ABSTRACT

YUN, TAEYOUNG. Development of a Viscoplastic Constitutive Model Using a Rate-Dependent Yield Criterion for HMA in Compression. (Under the direction of Dr. Y. Richard Kim).

This dissertation presents a uniaxial viscoplastic constitutive model that is capable of capturing the rate-dependent hardening-softening behavior of hot-mix asphalt (HMA) subject to compressive loading. Experimental support for such behavior is also given. In the constitutive model, Perzyna's over-stress theory and a rate dependent hardening-softening function are used as the flow rule and yield stress function, respectively.

A comprehensive material experimental program is performed to identify the characteristic behaviors of HMA, including dynamic modulus test, monotonic test, repetitive creep and recovery test, and flow number test under various loading conditions. From the dynamic modulus test, it is confirmed that the dynamic modulus of HMA in compression is the same as that in tension-compression; however, it is shown that the dynamic modulus is especially dependent on confining pressure at conditions where the material is softest (high temperatures and low frequencies). Further, it is found that when affected by confining pressure, that the modulus increases as the confining pressure increases. It is also confirmed that the time-temperature superposition principle holds true regardless of loading type, severity of damage or viscoplastic strain, as evidenced by a series of constant strain rate tests and repetitive creep and recovery tests. A finding previously undocumented for HMA that is found in this experimental research, is that the resistance to viscoplastic flow, the yield stress, shows rate-dependent hardening and softening behavior. The rate-dependent hardening and softening of the yield stress explains the significant increase of viscoplastic strain in the repetitive creep and recovery tests with long rest periods or with short loading pulses relative

to those with short rest periods or long loading pulses. The flow number test and tests combining repetitive creep and recovery and flow number tests are conducted to verify the model. The results indicate that the developed model is capable of accounting for the effects of rest period and loading sequence on viscoplastic strain development. These characteristics cannot be adequately captured with existing HMA viscoplastic models.

Development of a Viscoplastic Constitutive Model Using a Rate-Dependent Yield Criterion for HMA in Compression

by
Taeyoung Yun

A dissertation submitted to the Graduate Faculty of
North Carolina State University
in partial fulfillment of the
requirements for the Degree of
Doctor of Philosophy

Civil Engineering

Raleigh, North Carolina

2008

APPROVED BY:

_____	_____
Dr. Y. Richard Kim Chair of Advisory Committee	Dr. Roy H. Borden
_____	_____
Dr. Murthy N. Guddati	Dr. S. Ranji Ranjithan

DEDICATION

I dedicate this dissertation to my parents and sister. I also dedicate it to the person who made this work possible by endless support and understanding, my wife, Bokhee Kang.

BIOGRAPHY

Taeyoung Yun was born in Seoul, Korea on September 9, 1975. In 1994 he entered Chung-Ang University and earned Bachelor and Master degrees in Civil Engineering. During the following year he was also employed as a pavement researcher at the Korean Institute of Construction Technology in Gyeonggi-Do. In May 2004, he entered North Carolina State University for his graduate study in Civil Engineering.

ACKNOWLEDGEMENTS

Most of all, I would like to thank my parents, sister, and my wife for their endless support and understanding. Especially, I would like to thank my three-years-old son, Sungjin, who always makes me happy. Next, I would like to thank my advisory committee and all of the research group members for their help. Especially, I would like to thank my advisors, Dr. Y. Richard Kim and Dr. Murthy N. Guddati, for their support and advice. I could not have completed this work without the help and honest criticism of my brother and friend B. Shane Underwood. I will remember the moments when we had in-depth discussions about everything. All former and present group members, including Jusang Lee, Jaejun Lee, Sangyum Lee, Chulmin Back, Andrew Lacroix, Fadi Jadoun, Eric T. Hou, and Yeongtae Choi, also greatly contributed in various encouraging and practical ways.

TABLE OF CONTENTS

LIST OF TABLES

LIST OF FIGURES

1. INTRODUCTION

1.1. BACKGROUND AND OBJECTIVES

Hot mix asphalt (HMA) is a complicated material exhibiting both viscoelastic and viscoplastic behaviors. Further, HMA's composite nature means that the performance of this material is affected by the properties and interaction of the mix components when subjected to repeated traffic loading.

Rutting is one of the major forms of distresses in asphalt pavement. This distress results from the accumulation of vertical strains in the asphalt pavement layers and may be related to structural failure (i.e., rutting in the unbound layers) or material failure (i.e., rutting in the asphalt concrete layer). It is this latter type of rutting that is the focus of this dissertation. In order to predict the performance of asphalt concrete with reasonable accuracy, a better understanding of its deformation behavior under realistic conditions is required.

Researchers (Zhao 2002, Desai 2001, and Gibson 2003) have adopted various experimental testing protocols to identify the rutting behavior of HMA and developed constitutive models based on conventional viscoplasticity concepts. However, the difficulty in developing a constitutive model for HMA using this approach is that hardening rules based on the behavior

of metals or soils are not necessarily appropriate to describe the viscoplastic behaviors of HMA. In particular, models developed for metals and soils describe only elastic recovery during unloading, whereas HMA shows linear and/or nonlinear strain recovery during unloading due to the viscoelastic and composite properties of the material. Both of these components are found to be characteristic of HMA from the experimental component of this research.

The objective of this research is to develop a 1D viscoplastic constitutive model of HMA in compression that is capable of predicting the development of viscoplastic strain of HMA under various loading conditions and temperatures encountered in the field. In this study the rate-dependent hardening-softening concept is introduced into the yield stress function of the developed viscoplastic model in order to address rate-dependent hardening-softening of HMA under compressive stress. This is the first documented use of such an approach for modeling the permanent deformation behavior of HMA.

1.2. OUTLINE OF RESEARCH PRESENTED

This dissertation first presents, in Chapter 2, the theoretical background for identifying the

viscoelastoplastic characteristic behaviors of HMA and for developing the proposed viscoplastic constitutive model. Chapter 3 discusses relevant viscoplastic models that involve various plastic or viscoplastic materials. In Chapter 4, the materials, specimen fabrication, testing setup and the various types of testing performed in this research are discussed. The characteristic behaviors and physical interpretations of HMA found in existing solid mechanical theory and through various experimental tests are presented in Chapter 5. In Chapter 6, the development and validation of the viscoplastic constitutive model are presented. The conclusions and recommendations for future research are presented in Chapter 7.

2. THEORETICAL BACKGROUND

2.1. STRAIN DECOMPOSITION

A well-known assumption, founded in the theory of plasticity, is that total strain can be decomposed into elastic and plastic strains. Likewise, total strain can be decomposed into elastic strain, plastic strain, and creep strain according to the theory of viscoplasticity in order to account for the rate-dependent plastic strain of materials, as shown in Equation (2.1).

$$e_{ij}^{total} = e_{ij}^{e} + e_{ij}^{p} + e_{ij}^{c} = e_{ij}^{e} + e_{ij}^{vp}, \qquad (2.1)$$

where

e_{ij}^{e} = elastic strain,

e_{ij}^{p} = plastic strain,

e_{ij}^{c} = creep strain, and

e_{ij}^{vp} = viscoplastic strain.

In some studies that involve such rate-dependent materials, the rate-independent plastic strain and the rate-dependent creep strain are defined as viscoplastic strain because the distinction between plastic deformation and creep deformation is not well defined. The theoretical

background for the viscoplastic strain concept was first discussed by Perzyna (1971); since then more complicated models have been developed to explain the behavior of a material due to plasticity-creep interaction.

From a similar point of view, Schapery (1999) suggests that total strain may be separated into several components, such as elastic, viscoelastic, and viscoplastic strains. In this HMA constitutive modeling which addresses viscoelastoplastic material, elastic, linear viscoelastic, and strains due to microcracking damage are considered as the viscoelastic strain (e_{ij}^{ve}) and plastic strain and creep strain are considered as the viscoplastic strain (e_{ij}^{vp}) as shown in Equation (2.2).

$$e_{ij}^{total} = e_{ij}^{ve} + e_{ij}^{vp}, \tag{2.2}$$

where

e_{ij}^{ve} = elastic plus linear viscoelastic strain due to damage and

e_{ij}^{vp} = viscoplastic strain.

2.2. THEORY OF VISCOPLASTICITY

In conventional plasticity, viscoplastic concepts are generally presented as the expansion of

rate-independent plastic strain concepts. Therefore, the fundamental as well as rate-independent concepts of rate-dependent plasticity are described in Section 2.2.

2.2.1. Flow Rule

The general concept that underlines constitutive equations for plastic deformation was proposed by von Mises (1928) and is based on the theory of elasticity wherein the strain tensor is related to the stress through an elastic potential function, the complementary strain energy, U_e.

$$e_{ij}^{e} = \frac{\partial U_e}{\partial s_{ij}}, \tag{2.3}$$

where

e_{ij}^{e} = elastic strain tensor,

U_e = elastic complementary strain energy, and

s_{ij} = stress tensor.

The plasticity theory based on the above flow rule is called the plastic potential theory. When the state of stress reaches the yield criterion, f, plastic strain develops; this mechanism is called plastic flow. In order to generalize the concept to make it applicable to plasticity theory,

von Mises proposes a plastic potential function, $g\left(s_{ij}\right)$, and the plastic strain rate, de_{ij}^{p}, could be derived from the following flow rule:

$$de_{ij}^{p} = l\,\frac{\partial g}{\partial s_{ij}}, \tag{2.4}$$

where

de_{ij}^{p} = plastic strain rate,

l = positive scalar factor, and

$\frac{\partial g}{\partial s_{ij}}$ = gradient of the plastic potential, $g\left(s_{ij}\right)$.

In Equation (2.4), l is a proportional positive scalar factor that can be determined from the yield criterion. For some materials, the plastic potential function, g, and the yield function, f, can be assumed to be the same. These kinds of materials are considered to follow the associative flow rule of plasticity. In other words, the normality rule for this material is associated with the yield criterion, f. However, for other materials, the plastic potential function, g, and the yield function, f, are different. These materials are considered to follow the non-associative flow rule of plasticity and the flow rule of the material is derived from a plastic potential, g. In this case, $\frac{\partial g}{\partial s_{ij}}$ is not proportional to $\frac{\partial f}{\partial s_{ij}}$ and, therefore, the plastic strain direction is not normal to the yield surface, f. Basically, the viscoplastic

flow rule takes a similar form to the plastic flow rule with the exception that it takes advantage of the overstress function as a replacement of the scalar factor, l, as shown in Equation (2.5).

$$\dot{\varepsilon}_{ij}^{vp} = l\frac{\partial f}{\partial s_{ij}} = \frac{\Phi}{h_0}\frac{\partial f}{\partial s_{ij}} = \Gamma\Phi\frac{\partial f}{\partial s_{ij}}, \qquad (2.5)$$

where

Φ = overstress function, and

h_0 = viscosity.

Figure 2.1 represents the viscoplastic flow rule using a mechanical analog, which combines a dashpot and a slip element in parallel (Perzyna, 1963). In this case, the overstress function in Equation (2.5) is represented by the difference between applied stress (s) and yield stress (G), and viscosity (h_0) in this model.

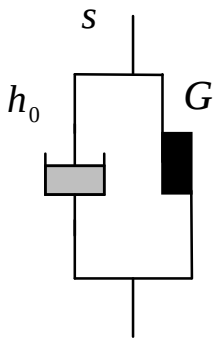

Figure 2.1 Mechanical analog for general viscoplastic model.

2.2.2. Yield Criterion

In viscoplasticity, the elastic limit of the material can be defined by a surface in stress space. Mathematically, the yield surface for general anisotropic materials is expressed as Equation (2.6).

$$f\left(s_{ij}\right)=0 \tag{2.6}$$

For an isotropic material, the orientation of the principal axes is immaterial, and the principal stresses, s_{11}, s_{22}, and s_{33} are sufficient to describe the state of stress. The principal stresses form the basis of integrity, presented generally as I_1, J_2, J_3. Therefore, the yield function becomes Equation (2.7) for the isotropic material.

$$f\left(s_{11},s_{22},s_{33}\right)=f\left(I_1,J_2,J_3\right)=0, \tag{2.7}$$

where

$I_1=s_{11}+s_{22}+s_{33}$,

$J_2=\frac{1}{2}s_{ij}s_{ij}$,

$J_3=\frac{1}{3}s_{ij}s_{jk}s_{ki}$,

$s_{ij}=s_{ij}-\frac{1}{3}s_{kk}d_{ij}$, and

d_{ij} = Kronecker delta.

Physically, I_1 represents the hydrostatic pressure and J_2 represents the distortional energy in the material, whereas no clear physical meaning is attached to J_3. Generally, yield criteria could be classified into two subgroups by the existence of dependence on hydrostatic stress. The isotropic hardening model is the simplest hardening model and is based on the assumption that the yield surface expands isotropically as the plastic strain develops. The typical isotropic hardening model is presented in Equation (2.8) and Figure 2.2(a). Because the load surface expands uniformly, it cannot account for the Bauschinger effect that is observed in various materials and describes the reduction of compressive yield strength due to a previously applied tensile stress, or vice versa.

Therefore, using only the isotropic hardening model frequently limits the characterization of the material behavior when both tension and compression loads are applied.

$$f\left(s_{ij}, K\right) = f\left(s_{ij}\right) - k = 0, \tag{2.8}$$

where

s_{ij} = deviatoric stresses, and

k = isotropic hardening parameter.

The kinematic hardening model assumes that during plastic deformation the yield surface translates as a rigid body in the stress space and has the same shape and size as the initial yield surface. The kinematic hardening model is represented by Equation (2.9) and Figure 2.2(b).

$$f\left(s_{ij}, a\right) = f\left(s_{ij} - a_{ij}\right) = 0, \tag{2.9}$$

where

s_{ij} = deviatoric stresses, and

a_{ij} = kinematic hardening parameters (coordinate of the center of the yield surface in the deviatoric stress space).

Equations (2.10) and (2.11) conceptually represent the kinematic hardening rules suggested by Prager (1956) and also by Armstrong-Frederick (1966) and Chaboche (1986), respectively. The kinematic hardening rate is a function of the viscoplastic strain rate in these equations, and the hardening rate is always zero when there is no change in viscoplastic strain.

$$da = g\left(d\varepsilon^{vp}\right) \text{ and} \tag{2.10}$$

$$da = g\left(d\varepsilon^{vp}, a\right), \tag{2.11}$$

where

$\dot{\alpha}$ = kinematic hardening stress, and

$\dot{\varepsilon}^{vp}$ = viscoplastic strain rate.

Therefore, when a material is subjected to one-directional loading, such as in a constant strain rate test or a repetitive creep and recovery test, the yield stress increases only in the direction of the developed viscoplastic strain and never decreases.

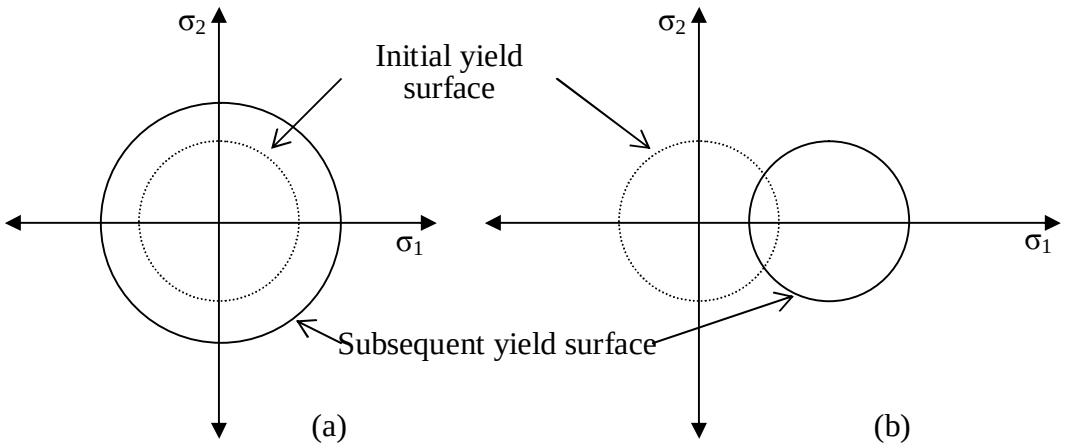

Figure 2.2 Schematic representation for isotropic hardening and kinematic hardening.

2.3. THEORY OF VISCOELASTICITY

Linear viscoelasticity is one of the fundamental theories used in modeling rate-dependent

materials and is used to explain the behavior of HMA in small strains. In this Section 2.3, the theory of linear viscoelasticity is presented.

2.3.1. Linear Viscoelasticity

As is well known, resistance to shear flow is a definitive property of viscous materials and the material shows time- or temperature-dependent behavior for a given stress or strain input history. In contrast, elastic materials are dependent only on the current stress or strain input regardless of the history of the input. Viscoelastic materials have characteristics of both viscous and elastic materials and, thus, show time- and temperature-dependent behavior. By assuming a linear system that satisfies homogeneity and superposition conditions as shown in Equation (2.12) and Equation (2.13) respectively, a typical constitutive relationship for linear viscoelastic materials can be expressed as shown in Equation (2.14) and Equation (2.15), depending on the type of input.

$$R\{A \cdot I\} = A \cdot R\{A\} \quad \text{and} \tag{2.12}$$

$$R\{I_1 + I_2\} = R\{I_1\} + R\{I_2\}, \tag{2.13}$$

where

I, I_1, I_2 = input histories, and

R = responses.

$$s = \int_0^t E(t-t)\frac{de}{dt}dt \quad \text{and} \tag{2.14}$$

$$e = \int_0^t D(t-t)\frac{ds}{dt}dt \ , \tag{2.15}$$

where

$E(t)$ = relaxation modulus, and

$D(t)$ = creep compliance.

The relaxation modulus and creep compliance are important material properties in company with the complex modulus in linear viscoelastic theory. Because these two properties are the responses for respective unit inputs, they are called *unit response functions*. These unit response functions can be obtained either by experimental tests performed in the linear viscoelastic (LVE) range or by converting another unit response function as suggested by Schapery (1984).

2.3.2. Time-Temperature Superposition Principle for Linear Viscoelastic Material

The effect of time and temperature on viscoelastic material behavior can be combined into a

single parameter, called *reduced time*, through the time-temperature superposition (t-TS) principle. Viscoelastic properties obtained in the linear viscoelastic range at different temperatures can be superposed to develop a single mastercurve by shifting them horizontally to a certain reference temperature. The horizontal distance required to superpose a curve to the reference curve is the log of the time-temperature shift factor (a_T). A material that has a single mastercurve by this method described above is called *thermorheologically simple* (TRS) material. Equation (2.16) represents mathematical definition of reduced time, and Figure 2.3 and Figure 2.4 present a typical mastercurve and shift factor function, respectively.

$$x = \frac{t}{a_T}, \tag{2.16}$$

where

a_T = time-temperature shift factor.

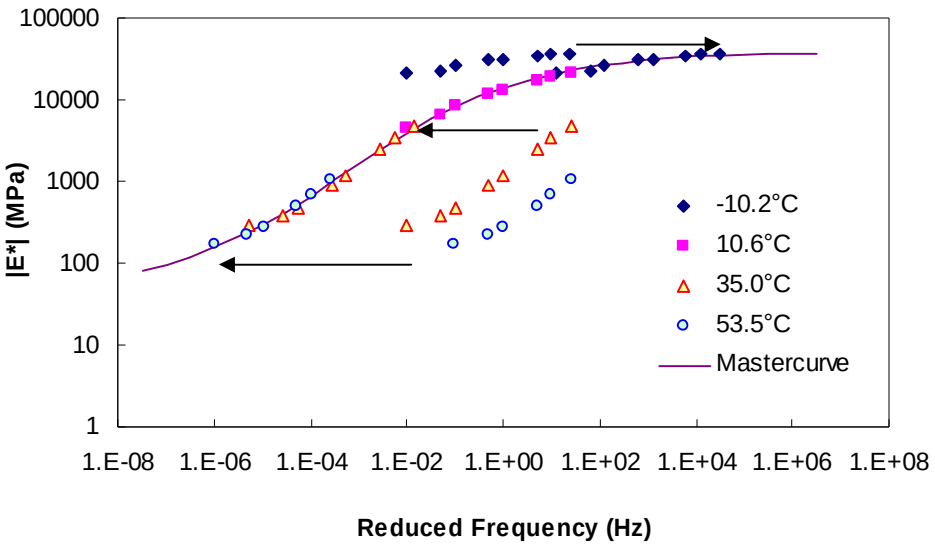

Figure 2.3 Dynamic modulus mastercurve (reference temperature of 10°C)

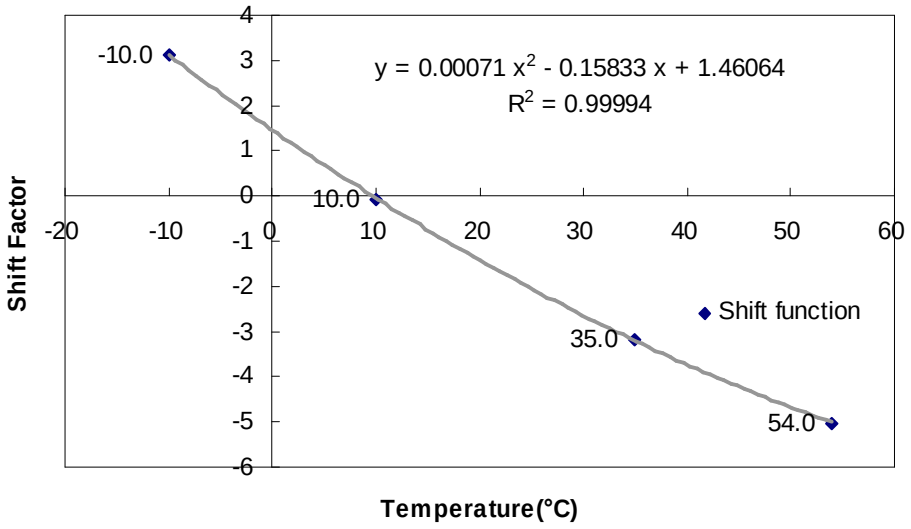

Figure 2.4 Shift factor function (reference temperature of 10°C)

2.3.3. Unit Response Function and Their Interrelationships

The unit response functions presented in Equation (2.14) and Equation (2.15) are often measured in the frequency domain using the complex modulus test, because it is often difficult to obtain unit response functions in the time domain due to the limitations of the machine's capacity or of testing time. The complex modulus provides the constitutive relationship between the stress and strain amplitudes of a material loaded in a steady-state sinusoidal manner. Then, the storage modulus can be determined from the complex modulus, and it can be converted to a time dependent property, such as $E(t)$ and $D(t)$ through the theory of linear viscoelasticity. When the storage modulus is expressed in terms of reduced angular frequency, w_R, as shown in Equation (2.17), it can be expressed using the Prony series representation given in Equation (2.18) (Park and Schapery 1999, Schapery 1961).

$$E'(w_R) = \left|E^*(w_R)\right| * \sin\left(f(w_R)\right) \quad \text{and} \tag{2.17}$$

$$E'(w_R) = E_\infty + \sum_{i=1}^{m} \frac{w_R{}^2 r_i E_i}{w_R{}^2 r_i{}^2 + 1}, \tag{2.18}$$

where

E_∞ = elastic modulus,

w_R = angular frequency(= $2p\ f_R \Delta t$),

Δt = time lag between stress and strain,

E_i = modulus of the i^{th} Maxwell element (fitting coefficient), and

r_i = relaxation time (fitting coefficient).

The coefficients determined from this process are then used with Equation (2.19) to find the relaxation modulus.

$$E(t) = E_\infty + \sum_{i=1}^{m} E_i e^{-t/r_i} \tag{2.19}$$

Using the theory of viscoelasticity, the exact relationship between the creep compliance and relaxation modulus is given by Equation (2.20).

$$\int_0^t E(t-\tau)\frac{dD(\tau)}{d\tau}d\tau = 1 \tag{2.20}$$

If the creep compliance can be written in terms of the Prony representation (Equation (2.21)), substituted into Equation (2.20) along with Equation (2.19) and simplified, the result can be expressed as a linear algebraic equation, Equation (2.22). The coefficients, {D}, in this equation are solved by any proper numerical method.

$$D(t) = D_g + \sum_{j=1}^{n} D_j\left(1 - e^{-t/t_j}\right) \text{ and} \tag{2.21}$$

$$[A]\{D\}=[B], \tag{2.22}$$

where

$$[A]=\sum_{j=1}^{M}\left[\sum_{m=1}^{N}\frac{r_m E_m}{r_m - t_j}\left(e^{\frac{-t}{r_m}}-e^{\frac{-t}{t_j}}\right)+E_\infty\left(1-e^{-\frac{t}{t_j}}\right)\right],$$

$\{D\}=D_j$, and

$$[B]=1-\frac{1}{E_\infty+\sum_{m=1}^{N}E_m}\left(E_\infty+\sum_{m=1}^{N}E_m e^{\frac{-t}{r_m}}\right).$$

Once the coefficients, D_j, are determined, they are substituted into Equation (2.21) to find the creep compliance.

2.3.4. Elastic-Viscoelastic Correspondence Principle

As described earlier, linear viscoelastic material shows time- and temperature-dependent behavior, and sometimes the time- and temperature-dependent property makes it difficult to understand the behavior of the material intuitively. The elastic-viscoelastic correspondence principle suggested by Schapery (1984), enables linear viscoelastic material to be considered as linear elastic material and, therefore, the material behavior can be understood more easily. The constitutive relationships of linear viscoelastic material in the uniaxial state of stress are

found is in the form of the following convolution integral, Equation (2.23), and the material property needed in Equation (2.23) is the relaxation modulus that can be obtained by converting the complex modulus through the interconversion relationship explained in the previous Section 2.3.3.

$$s = \int_0^x E(x-t)\frac{de}{dt}dt \ , \tag{2.23}$$

where

x = reduced time ($=\frac{t}{a_T}$),

t = physical time,

a_T = time-temperature shift factor,

$E(t)$ = relaxation modulus, and

t = integration variable.

Now, the pseudo strain is defined as shown in Equation (2.24) for a uniaxial state of stress.

$$e^R = \frac{1}{E_R}\int_0^x E(x-t)\frac{de}{dt}dt \ , \tag{2.24}$$

where

e^R = pseudo strain, and

E_R = reference modulus (an arbitrary constant).

Applying the definition of pseudo strain in Equation (2.24) to Equation (2.23) results in Equation (2.25).

$$s = E_R e^R \tag{2.25}$$

In Equation (2.25), E_R is an arbitrary constant, and by forcing the E_R value to one, Equation (2.25) becomes the same as Equation (2.24) and represents the pseudo strain as the linear viscoelastic stress.

3. VISCOPLASTIC MODELS

To predict the rutting performance of HMA, much effort has been made to develop constitutive models capable of describing the permanent strain development in HMA. Uzan (1985) suggests a viscoplastic model with strain-hardening features. As the simplest model, the Uzan model is also able to describe monotonic behavior in tension, as shown by several researchers (Schapery 1999, Chehab et al. 2003). Scarpas (1997) presents a viscoplastic model for HMA that incorporates Perzyna's flow rule with Desai's yield function (Desai et al. 1987). Gibson (2006) suggests a simplified HISS-Perzyna model that shows a reasonable viscoplastic strain prediction. However, the difficulty in developing a constitutive model for HMA is that hardening rules based on the behavior of metals or soils are not necessarily appropriate to describe both the viscoplastic and viscoelastic behaviors of HMA. That is, models developed for metals and soils describe only elastic recovery during unloading, whereas HMA shows nonlinear strain recovery during unloading due to the viscoelastic property of the material. An important observation supporting this phenomenon was made by Saadeh (2005).

3.1. SIMPLE STRAIN-HARDENING MODEL

Uzan (1985) and Schapery (1999) suggest a simple relationship, evidenced by Equation (3.1), which assumes that viscosity obeys a power law in viscoplasticity. Several researchers (Schapery 1999, Chehab et al. 2003) have shown that the model is applicable to monotonic behavior in tension.

$$d\varepsilon_{vp} = \frac{g(s)}{h(e_{vp})}, \tag{3.1}$$

where

$g(s)$ = stress function, and

h = viscosity.

Assuming that h is a power law in the viscoplastic strain, Equation (3.2) becomes

$$d\varepsilon_{vp} = \frac{g(s)}{A e_{vp}^{\ p}}, \tag{3.2}$$

where A and p are model coefficients. Rearranging and integrating yield

$$e_{vp}^{\ p} de_{vp} = \frac{g(s)dt}{A}, \text{ and} \tag{3.3}$$

$$e_{vp}^{p+1} = \frac{p+1}{A}\int_0^t g(s)\,dt\,. \tag{3.4}$$

Raising both sides of Equation (3.4) to the 1/(p+1) power yields

$$e_{vp} = \left(\frac{p+1}{A}\right)^{\frac{1}{p+1}}\left(\int_0^t g(s)\,dt\right)^{\frac{1}{p+1}}. \tag{3.5}$$

Letting $g(s) = Bs_1^q$, and coupling coefficients A and B into coefficient Y, Equation (3.5) becomes

$$e_{vp} = \left(\frac{p+1}{Y}\right)^{\frac{1}{p+1}}\left(\int_0^t s^q dt\right)^{\frac{1}{p+1}}. \tag{3.6}$$

In the current work, the coefficients, p, q and Y, are pressure-dependent quantities. Typically, viscoplastic models are characterized using creep and recovery tests. These tests allow the relatively easy separation of the viscoplastic and viscoelastic components. However, it is difficult (if not impossible in some machines) to maintain a zero load during the recovery period of the creep and recovery test in tension. Therefore, in tension, viscoplastic characterization uses constant rate tests in which the VECD model is used to first predict the viscoelastic strains. These viscoelastic strains are then subtracted from the measured strains to provide the viscoplastic strains that are needed for curve fitting in Equation (3.6).

The advantage of this model is that it is easy to implement and does not consume much computational time. The ability of this model to predict the HMA behavior under complex loading histories in tension is reported by Underwood et al. (2006). However, this model's major weakness is its one-dimensional nature, which is not sufficient to describe the behavior of HMA in pavements. This deficiency is particularly troublesome in compression where confinement is known to play a major role in the permanent deformation behavior of HMA. In the following subsections, more general viscoplastic models are presented.

3.1.1. A Phenomenological Model Considering Pulse Time Effects

As a first step towards developing a mechanistic material model for the behavior of HMA in compression, a series of analyses was performed on variable loading time (VT) and variable load level (VL) test data, and a phenomenological model was developed. The modeling approach adopted in the phenomenological model is based on the existing strain-hardening model presented for describing the tensile behavior in Equation (3.1). As shown in Equation (3.1), the viscoplastic strain rate is represented by the combination of two functions, $f(\sigma)$ and $g(\varepsilon_{vp})$, which allow the stress rate dependency and strain hardening to be taken into

consideration in the model. Equation (3.1) can be generalized as Equation (3.7), which accounts for the effect of the pulse time.

$$\dot{\varepsilon}_{vp} = F\left(e_{vp}, s, t_p\right), \tag{3.7}$$

where t_p is the loading time. The exact form of the function, F, is presented along with experimental data in the following sections.

Tests Performed in This Study

Three types of repetitive creep and recovery tests were performed for the phenomenological model development. They include the creep and recovery test with variable load levels (VL test), the creep and recovery test with variable loading times (VT test), and the creep and recovery test with a constant load level and constant loading time (CLT test). All the tests were conducted at 55°C under the confining pressure of 500 kPa. Experimental details for these tests are given below, because this particular study uses different test conditions than those outlined in Chapter 4.

Creep and Recovery Test with Variable Loads): The VL test was performed with 200 kPa as the starting load level. An incremental factor of 1.0245 was used for the subsequent load

levels to increase the load level until the complete failure of the specimen. The loading time and rest period were 0.1 second and 10 seconds, respectively.

Creep and Recovery Tests with Variable Loading Time: The VT test was performed with a loading block consisting of 30 different loading times. The loading times varied from 0.005 second to 2.0 seconds with an incremental factor of 1.1356. The rest period for each loading cycle was 30 times that of each loading time. The VT tests were performed at three different load levels, 1800, 2000, and 2200 kPa.

Creep and Recovery Test with Constant Load Level and Loading Time: In the CLT test, a constant load level and constant loading time were used for each test. Load levels and loading times were changed between tests. Three load levels of 1800 kPa, 2000 kPa and 2200 kPa were used with the loading time of 1.6 seconds. For the 2000 kPa load level, the creep and recovery tests were conducted with three additional loading times of 0.1, 0.4, and 6.4 seconds.

The VL and VT tests were conducted to understand the effects of load level and loading time on the permanent deformation behavior of HMA and to calibrate the phenomenological model, and the CLT tests were conducted to verify the calibrated model.

Model Characterization

By observing the viscoplastic strain rate versus the viscoplastic strain variable loading time in Figure 3.1, a constitutive relationship between these viscoplastic media is defined, as shown in Equation (3.8).

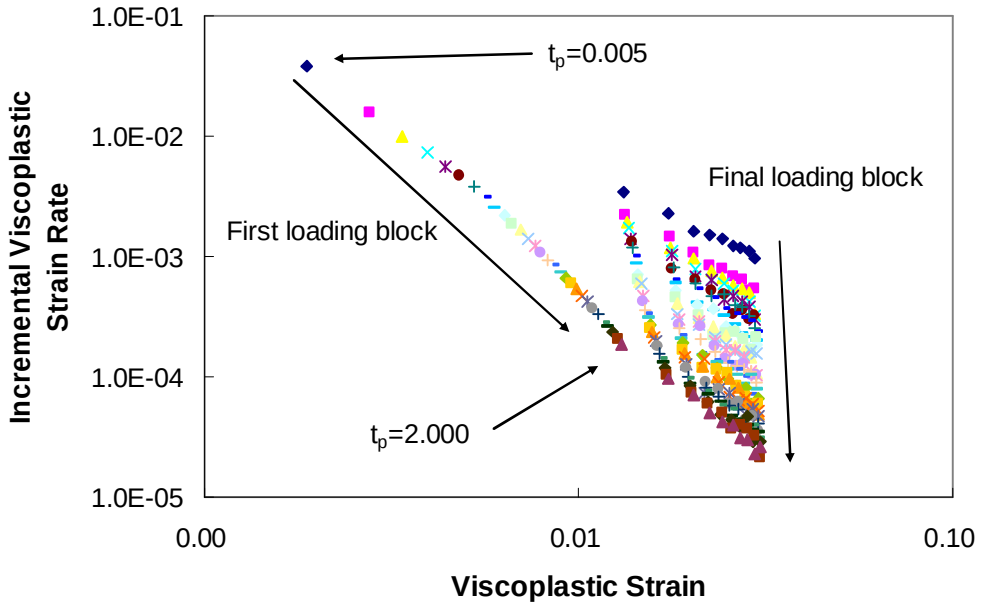

Figure 3.1 Incremental viscoplastic strain rate vs. viscoplastic strain (500 kPa confinement, 2000 kPa).

$$\log \dot{\varepsilon}_{vp} = a\left(t_p\right) \log e_{vp} + D\left(t_p, s\right), \tag{3.8}$$

where

$a(t_p)$ = material function of loading time, and

$D(t_p, s)$ = intercept of the curve on the viscoplastic strain rate axis.

In Equation (3.8), $a(t_p)$ is a function of the loading time, and $D(t_p, s)$ is a function of the load level and loading time. Equation (3.8) can be represented in Equation (3.9), which is a generalized form of Equation (3.7).

$$\begin{aligned} \dot{e}_{vp} &= \left[\left(e_{vp} \right)^{a(t_p)} \left(t_p \right)^b 10^d \right] 10^{c(s)} \\ &= \frac{f(s)}{g(e_{vp}) k(t_p)} \end{aligned} \tag{3.9}$$

where

$k(t_p)$ = function of loading time.

Equation (3.8) requires the determination of $a(t_p)$ and $D(t_p, s)$ to calculate the viscoplastic strain rate for a given viscoplastic strain. Values of $a(t_p)$ and $D(t_p, s)$ for given loading times can be found by fitting log functions against each viscoplastic strain rate versus viscoplastic strain curve corresponding to a given loading time. At this time, the values of $a(t_p)$ can be represented by the second logarithm function, as shown in Equation (3.10).

$$a\left(t_p\right) = a_1 \log t_p + a_2 , \tag{3.10}$$

where the coefficients a_1 and a_2 are material-dependent constants. In order to determine the form of $D\left(t_p, s\right)$, it is assumed that $D\left(t_p, s\right)$ can be represented by the summation of the loading time term and the load level term, as shown in Equation (3.11).

$$D\left(t_p, s\right) = b \log t_p + c\left(s\right) + d , \tag{3.11}$$

where the function $c\left(s\right)$ is given by $c_1 \log\left(s\right)$ when the stress is less than 1000 kPa and by $c_2 s$ when the stress is greater than 1000 kPa. The coefficient, b, is determined by fitting Equation (3.11) against $D\left(t_p, s\right)$ from the VT test. At this time, it is assumed that $c\left(s\right)$ and d constitute one constant that accounts for the effect of load level. The function, $c\left(s\right)$, is then fitted by the logarithmic function and the linear function. Finally, coefficient, d, is determined by fitting Equation (3.11) for the viscoplastic strain rate versus the viscoplastic strain curves of the VL and VT tests. Figure 3.2 and Figure 3.3 show the fitting results and the coefficients that have been determined. Figure 3.4 presents predictions for the VT and VL tests, which are then used for the characterization process.

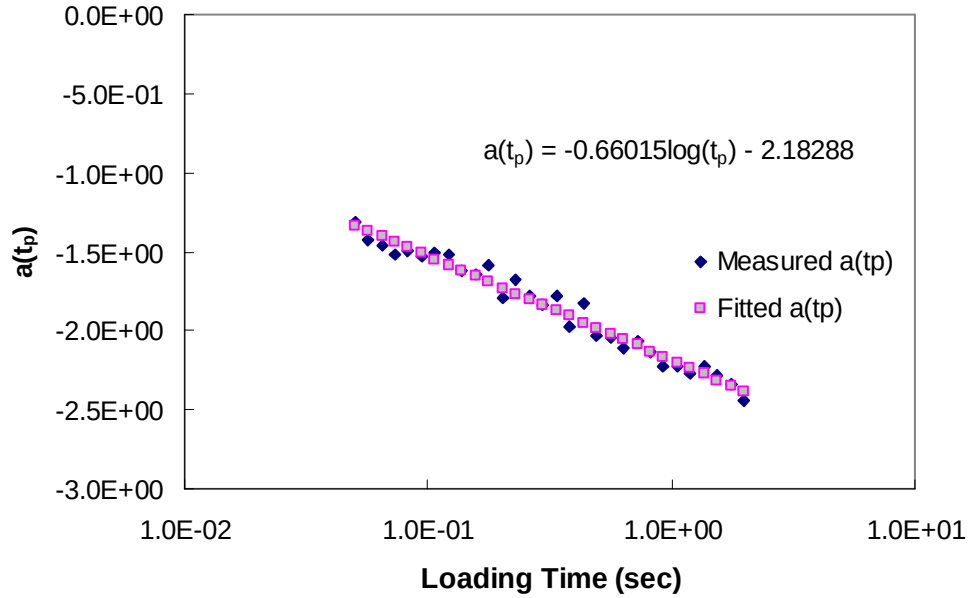

Figure 3.2 Determined fitting results and coefficients of function $a(t_p)$.

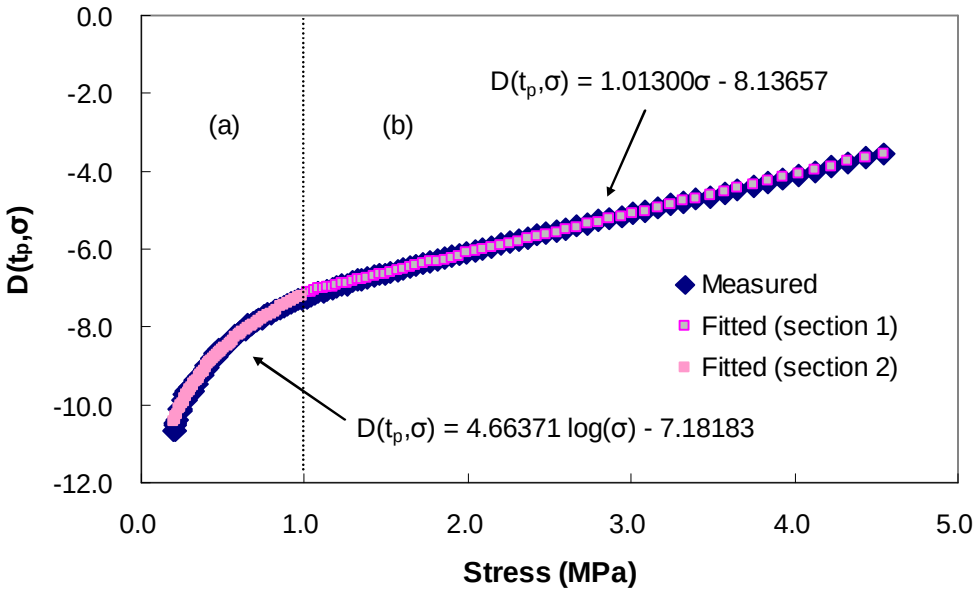

Figure 3.3 Determined fitting results and coefficients of function $D(t_p,\sigma)$.

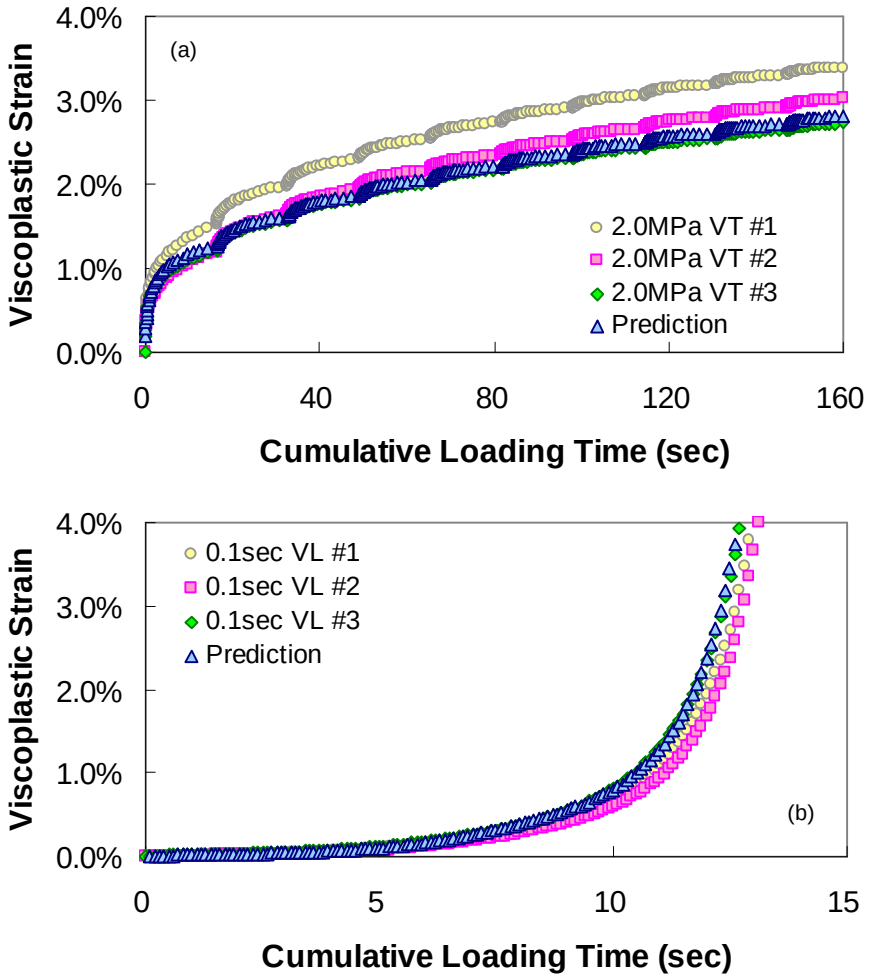

Figure 3.4 Prediction for VT and VL tests: (a) VT and (b) VL.

Verification of the Model

Figure 3.5 shows predictions for the CLT tests. Although the model is able to account for differences in the viscoplastic development for the various loading times, overall predictions are not as accurate.

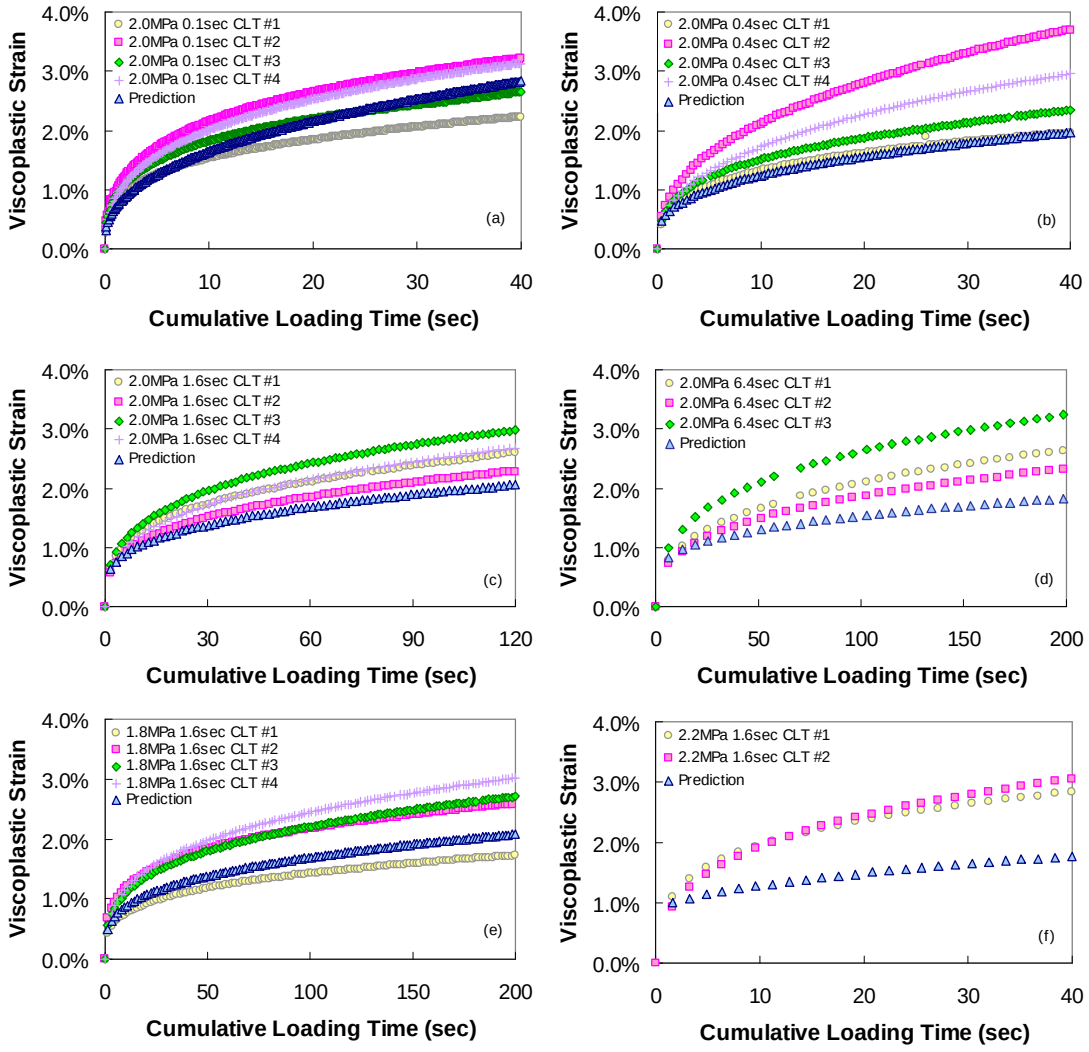

Figure 3.5 Predictions for the CLT tests (Legends stand for load level – loading Time – CLT – replicate number).

Several causes for the discrepancy between the viscoplastic strain predictions and measurements can be suggested. However, it seems that the inability of the model to consider strain history is a highly probable cause for this discrepancy, given that the fitting results for

the VT and VL tests are acceptable.

3.2. HIERARCHICAL SINGLE SURFACE - PERZYNA MODEL

The hierarchical single surface (HISS) plasticity model provides a general formulation for the elastoplastic characterization of material behavior. This model, which is potentially able to incorporate isotropic and kinematic hardening and associated and non-associated plasticity characterizations, can be used to represent a material response based on the continuum plasticity theory. Therefore, the HISS model allows the selection of a more appropriate derivative model for a given material in a specific engineering application. Various well-known plasticity models – such as the Von Mises, Mohr-Coulomb, Drucker-Prager, continuous yielding critical-state, and capped models – can be derived as special cases of the HISS model.

The HISS-Perzyna model, suggested by the Delft University of Technology and the University of Maryland, has been investigated with respect to the data set obtained from experimental tests. A prediction using the Delft University of Technology model could not be made because of numerical problems. However, the characterization process using the t-TS

principle and coefficients of the model are described in Section 3.2.1.

3.2.1. HISS Model Implemented by the Delft University of Technology

Equation (3.12) represents the HISS criterion suggested by Desai (1986). In the criterion, n and α determine the shape of the yield stress in deviatoric-hydrostatic stress space, and γ represents ultimate yield stress. R represents the cohesion of the material and determines the position of the yield stress with respect to the hydrostatic stress axis. Because the yield stress of the HISS criterion varies depending on the first stress invariant, I_1, the model exhibits a spindle shape of its yield surface when the shape of the yield surface is assumed to be circular ($\beta=0$) in the deviatoric stress space, as shown in Figure 3.6.

$$f = \frac{J_2}{P_a^2} - \frac{\left[g\left(\frac{I_1 - R}{P_a}\right)^2 - a\left(\frac{I_1 - R}{P_a}\right)^n \right]}{\sqrt{\left(1 - b\,\frac{3\sqrt{3}J_3}{2\left(J_2\right)^{\frac{3}{2}}}\right)}} = 0, \qquad (3.12)$$

where

g = softening parameter,

a = hardening parameter

R = tensile strength of material when deviatoric stress is zero,

n = parameter determining shape of yield stress,

b = parameter determining shape of yield stress in deviatoric stress space, and

P_a = atmosphere pressure.

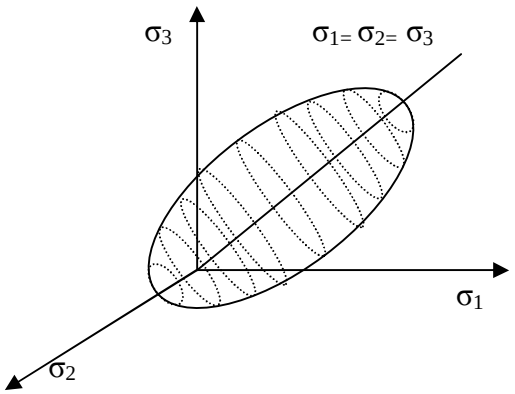

Figure 3.6 Typical yield surface of HISS model.

Erkens (2003) suggests a HISS criterion whose parameters are the strain rate-dependent functions for a given HMA mixture. For the characterization, a series of constant strain rate tests in tension and in compression are performed at several strain rates and temperatures. Then, predictions are made for indirect tension (IDT) specimens subjected to constant strain rate loading. Because this model requires constant strain rate testing that uses several

different strain rates and temperatures for characterization, it is important to determine the appropriate range of the strain rates and temperatures to minimize the amount of experimental effort. Although it appears that the model can successfully explain the viscoplastic behavior when subjected to monotonic loading, numerical issues related to parameter determination and prediction still remain. In addition, because the model is characterized using constant strain rate tests, it cannot fully explain the behavior of HMA under discontinuous loading, such as repetitive creep and recovery loading.

The model suggested by researchers at the Delft University of Technology requires the development of several relationships between the material parameters and the strain rates obtained from constant strain rate tests. In this research, the t-TS principle is utilized to simplify the modeling effort and to reduce the number of relationships required. With the assumption that the yield stress in deviatoric stress space presents as circular, ($b = 0$), Equation (3.12) can be reduced to Equation (3.13).

$$\sqrt{J_2} = \sqrt{g\left(I_1 - R\right)^2 - a\left(I_1 - R\right)^n}\,, \tag{3.13}$$

where

g = softening parameter,

a = hardening parameter,

R = tensile strength of material when deviatoric stress is zero, and

n = parameter that determines shape of yield stress.

Figure 3.7 shows peak stresses for a series of compressive and tensile constant strain rate tests; the strain rates are listed in Section 4.4.2.

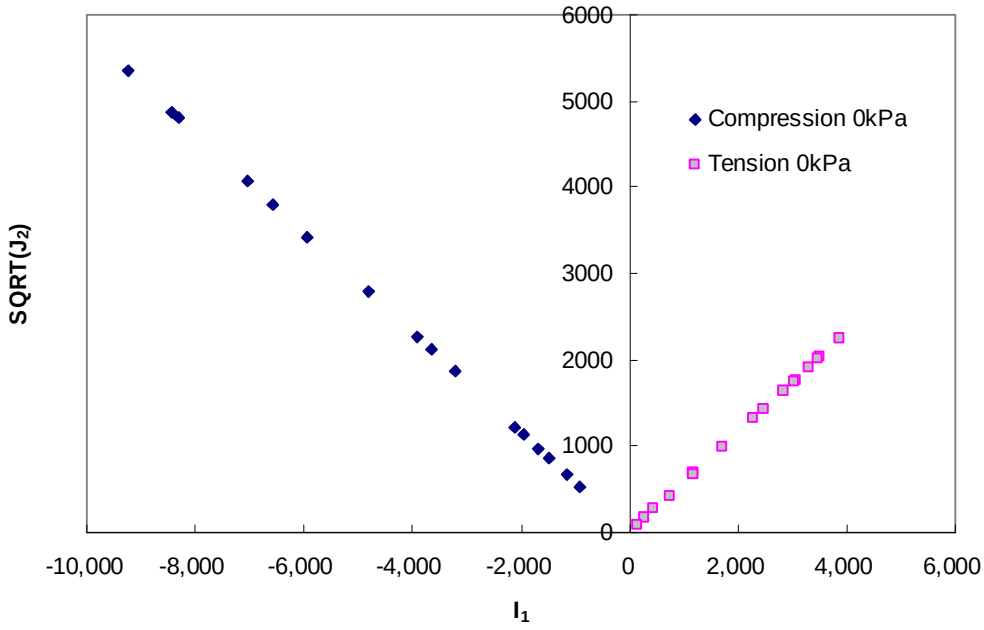

Figure 3.7 Compressive and tensile peak stress in SQRT(J_2)-I_1 space.

These peak stresses are used as fundamental quantities to develop relationships between the material parameters and the reduced strain rates. R and g_0 can be determined as functions of the reduced strain rate by plotting the compressive and tensile peak stresses obtained from the constant strain rate tests under a certain strain rate and then taking the slope and x-intercept of the line. In the model, R and g_0 represent the tensile strength of hydrostatic stress and the softening of the material in the post-peak region, respectively. The parameter, n, governs the overall shape and size of the yield function and is believed to be related to the dilation of the material. The beginning of dilation can be defined as the stress at the minimum plastic volumetric strain, because the plastic deviatoric strain and elastic strain (or viscoelastic strain) is assumed not to be associated with the volumetric change of a material. In addition, because HMA specimens dilate after a little compression as the compressive stress increases, the dilation stress can be determined. Once the dilation stresses are determined for several strain rates, the value of *n* can be determined using Equation (3.14).

$$n = \frac{2}{1 - \frac{J_{2,dilation}}{g\left(I_{1,dilation} - R\right)^2}}, \tag{3.14}$$

where,

$I_{1,dilation}$ = I_1 at the beginning of dilation, and

$J_{2,dilation}$ = J_2 at the beginning of dilation.

Once n is determined, α_0 can be readily determined using Equation (3.15).

$$a_0 = g_0 \left(\frac{R}{P_a} \right)^{2-n} . \tag{3.15}$$

The sigmoidal function is used to represent relationships between the reduced strain rate and the material parameters. The form of the function and the coefficients determined for each parameter are listed in Equation (3.16) and Figure 3.8 shows a comparison of measured values versus predicted values at various reduced strain rates.

$$\log(\gamma_0 \text{ or } R) = a + \frac{b}{1 + exp\left(d - e\log\left(\dot{\varepsilon}_{reduced}\right)\right)}. \tag{3.16}$$

Table 3.1 Delft material model coefficients functions

	a	b	d	e
R	316.86	17074.55	-9.28	1.75
γ_0	0.20	-0.15	-13.91	2.13
n	2.00	2075.86	0.48	1.06
α_0	-0.63	-93.39	-5.01	1.35

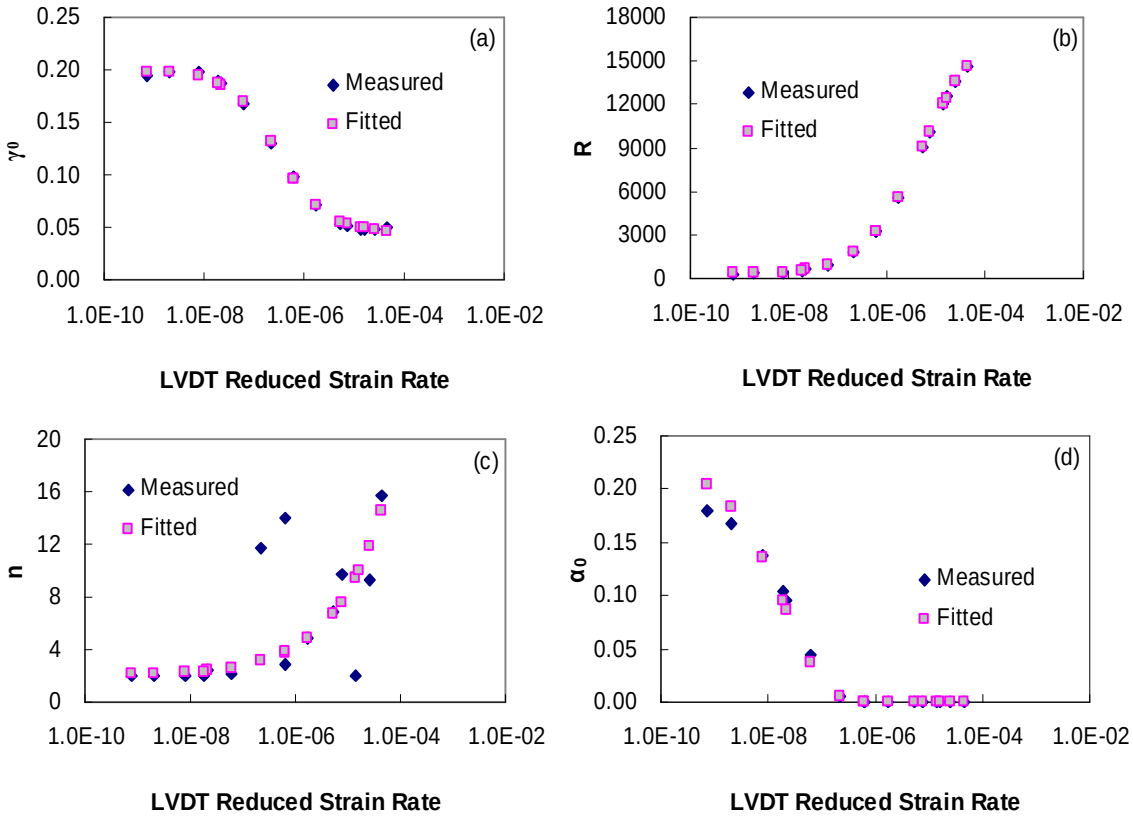

Figure 3.8 Determined parameter functions (sigmoidal function).

Figure 3.9 shows the strain rate-dependent yield surface that is constructed using the characterized parameters when the viscoplastic strain is equal to zero (i.e., the initial yield surface). It is observed that the initial yield surface increases as the temperature decreases; that is, the reduced strain rate increases. This behavior coincides with observations from constant strain rate tests whereby more viscoplastic strains are developed under a small reduced strain rate (or higher temperature).

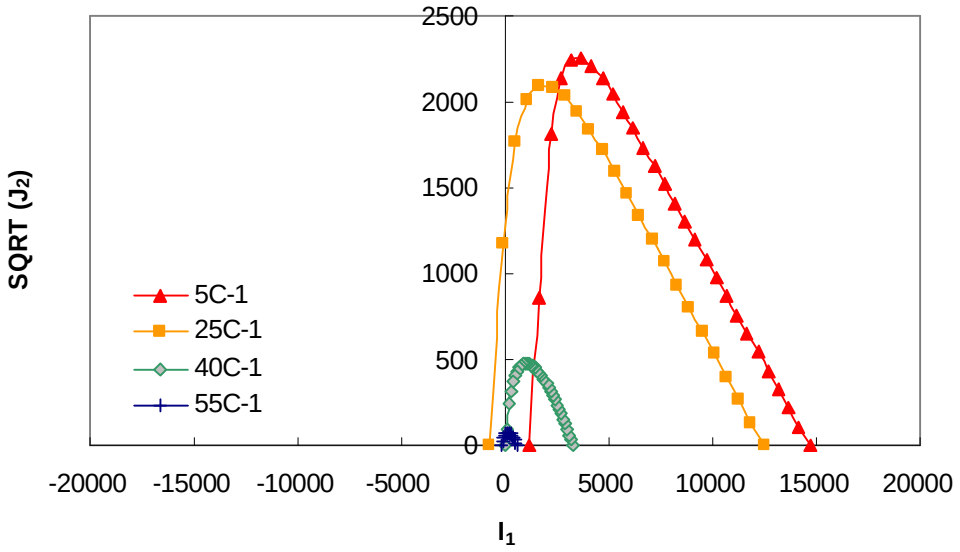

Figure 3.9 Rate-dependent initial yield surface.

As shown in Equation (3.13), the second term in the square root must always be smaller than the first term in order to construct a valid yield surface. However, because of the numerical errors involved in the characterization process of a and n, the prediction program was often required to calculate the square root of a negative number during the analysis. This situation can be encountered without t-TS, as mentioned by Erkens (2002).

3.2.2. HISS Model Implemented by the University of Maryland

Gibson (2006) suggests a viscoplastic model based on the simplified HISS model and using

Perzyna's flow rule. Repetitive creep and recovery tests are used for both calibration and prediction, and numerical optimization techniques are adapted for calibrations, unlike Erkens' model. As shown in Equation (3.17), g, which represents both the ultimate yield stress and the softening of the material, is considered a constant, and R is a function of the viscoplastic strain. In Erkens' study, however, g and R are functions of the viscoplastic strain rate and temperature.

$$F = J_2 - \left[g\left(I_1 + R(x)\right)^2 + a\,(x)\left(I_1 + R(x)\right)^n \right], \tag{3.17}$$

where,

x = viscoplastic strain trajectory,

g = softening parameter (constant),

a = hardening parameter (function of viscoplastic strain), and

R = tensile strength of the material when the deviatoric stress is zero.

The main contribution of this research is to apply the t-TS principle to a conventional viscoplastic constitutive model and confirm the validity of the superposition principle. As shown in Equation (3.17), a simplified HISS-Perzyna model was suggested by researchers at the University of Maryland (Gibson, 2006). Equation (3.18) represents a general form of the

hardening function used for the suggested model and Figure 3.10 represents predictions made by Uzan's model and Gibson's model.

$$a = a_0 e^{-k \cdot e_{vp}}, \tag{3.18}$$

where the parameters a_0 and k are material constants.

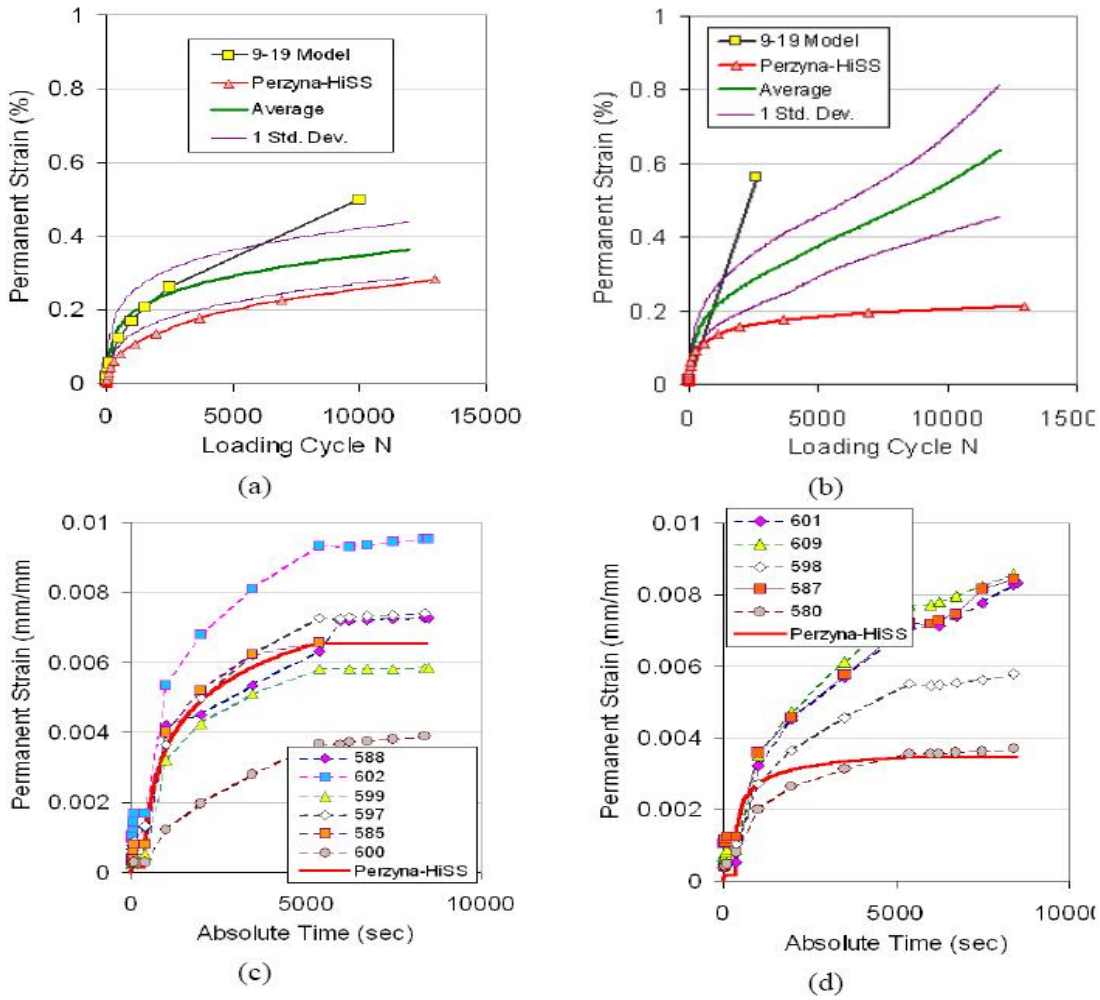

Figure 3.10 Predictions for repetitive loading conditions ((a) haversine 0.1-0.1 second at 37°C, (b) haversine 0.9-0.9 second at 54.4°C, (c) haversine 0.1-0 second at 37°C, (d) haversine 0.9-0 second at 54.4°C, Nelson Gibson 2006, ISAP)

However, the observation made in Section 5.3 indicates that a single hardening function, Equation (3.18), is not sufficient to represent the characteristic behavior of the material, such as softening during unloading.

Therefore, one more variable, the viscoplastic strain increment during loading, is introduced into Equation (3.18). Equation (3.19) represents the modified function, α, to incorporate the variation of the viscoplastic strain rate during the pulse time in the existing model. a_1 and a_2 in Equation (3.19) describe general variations of α in terms of viscoplastic strain and a local variation of α in terms of incremental viscoplastic strain in a pulse, respectively.

$$a = k_1 a_1 a_2 , \tag{3.19}$$

where

$a_1 = e^{-k_2 e_{vp}}$, and

$a_2 = \left(1 - e^{-k_2 \Delta e_{vp}}\right)$.

Figure 3.11 presents the variation of α determined by using a modified alpha-viscoplastic relationship for five 6.4-second pulses with 1800 kPa of load level. As shown, a is no longer a simple decreasing function of the viscoplastic strain but has multiple decreasing

functions in which independent variables constitute incremental viscoplastic strain during each loading pulse and overall viscoplastic strain. The incremental viscoplastic strain is reset to zero each time the material is unloaded.

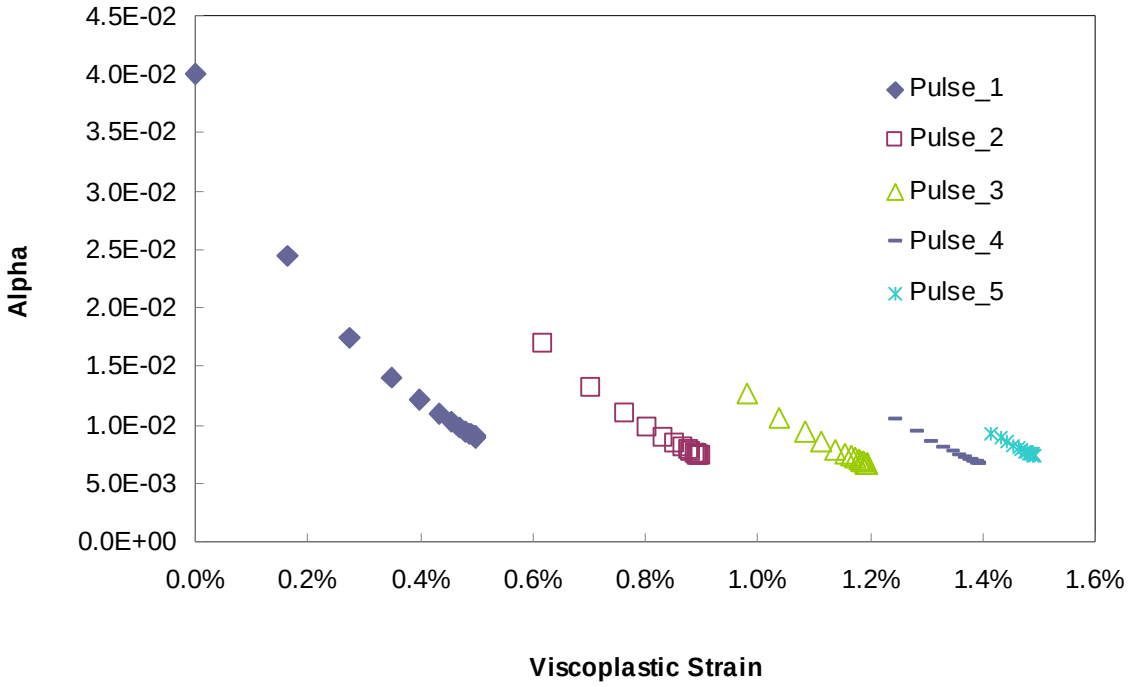

Figure 3.11 Variation of alpha for 1800 kPa CLT loading (500 kPa confinement).

Figure 3.12 presents measured and predicted viscoplastic strains by using a modified hardening function. The model is able to describe viscoplastic strain development for various loading conditions, such as for the VT, reversed variable time (RVT) test and CLT; this

capability is not possible in the existing HISS-Perzyna model.

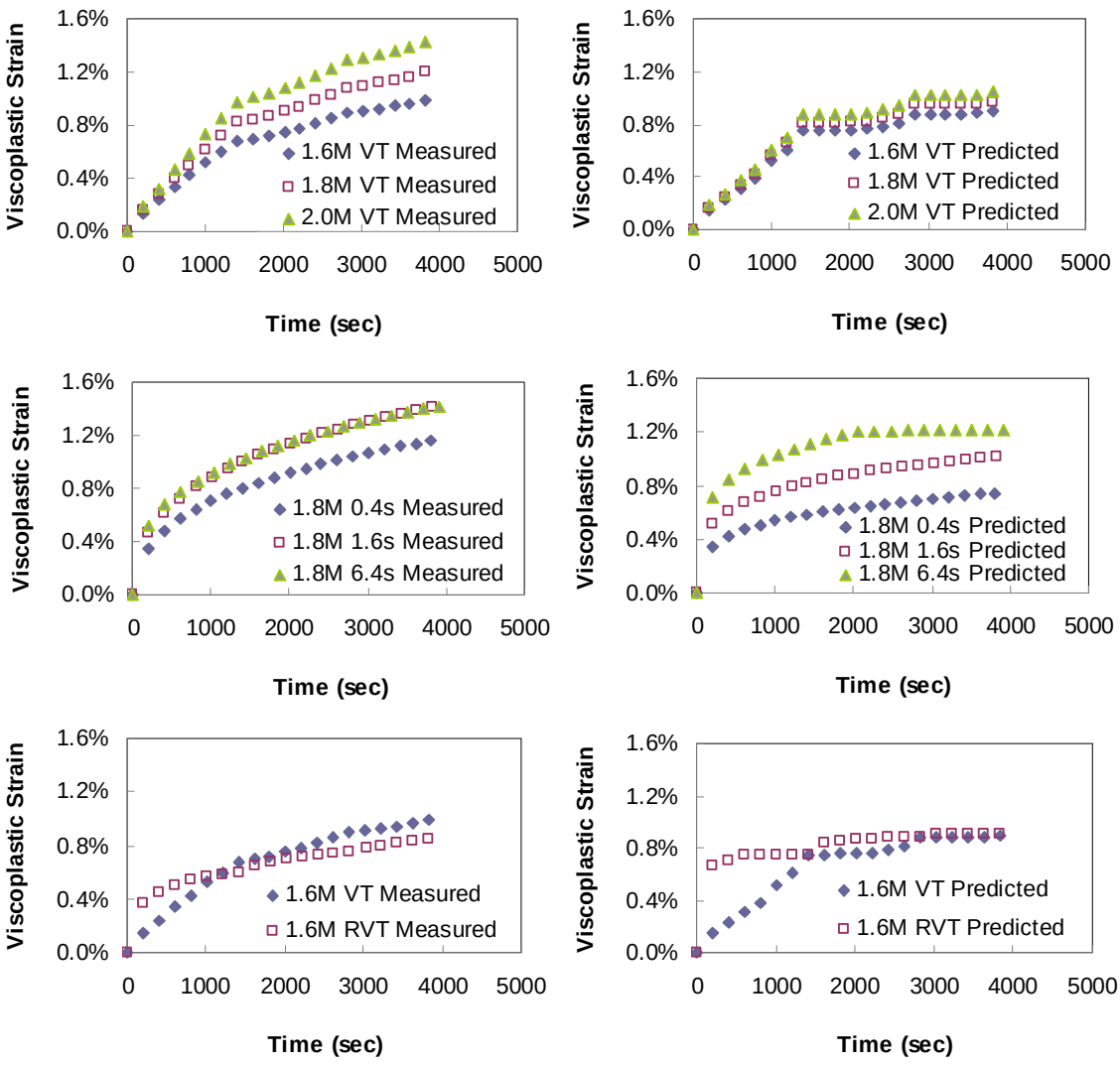

Figure 3.12 Viscoplastic strain predictions (500 kPa confinement).

However, even though incremental viscoplastic strain in a pulse describes multiple hardening

rates at certain viscoplastic strains, it is more reasonable to assume that the multiple hardening rates are caused by the viscoelastic property of the material, given the rate dependency of the softening behavior. Therefore, a viscoplastic model with a rate-dependent hardening-softening function has been developed and is presented in Chapter 6.

3.3. UNIFIED MODEL

In the theory of viscoplasticity, the term *unified constitutive model* refers to models that describe rate-dependent viscoplastic strain for steel or polymer. However, in other disciplines, the unified constitutive model is used to represent not only viscoplastic strain but also viscoelastic strain. Because this type of model takes a more flexible form of hardening equations than other viscoplastic models, it is worth reviewing the approaches used in the unified model.

3.3.1. Linear Kinematic Hardening Model

The simplest unified constitutive model is the linear kinematic hardening model suggested by Krieg (1977), as shown in Equations (3.20) and (3.21). The inelastic strain rate has a linear

relationship with the overstress, $s - a$. The back stress rate is a function of the back stress in the previous time step and the strain rate in the current time step. Because the model is designed to explain inelastic strain, which is the summation of viscoelastic strain, plastic strain, and viscoplastic strain, the inelastic strain rate can be negative depending on the stress history. Note that the back stress rate, $\dot{\alpha}$, is nothing but another representation of the Maxwell model of a mechanical analog.

$\dot{\varepsilon}^{in} = C(s - a)$, and (3.20)

$\dot{\alpha} = A\dot{\varepsilon}^{in} - Ba$, (3.21)

where

$\dot{\varepsilon}^{in}$ = inelastic strain,

A, B, and C = material constants, and

a = back stress.

3.3.2. Chaboche Model

In general, the viscoplastic strain of a material obeys a power law, and the hardening of the material can be represented by kinematic and isotropic hardening, as shown in Equation

(3.22).

$$\dot{\varepsilon}_{ij}^{vp} = \Phi(s, a, k)\frac{\partial F}{\partial s_{ij}} = \left\langle \frac{F(s-a)-k}{D} \right\rangle^{n} \frac{\partial F}{\partial s_{ij}}, \tag{3.22}$$

where

Φ = magnitude of strain rate,

a = kinematic hardening function (back stress function), and

k = isotropic hardening function.

Chaboche (1986) suggests a viscoplastic model consisting of the above flow rule and hardening function represented by a summation form of back stress. By using decomposed back stress, the model is capable of describing nonlinear hardening with enhanced accuracy for a wider range of viscoplastic strain. Equation (3.23) shows the back stress function in the Chaboche model; it becomes the Armstrong-Frederick model when $n = 1$.

$$a = \sum_{i=1}^{n} a_i(e_{vp}), \tag{3.23}$$

where $a_i(e_{vp})$ is the ith back stress, which is a function of the viscoplastic strain.

3.3.3. Krempl and Ho Models

As an advanced and recent form of the linear kinematic hardening model, Krempl (1978 and 2003) proposes a viscoplastic model based on the overstress concept. The constitutive model also includes a description of the time-dependent recoverable strain of the materials. It begins with the assumption that the coefficients of viscoelasticity are nonlinear functions. Equation (3.24) is the differential equation used to derive the model.

$$m\left(s-g\left(e\right)\right)\times\dot{e}+g\left(e\right)=s+k\left(s-g\left(e\right)\right)\times\dot{s}, \qquad (3.24)$$

where

$m\left(s-g\left(e\right)\right)$ = positive, bounded and even function,

$k\left(s-g\left(e\right)\right)$ = positive, bounded and even function,

$g\left(e\right)$ = odd function of strain, and

$s-g\left(e\right)$ = overstress.

When the functions $m\left(s-g\left(e\right)\right)$ and $k\left(s-g\left(e\right)\right)$ become constant, and $g\left(e\right)$ is linear in e, Equation (3.24) reduces to the differential equation of a standard linear solid model that represents viscoelastic behavior. The equation can then be expanded to the regular convolution integrals of linear viscoelasticity. Because Equation (3.25) holds true for slow

loading (Cernocky and Krempl 1978), the relationship between the strain rate and stress can be expressed as Equation (3.26), the simplest form of the viscoplastic model.

$$E = \frac{m\left(s - g\left(e\right)\right)}{k\left(s - g\left(e\right)\right)}, \tag{3.25}$$

where E is the material elastic modulus.

$$\dot{e} = \frac{\dot{s}}{E} + \frac{s - g\left(e\right)}{E \times k\left(s - g\left(e\right)\right)} \tag{3.26}$$

More complicated model forms are available to describe hardening, dynamic and static softening, relaxation, and negative and positive rate sensitivities. However, as shown in Equation (3.26), Krempl's constitutive models do not include either loading and unloading conditions or the concept of yield stress because they are derived from the general concept of viscoelasticity. Therefore, it is not appropriate to describe only the viscoplastic behavior of HMA, even though the model gives an idea of the rate dependency of viscoplastic properties under unloading conditions. Ho (2006) proposes a model capable of defining yield stress by introducing Macauley's bracket into the second term of Equation (3.26). Because the model is based on Equation (3.26), the back stress function is related to the kinematic stress function, as shown in Equation (3.28).

$$\dot{\varepsilon}^{in} = B\left\langle \frac{|s - H| - R}{D} \right\rangle^{m} \frac{(s - G)}{|s - G|}, \tag{3.27}$$

where

D = drag stress,

R = isotropic hardening function,

H = kinematic stress function ($\dot{H} = E\dot{\varepsilon}^{in}$),

G = back stress, and

$$\dot{G} = y\left[\dot{\varepsilon}^{in} - \frac{(G - H)}{R}\left|\dot{\varepsilon}^{in}\right|\right] + \dot{H}, \tag{3.28}$$

where, B , m , and y are material constants, which must be characterized from experimental results. In contrast to Krempl's model, this model does not allow a change in the material state during unloading, because the state of the material is a function only of the viscoplastic strain rate.

4. EXPERIMENTAL PROGRAM

4.1. MATERIALS

Component materials used in this study were obtained from the Federal Highway Administration (FHWA) Turner-Fairbanks Highway Research Center. Four stockpiles, #68, #78, #10 and sand (FHWA designation B-6265, B-6264, B-6306 and B-6263, respectively), were sampled and transported to North Carolina State University (NCSU) for fabrication. It should be noted that for the Accelerated Loading Facility (ALF) lanes, hydrated lime was first mixed with the #10 stockpile before mixing it with the asphalt binder. The decision was made not to use this stockpile for fabrication; instead, hydrated lime was added separately on a specimen by specimen basis at NCSU. In addition to acquiring aggregates, PG 70-22 (B-6298) was also acquired.

The aggregate structure for each of the mixtures was constant and was a coarse 12.5 mm nominal maximum size aggregate (NMSA) mixture comprised of 18.0% #68 stone, 36.4% #78 stone, 17.1% #10 stone, 27.5% sand and 1.0% lime. For the multiaxial tension work, a slightly modified mixture was used. This mixture contained the same binder and gradation as

the control mixture; however, the #78 aggregate for this mixture was obtained almost four years after the original aggregate was obtained. To reflect the later date of aggregate acquisition, this mixture is referred to as Control-2006. The blended gradation is shown in Figure 4.1. Four asphalt binders, three polymer-modified and one unmodified, of similar performance grade were used for this study. The asphalt content for each mixture was set at 5.3% by total mixture mass.

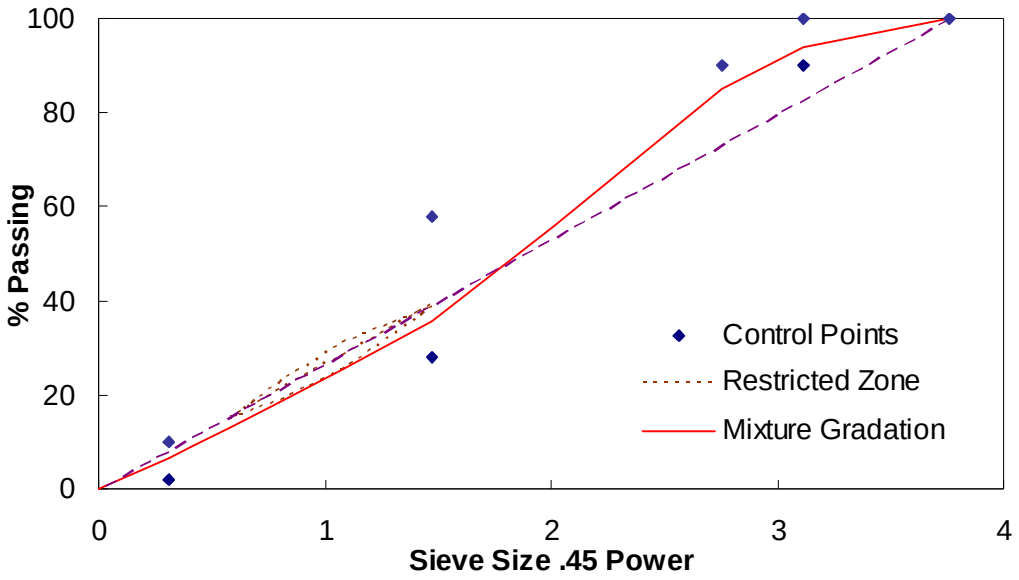

Figure 4.1 Mixture gradation chart.

4.2. SPECIMEN FABRICATION

All specimens were compacted by the Servopac Superpave gyratory compactor, produced by IPC Global of Australia, to a height of 178 mm and a diameter of 150 mm. To obtain specimens of uniform air void distribution, these samples were cored and cut to a height of 150 mm with a diameter of 100 mm for compression testing. Details can be found elsewhere (Daniel 2001, Chehab 2002). After obtaining specimens of the appropriate dimensions, air void measurements were taken via the CoreLok method, and specimens were stored until testing. It is noted that the air voids for all tests in this study are between 3.5% and 4.5%. During storage, specimens were sealed in bags and placed in an unlit cabinet to reduce aging effects. Furthermore, no test specimens were stored longer than two weeks before testing.

4.3. TEST SET-UP

An MTS closed-loop servo-hydraulic loading frame was used for all the tests. Depending on the nature of the test, either an 8.9 kN or a 25 kN load cell was used. An environmental chamber, equipped with liquid nitrogen coolant and a feedback system, was used to control and maintain the test temperature.

Measurements of axial and, in some instances, radial deformations were taken during loading. Axial measurements were taken at 90° intervals over the middle 100 mm of the specimen with loose-core linear variable differential transformers (LVDTs) from IPC Global. Radial deformations, when taken, were measured at 90° intervals with spring-loaded LVDTs from IPC Global. These measurements were taken on the central plane of the specimen. Load, crosshead movement, triaxial cell pressure (when appropriate) and deformation data for the specimen were acquired using National Instruments hardware and collected with LabView software.

For the uniaxial constant crosshead rate compression tests, a circular hole 3 mm deep and 14 mm in diameter was made at the center of the top surface of the specimen. The top plate had a key with the same dimensions in its center. The key and the hole were used to prevent the specimen from sliding during the test. For the creep and recovery test specimens, an aluminum end plate was used to minimize the creep due to the weight of the end plate. A 0.3048 mm thick rubber membrane of 100 mm diameter and lubricant were used to avoid the end effect caused by friction between the end plate and the surface of the specimen.

The preparation protocols for confined tests are similar to those of an unconfined set-up,

except that before testing the specimen is encased in a latex membrane. To ensure proper drainage during the compression tests, the bottom lubricated membrane was punctured with a hole approximately 25 mm in diameter. This ability to drain ensured that no excess pore pressure developed during testing. Following the protocol presented in NCHRP 465 (Witczak et al. 2000), the specimen was encased in a latex membrane after attaching LVDT mounting studs. Early observations indicated that extreme care must be taken when attaching LVDTs, and that failure to remove all air pockets between the membrane and specimen, particularly around the LVDT studs, results in unusual and inconsistent results. In this study, a hole in the membrane approximately 2.5 mm in diameter was punctured at the center of each LVDT mounting stud. This opening was then stretched around the LVDT studs, and all surrounding air pockets were removed. Studs were mounted and prepared similarly for radial measurements. Mounts were prepared for radial measurements instead of directly measuring the membrane-encased specimen, because during pressurization it was found that deformation of the membrane was significant. Finally, after all the LVDT mounting brackets were attached, acrylic latex caulk was used to seal the areas around the mounts.

4.4. TEST PROTOCOLS

Four tests were conducted in this study; the complex modulus test, constant crosshead rate monotonic test, repetitive creep and recovery test, and flow number test. The experimental protocols for these tests are explained in the following.

4.4.1. Complex Modulus Test

The complex modulus test was performed in stress-controlled mode in axial compression according to AASHTO TP62-03. The test was performed at frequencies of 25, 10, 5, 1, 0.5, 0.1, 0.05, and 0.01 Hz and temperatures of -10°, 10°, 35°, and 54°C. The confining pressures applied in the complex modulus tests were 0, 150, 250 and 500 kPa. The load level was adjusted for each condition to produce a total strain amplitude of about 50 to 70 microstrains. The tests were used to validate the t-TS principle for HMA.

4.4.2. Constant Crosshead Rate Test

The constant crosshead rate (monotonic) tests were conducted in uniaxial and triaxial compression mode until failure at different on-specimen LVDT strain rates (0.0000096 to

0.03 strains/sec) and temperatures (5°C and 55°C), as shown in Table 4.1.

Table 4.1 Controlled crosshead testing matrix under uniaxial and triaxial condition

Test ID	Confining Pressure (kPa)		Temp. (°C)	Crosshead Strain Rate	Reduced Strain Rate @ 25°C
	0	500			
5-1	v	v	5	5.75E-05	4.05E-02
5-2	v	v		3.83E-05	2.70E-02
5-3	v	v		1.92E-05	1.35E-02
5-4	v	v		9.60E-06	6.76E-03
25-1	v	v	25	1.35E-02	1.35E-02
25-2	v	v		4.50E-03	4.50E-03
25-3	v	v		1.50E-03	1.50E-03
25-4	v	v		5.00E-04	5.00E-04
40-1	v	v	40	3.01E-02	5.00E-04
40-2	v	v		1.00E-02	1.66E-04
40-3	v	v		3.00E-03	4.98E-05
40-4	v	v		1.00E-03	1.66E-05
55-1	v	v	55	2.99E-02	1.66E-05
55-2	v	v		1.00E-02	5.55E-06
55-3	v	.		3.00E-03	1.67E-06
55-4	v	.		1.00E-03	5.60E-07

To simplify the discussion of the monotonic test results, a test identification (ID) system (e.g., 55-1, 55-2, etc.) is used to describe the data for the remainder of this paper. The first number in the test ID is the test temperature, and the second number indicates the ranking of the strain rate, with 1 being the fastest and 4 being the slowest. The tests were used to determine the damage characteristic curve of the VECD model. Instead of testing several replicates at a limited set of rates and temperatures, tests were conducted at four different rates for each temperature with one replicate per rate.

4.4.3. Repetitive Creep and Recovery Tests

Repetitive creep and recovery tests were conducted in multiaxial compression at 40°C and 55°C. These tests consist of the repeated application of creep and recovery cycles. For characterization, two different conditions were applied: one with a fixed-stress level and increasing loading time without change of rest period as the loading cycle increases (i.e., a variable time or VT test with a constant rest period), and the other with the same load level and loading time conditions but with a change of rest period as the loading cycle increases (i.e., a variable loading time with variable rest period, or VTVR test). To gain insight into the

material behavior with respect to sequence of loading, a VT test was performed in the reverse order of the characterization i.e., a reverse VT, also known as an RVT test. For model verification, several different test conditions were used: VT testing with two different rest periods, 0.05 second and 1 second, a test with constant load and constant time (CLT) test, a variable load and variable time test (VLT), flow number test, and finally a VT test followed by a flow number test. A summary of the test methods and the confining pressures used with each is shown in Table 4.2. The following sections provide a description of each test method.

Table 4.2 Creep and recovery testing matrix for control mixture in compression

		Confining Pressure (kPa)	
		140	500
VT		v	v
RVT		v	v
VL		v	v
VLT		v	v
CLT	0.1s	v	.
	0.4s	v	v
	1.6s	v	v
	6.4s	v	v

Variable Time (VT) and Reversed Variable Time (RVT) Test

Repetitive creep and recovery tests with variable loading times were performed to achieve three major goals: identify the effect of loading time (i.e., rate-dependent hardening as a function of loading rate or time) on viscoplastic strain development; verify the t-TS principle, and characterize the viscoplastic model. For the VT tests, the level of deviatoric stress remained the same until the end of the test, but the duration of the loading was varied. The first loading block started with a 0.05-second loading pulse followed by 200 seconds of rest. Longer loading pulses with 200 seconds of rest were applied subsequently until the loading block ended. Figure 4.2 schematically represents the VT test with a rest period of 200 seconds at a deviatoric stress of 827 kPa and at confining pressure of 140 kPa as an example. This loading block was repeated depending on the deviatoric stress and confining pressure of the test. As shown in Table 4.3, at a confining pressure of 140 kPa, five different stress histories are given for the VT tests. Two of them were performed to verify the t-TS principle with damage. For this verification, VT testing with a deviatoric stress of 827 kPa was first performed at 55°C. (The 200-second rest period results are used here) Next, this time history is used with the t-TS shift factors to compute the equivalent reduced time history at 40°C.

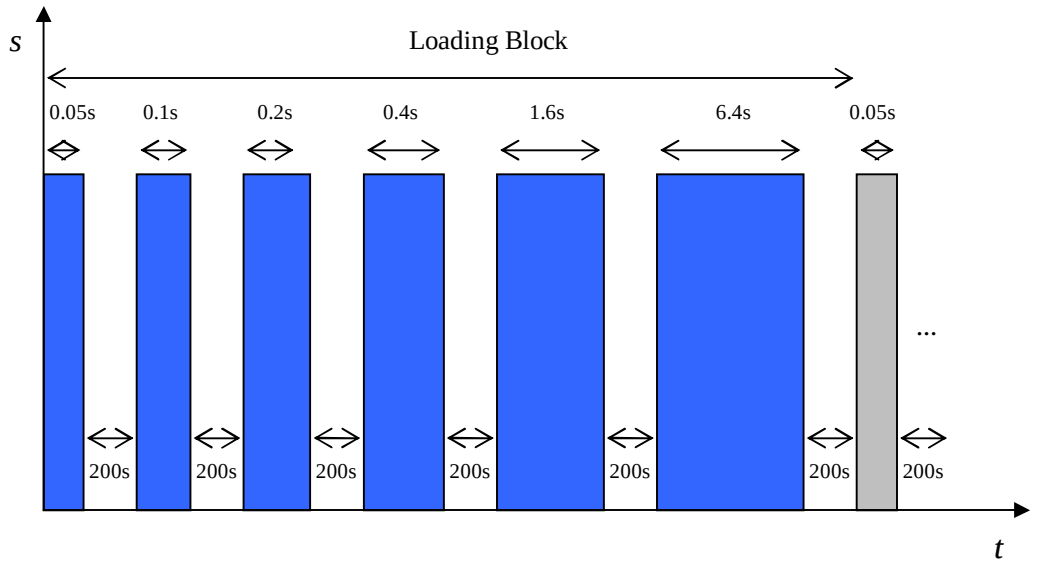

Figure 4.2 Stress history of VT testing (140 kPa confinement).

Table 4.3 Test conditions for the VT and RVT tests

Test ID	Confining Pressure (kPa)	Deviatoric Stress (kPa)	Pulse Time (sec) (rest period)						
140 kPa-827 kPa (55°C) VT 200s 140 kPa-552 kPa (55°C) VT 200s	140	827 552	0.05 (200)	0.1 (200)	0.2 (200)	0.4 (200)	1.6 (200)	6.4 (200)	.
140 kPa-827 kPa (40°C) VT		827	0.82 *(40)	1.63 *(40)	3.27 *(40)	6.53 *(40)	26.12 *(50)	104.49 *(60)	
140 kPa-827 kPa (55°C) VT 1.0s		827	0.05 (1)	0.1 (1)	0.2 (1)	0.4 (1)	1.6 (1)	6.4 (1)	.
140 kPa-827 kPa (55°C) VT 0.05s		827	0.05 (0.05)	0.1 (0.05)	0.2 (0.05)	0.4 (0.05)	1.6 (0.05)	6.4 (0.05)	.
500 kPa-1600 kPa (55°C) VT 500 kPa-1800 kPa (55°C) VT 500 kPa-2000 kPa (55°C) VT	500	1600 1800 2000	0.05 (200)	0.1 (200)	0.25 (200)	0.4 (200)	1.6 (200)	2.0 (200)	6.4 (200)

*Physical time at 40°C, which is equivalent in reduced time to physical time at 55°C.

However, because the testing time was estimated to take several days (the equivalent time of 200 seconds at 55°C is approximately 3265 seconds at 40°C), the following analysis was performed to finish the VT testing within a reasonable time. In this analysis, the measured strain history during the unloading portion of several loading pulses is used to compute the strain rate, which is plotted against the rest period time in Figure 4.3. To avoid issues related to the initial loading of a test, the 0.05-second data are taken from the second loading block, whereas the other pulse times are taken from the first loading block of the VT test. As shown in Figure 4.3, most of the strain rates become quite small after around 40 seconds, except for the rest periods following the 1.6- and 6.4-second loading pulses. For this reason, 40 seconds is used to compute the reduced time for pulse times less than 1.6 seconds (653 seconds at 40°C), 50 seconds is used for a pulse time of 1.6 seconds (816 seconds at 40°C), and 60 seconds is used for a pulse time of 6.4 seconds (980 seconds at 40°C).

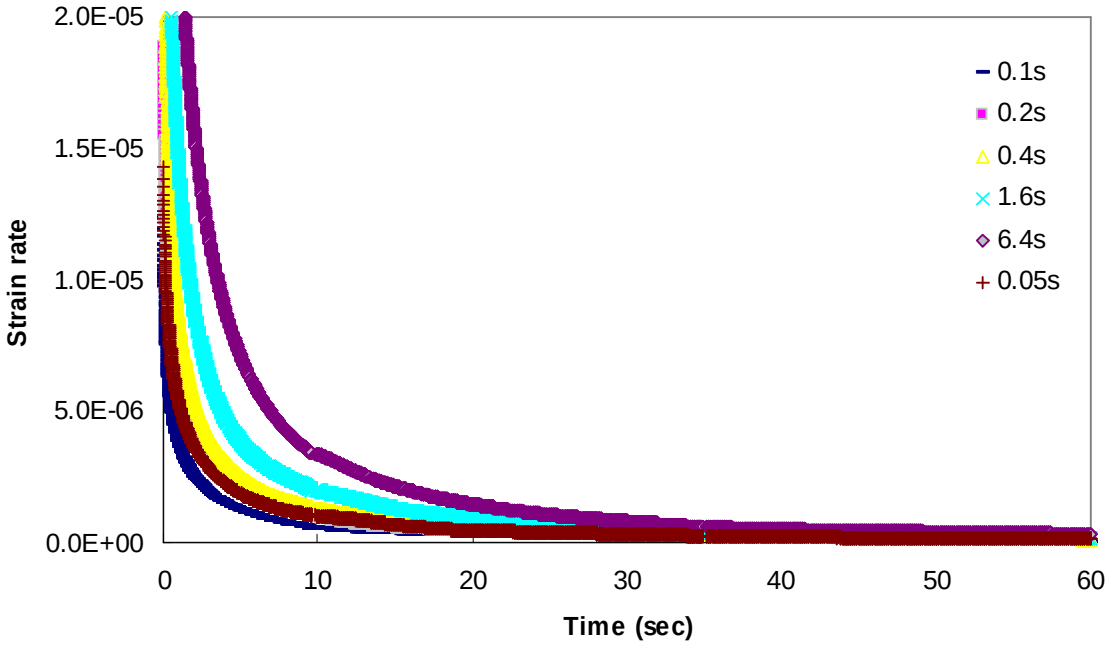

Figure 4.3 Variation of strain rate during unloading.

Note that strain rates reach an asymptotic value of zero more quickly as the strain level increases; thus, it is conservative to consider the times used in the first loading block as the reference times. The other VT tests were performed to evaluate the significance of the rest period on viscoplastic strain development, whereas the RVT test was performed to evaluate the significance of the loading sequence. In RVT testing, the loading conditions are the same as for VT testing with a rest period of 200 seconds at a deviatoric stress of 827 kPa; however, the sequence of loading is the opposite of that in the VT tests.

Variable Loading Time with Variable Rest Period (VTVR) Test

The repetitive creep and recovery with variable loading time and rest period (VTVR) test was performed to capture the rate-dependent softening behavior of the HMA. The loading conditions are the same as for VT testing, except for the rest period following each loading pulse, as shown in Table 4.4.

Table 4.4 Test conditions for the VTVR test

Test ID	Confining Pressure (kPa)	Deviatoric Stress (kPa)	Pulse Time (sec) (rest period)					
140 kPa-827 kPa (55°C) VTVR	140	827	0.05 (0.05) (0.1) (0.2) (0.4) (0.8)	0.1 (0.05) (0.1) (0.2) (0.4) (0.8)	0.2 (0.05) (0.1) (0.2) (0.4) (0.8)	0.4 (0.05) (0.1) (0.2) (0.4) (0.8)	1.6 (0.05) (0.1) (0.2) (0.4) (0.8)	6.4 (0.05) (0.1) (0.2) (0.4) (0.8)

For example, in the first loading group, each loading pulse was followed by a rest period of 0.05 second and, then, a rest period of 200 seconds was allowed at the end of the loading group to measure the viscoplastic strain developed by the loading group. The rest period for each pulse was set to 0.1 second in the second loading group. Similarly, in the fifth loading

group, the rest period was set to be 0.8 second and a rest period of 200 second was allowed at the end of the loading group. The five loading groups, including rest periods of 0.05, 0.1, 0.2, 0.4, and 0.8 second were repeated seven times to acquire enough viscoplastic strain to characterize the rate-dependent softening function of the developed viscoplastic constitutive model.

Variable Load (VL) Test

The repetitive creep and recovery with a variable load level (VL) test was performed to evaluate model performance for a loading pulse with variable load levels. In this VL test, the loading time remained constant until the end of the test, whereas the load level was varied. One loading block consists of eight increasing loading pulses. The deviatoric stress of the first load in the loading group was the same as that of the third load in the preceding loading group. For testing with a confining pressure of 140 kPa, the first deviatoric stress was 137.9 kPa and was stepped by $1.2^{(n-1)}$ as the number of loads, n, increased, as shown in Figure 4.4.

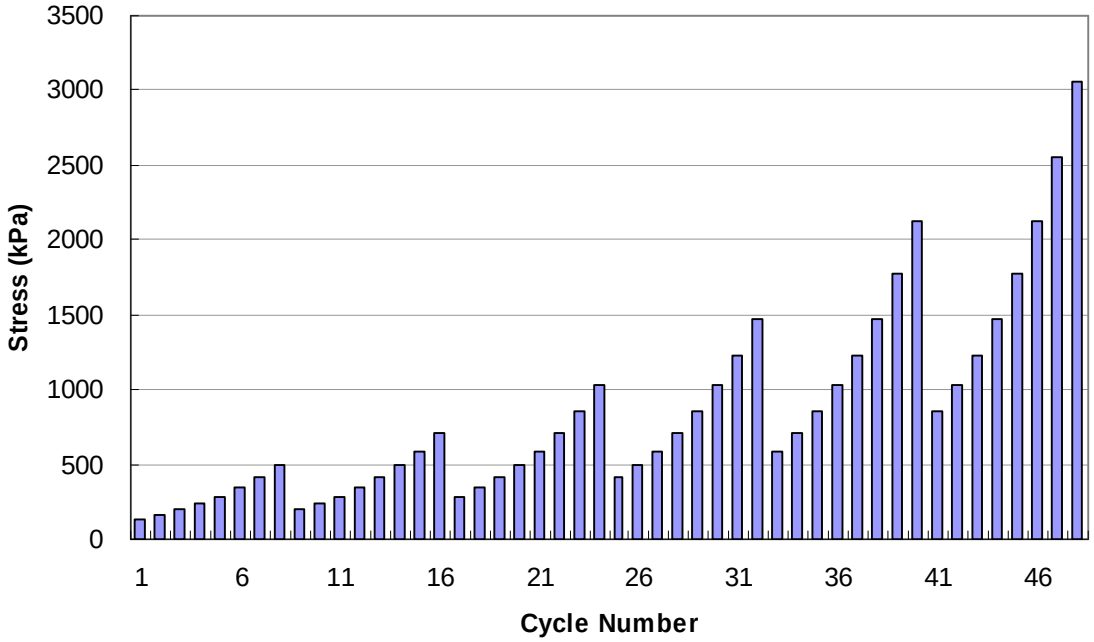

Figure 4.4 Stress history of VL testing (140 kPa confinement VL).

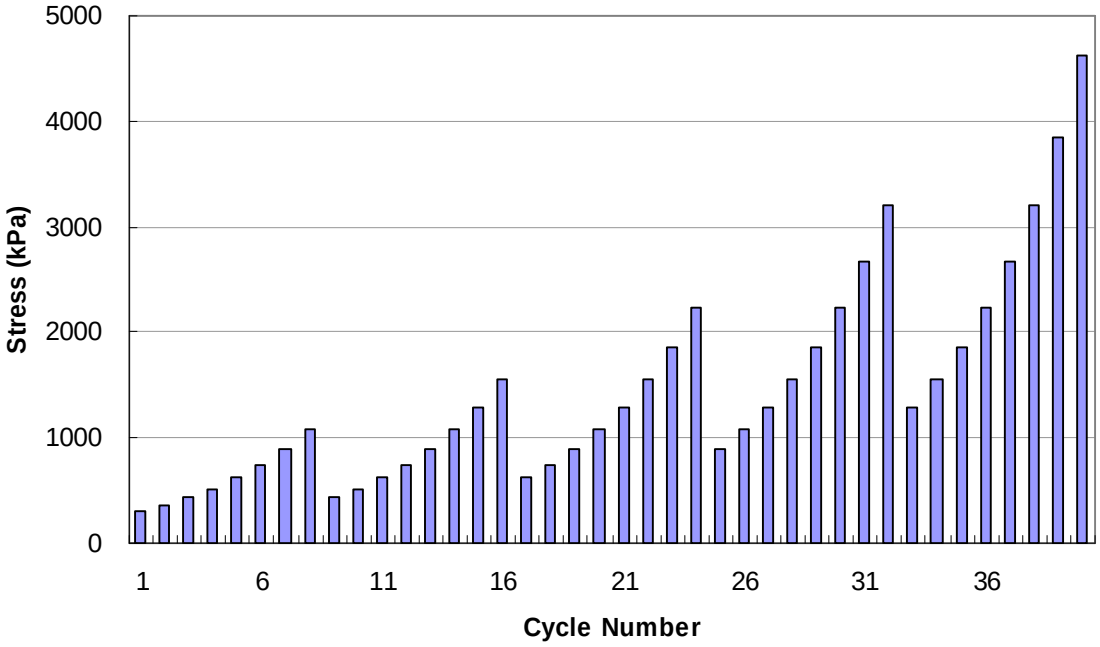

Figure 4.5 Stress history of VL testing (500 kPa confinement VL).

The confined testing began with a deviatoric stress of 300 kPa for the 500 kPa confining pressure test, as shown in Figure 4.5. For both cases, the loading time was set to 0.4 second, and the loading was repeated until the specimens failed.

Constant Load and Time (CLT) Test

CLT testing was conducted to confirm the effects of loading time on the viscoplastic strain development and to verify the developed model. During CLT testing, the loading time, rest period, pulse shape (i.e., square pulse), and load level were kept constant as shown in Table 4.5. The deviatoric stresses of 827 kPa and 1800 kPa were used for deviatoric stresses of 140 kPa and 500 kPa, respectively. Three different loading times of 0.4, 1.6, and 6.4 seconds were used with a rest period of 200 seconds for the 500 kPa confinement tests , whereas four different loading times of 0.1, 0.4, 1.6, and 6.4 seconds were used with a rest period of 0.9 second for 140kPa confinement tests. For the test conditions with 140 kPa confinement, the rest period of 200 seconds was applied to measure the viscoplastic strain when the cumulative loading times reached the specified target cumulative loading time, specified as shown in Table 4.6.

Table 4.5 Test conditions for the CLT tests

Test ID	Confining Pressure (kPa)	Deviatoric Stress (kPa)	Pulse Time (sec) (Rest Period)
140 kPa-827 kPa CLT (55°C) 0.1s-0.9s	140	827	0.1 (0.9)
140 kPa-827 kPa CLT (55°C) 0.4s-0.9s			0.4 (0.9)
140 kPa-827 kPa CLT (55°C) 1.6s-0.9s			1.6 (0.9)
140 kPa-827 kPa CLT (55°C) 6.4s-0.9s			6.4 (0.9)
500 kPa-1800 kPa CLT (55°C) 0.4s-200s	500	1800	0.4 (200)
500 kPa-1800 kPa CLT (55°C) 1.6s-200s			1.6 (200)
500 kPa-1800 kPa CLT (55°C) 6.4s-200s			6.4 (200)

Table 4.6 Target cumulative loading times to measure viscoplastic strain in the CLT and flow number tests.

Pulse Time (sec)	Target Cumulative Loading Time (sec)											
0.1	4	8	16	32	64	96	128	160	224	288	352	416
0.4	4	8	16	32	64	96	128	160	224	288	352	416
1.6	.	8	16	32	64	96	128	160	224	288	352	416
6.4	.	.	.	32	64	96	128	160	224	288	352	416

Variable Load and Time (VLT) Test

VLT testing incorporates the loading history of the VT testing with that of the VL testing. The test began with a deviatoric stress of 100 kPa and a loading time of 0.05 second, as shown in Figure 4.6, Figure 4.7, and

Table 4.7. After 200 seconds of rest period following the first loading pulse, another loading pulse using the same deviatoric stress but with and increased loading time, similar to the VT testing, was also followed by 200 second of rest. Once VT testing with this deviatoric stress was completed (i.e., a loading block), the deviatoric stress was increased to the next stress level, as shown in Figure 4.6 and Figure 4.7 for a confining pressure of 140 kPa and 500 kPa, respectively. This sequence was repeated until the specimen failed.

Table 4.7 Loading times in a loading group for VLT test

Confining Pressure (kPa)	Pulse Time (sec)					
140	0.05	0.1	0.2	0.4	1.6	6.4
500	0.05	0.1	0.25	0.4	1.6	6.4

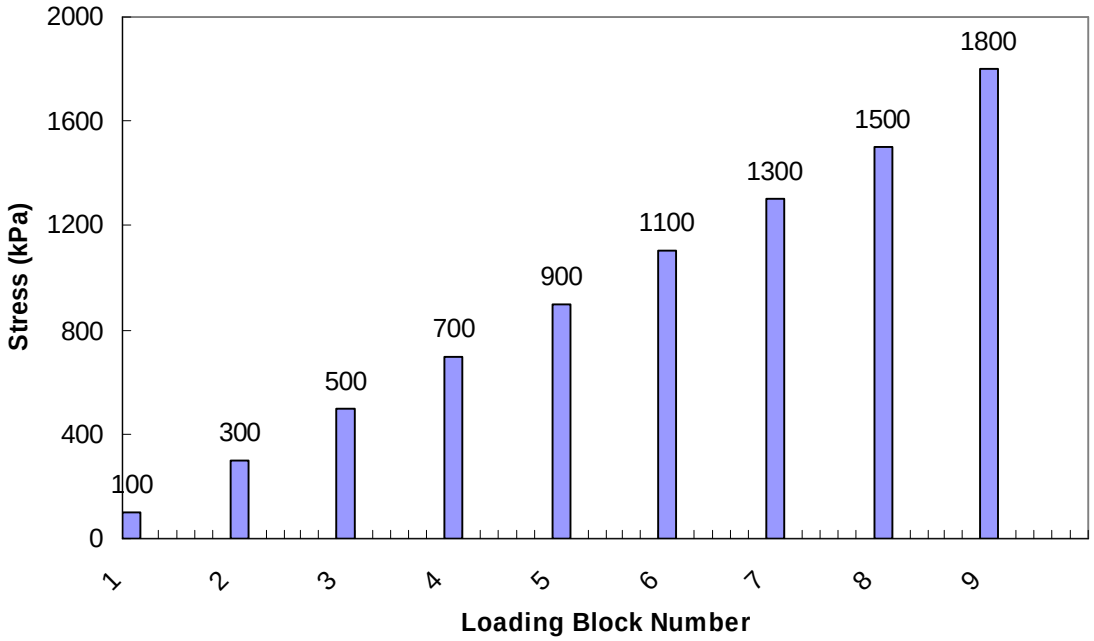

Figure 4.6 Stress history of VLT testing (140 kPa confinement).

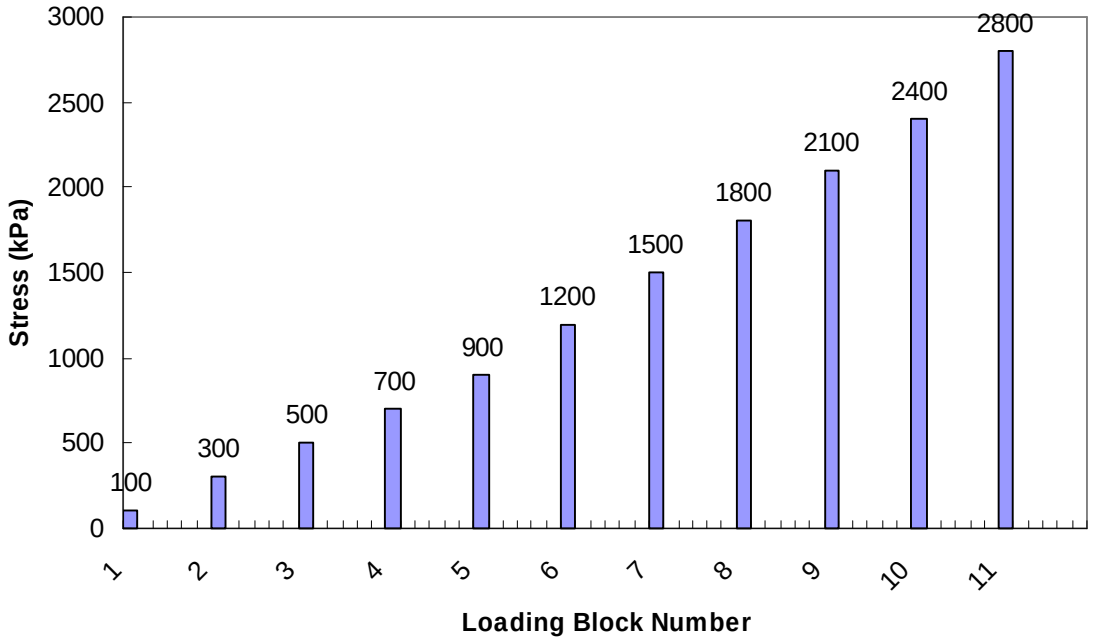

Figure 4.7 Stress history of VLT testing (500 kPa confinement).

4.4.4. Flow Number Tests

Because of its simplicity, the flow number test is considered to be a simple performance test of the permanent deformation of HMA mixtures. As shown in Table 4.8, the pulse time, rest period, loading shape (i.e., haversine pulse), and load level are kept constant until the end of testing. In this study, four different pulse times (i.e., 0.1, 0.4, 1.6, and 6.4 seconds) were selected for the verification and the viscoplastic strains at the target cumulative loading times were determined by lengthening the rest period to 200 seconds as well as by CLT testing. The target cumulative loading times used to measure viscoplastic strain are also the same as those used in CLT testing, as shown in Table 4.5.

Table 4.8 Test conditions for the flow number tests

Test ID	Confining Pressure (kPa)	Deviatoric Stress (kPa)	Pulse Time (sec) (Rest Period)
140 kPa-827 kPa Flow (55°C) 0.1s-0.9s	140	827	0.1 (0.9)
140 kPa-827 kPa Flow (55°C) 0.4s-0.9s			0.4 (0.9)
140 kPa-827 kPa Flow (55°C) 1.6s-0.9s			1.6 (0.9)
140 kPa-827 kPa Flow (55°C) 6.4s-0.9s			6.4 (0.9)

4.4.5. Combination of the VT and Flow Number Tests

The combination of the VT and flow number tests was considered to evaluate the performance of the developed model under more complicated loading conditions. In this testing, the loading time, pulse shape, rest period, and load level were varied. As shown in Figure 4.8, the loading condition for the VT test with a rest period of 200 seconds was used for the first two loading block; then, a flow number test followed by a VT test were repeated.

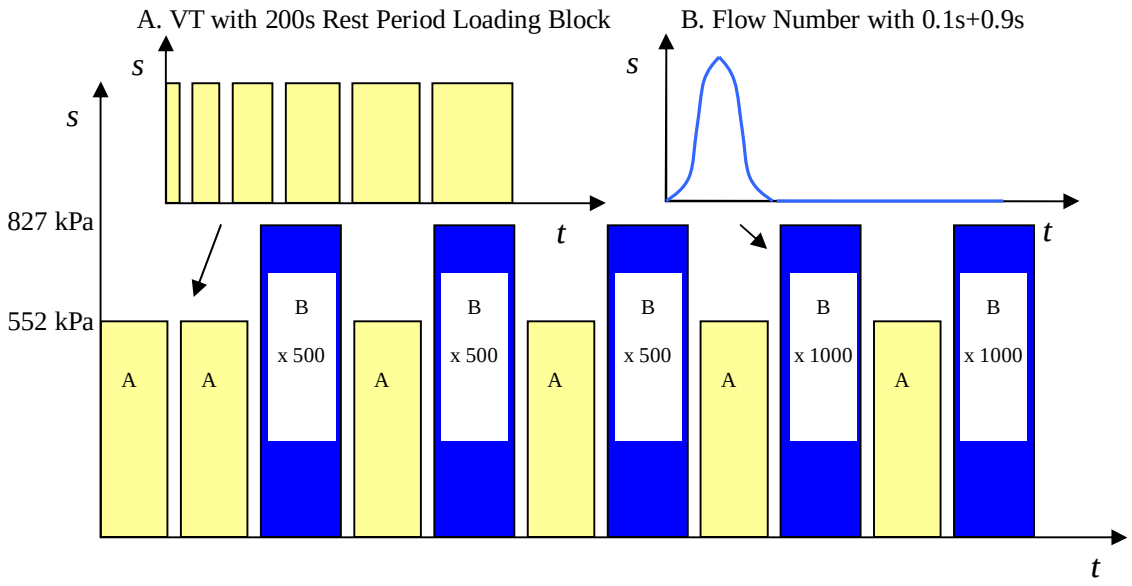

Figure 4.8 Schematic representation for stress history of combination of VT and flow number test (140 kPa confinement)

The VT loading block consisted of 6 loading pulses, 0.05, 0.1, 0.2, 0.4, 1.6, and 6.4 seconds,

each followed by rest periods of 200 seconds, and the flow number loading block consisted of a haversine loading pulse of 0.1 second and a rest period of 0.9 second. As shown in Figure 4.8, the loading pulse and rest period for the flow number test were repeated 500 times for the first three flow number loading blocks and 1000 times for the remaining blocks. At the end of each flow number loading block, 200 seconds of rest were allowed to measure the viscoplastic strains. The deviatoric stresses for the VT test and flow number test were 552 kPa and 827 kPa, respectively.

5. THE CHARACTERISTIC BEHAVIORS OF HMA IN COMPRESSION

5.1. TIME-TEMPERATURE SUPERPOSITION PRINCIPLE

The principle of t-TS is one of the fundamental and most important concepts for HMA modeling, because it provides a strong mechanical background and significantly reduces the experimental efforts. In the following sections, tests performed to verify the t-Ts principle of HMA in compression are represented and discussed.

5.1.1. Time-Temperature Superposition within the Linear Viscoelastic Range

The dynamic modulus mastercurve is constructed by shifting the dynamic modulus curves at multiple temperatures along the log frequency axis, as shown in Figure 2.3. Figure 5.1(a) and (b) represent the dynamic modulus test results for the four confining pressures (0, 140, 250, and 500 kPa), and Figure 5.2(a) and (b) represent phase angle mastercurves and shift factors, respectively.

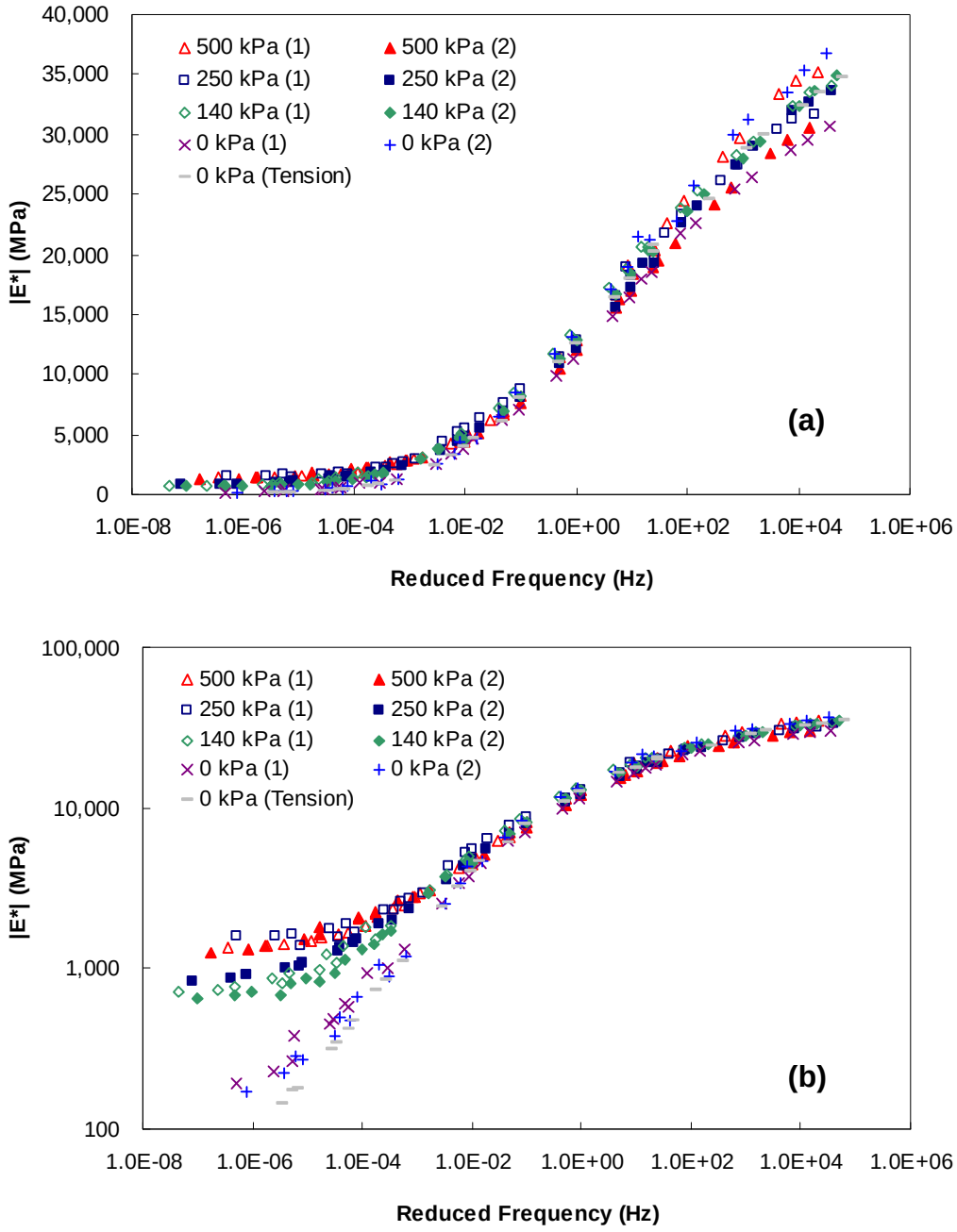

Figure 5.1 Dynamic modulus mastercurve for four different confining pressures in (a) semi-log space, (b) log-log space.

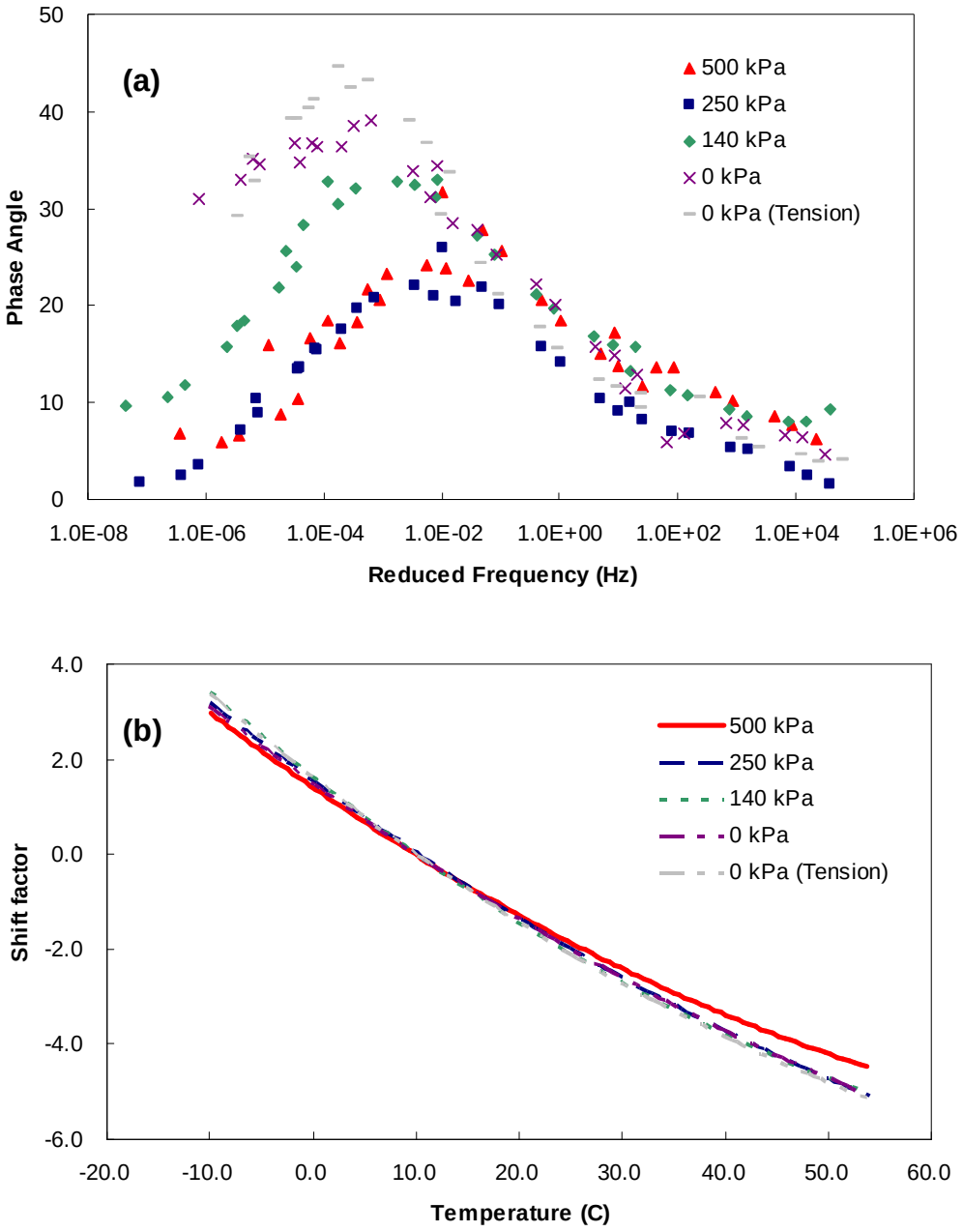

Figure 5.2 (a) phase angle mastercurves and (b) shift functions for four different confining pressures

Overall, it is clearly observed that t-TS principle is valid for this mixture regardless of stress conditions, but the dynamic modulus is dependent on confining pressure at low reduced frequencies. Furthermore, it is seen from Figure 5.1 that the slope of the confined mastercurve is not as steep as the slope of the unconfined mastercurve, thus suggesting reduced rate dependence in the material under confined stress. In addition, by examining the phase angle mastercurves in Figure 5.2(a), it is seen that at lower reduced frequencies the material behaves more elastically under confining pressure than it does in the uniaxial state. It is also observed that this effect is not very dependent on the confining stress level. The net effect of the increased dynamic modulus is an increase in the relaxation modulus, which is shown for the different confining pressures in Figure 5.3. From Figure 5.3, it is observed that the relaxation modulus begins to diverge at around 0.01 ~ 1 second in reduced time. These times generally correspond to a physical time of between $1E^{-5}$ and $2E^{-7}$ seconds at 54°C, and $1E^{-4}$ and $1E^{-7}$ seconds at 40°C. Therefore, it is important to consider the effect of confining pressure in describing the compressive behavior of HMA, because the time at which the relaxation modulus starts to diverge is within the range of reduced time that is to be used in the rutting analysis.

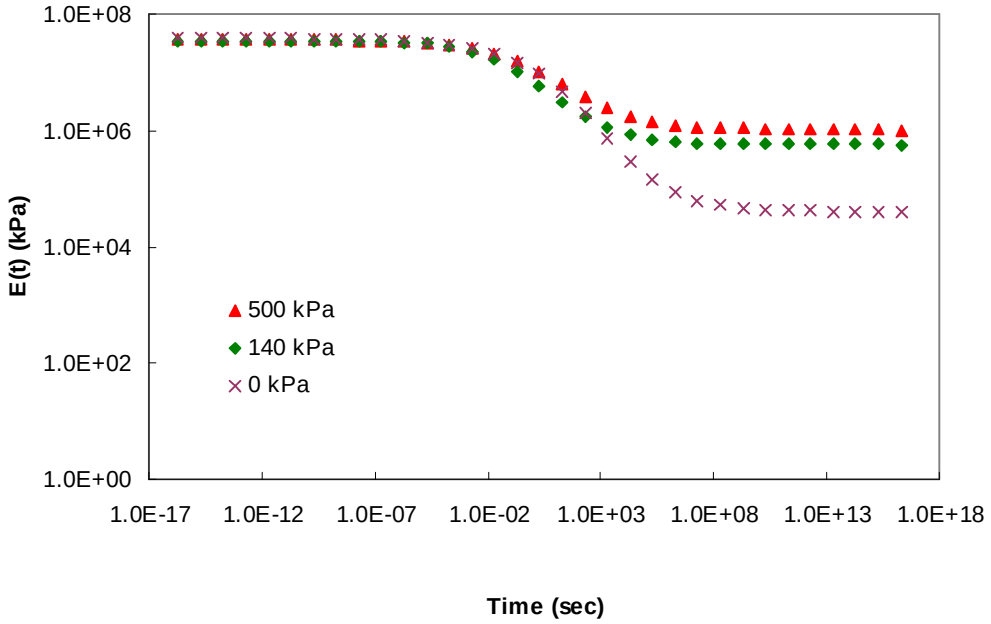

Figure 5.3 Effect of confining pressures on relaxation modulus

These observations are consistent with those made by other researchers (Pellinen 2001, Kim and Chehab 2004) for asphalt concrete and are also the same as those found from unbound paving materials (i.e., higher stiffness increases the confining pressure). The behavior, therefore, appears to be related to the ability of the asphalt cement to resist dilation of the aggregate skeleton. However, it should be kept in mind that the deformation that is applied in these tests is generally small, on the order of 60 με, which is not enough to introduce significant aggregate reorientation. Nevertheless, it seems reasonable to assume that the mechanisms responsible for the increased stiffness under confining pressure are at least

similar to those of unbound materials. This hypothesis may also suggest that the effect of confining pressure can be considered without the need to significantly reconsider the linear viscoelastic properties of the material.

5.1.2. Time-Temperature Superposition with Growing Damage and Viscoplastic Strain

In order to verify the t-TS principle for the compression stress state with damage and viscoplastic strain, stress characteristic curves were constructed from constant strain rate test results by utilizing shift factors determined from the dynamic modulus tests. Further verification was also performed using repetitive creep and recovery tests.

First of all, for the verification of the t-TS principle for monotonic loading, a wide range of eight reference strain values was chosen according to the results of both the uniaxial and triaxial compressive constant strain rate tests, as shown in Figure 5.4. According to the procedure discussed in detail elsewhere (Chehab 2002, Kim et al. 2005), stress and time values were determined for all of these tests at fixed strain levels. These plots of stress versus time are shown in Figure 5.5 and Figure 5.6. Then, shift factors obtained from small-strain linear viscoelastic testing were applied to determine the reduced time that corresponds to

each physical time.

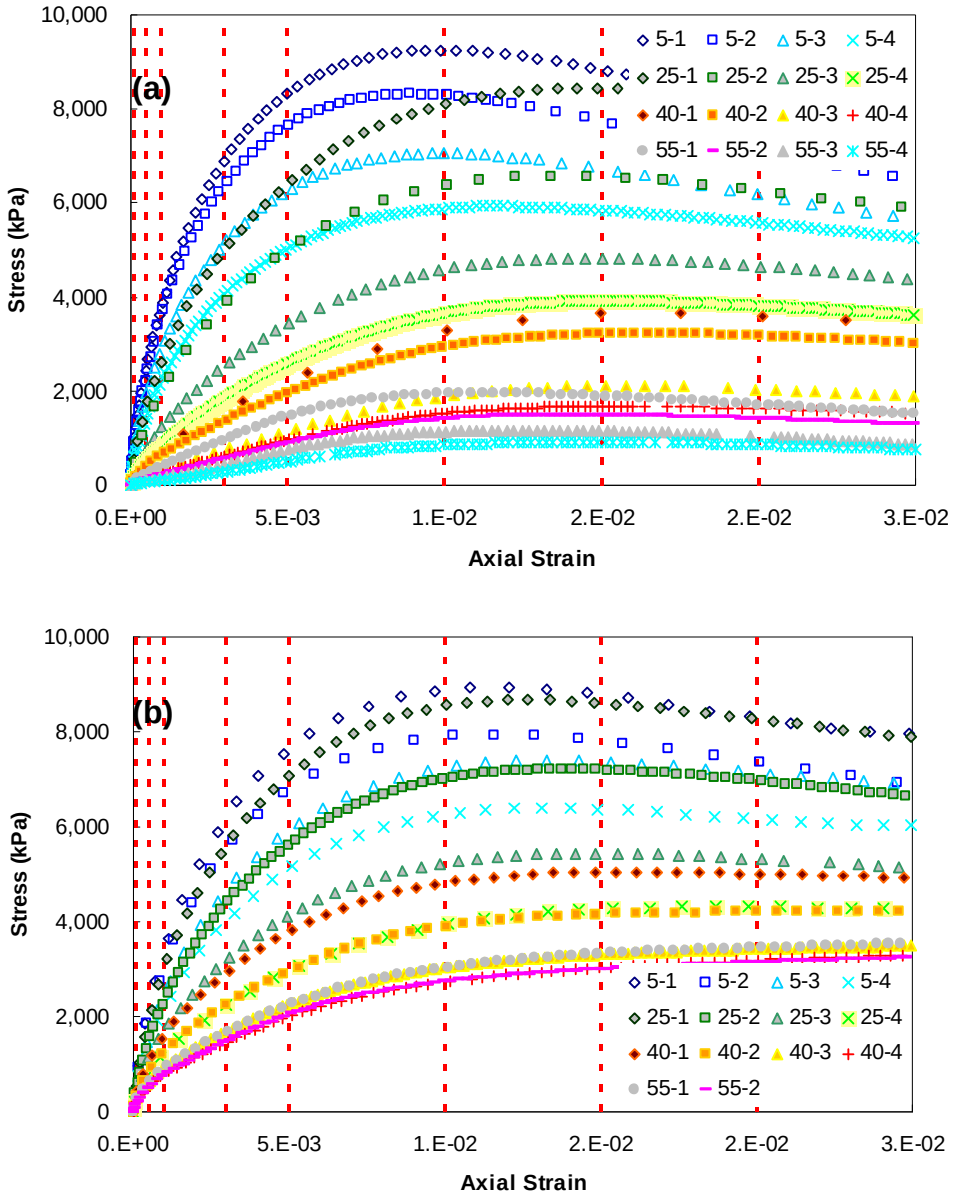

Figure 5.4 Strain levels examined for verifying the time-temperature superposition principle under growing damage and confining pressure of: (a) 0 kPa and (b) 500 kPa.

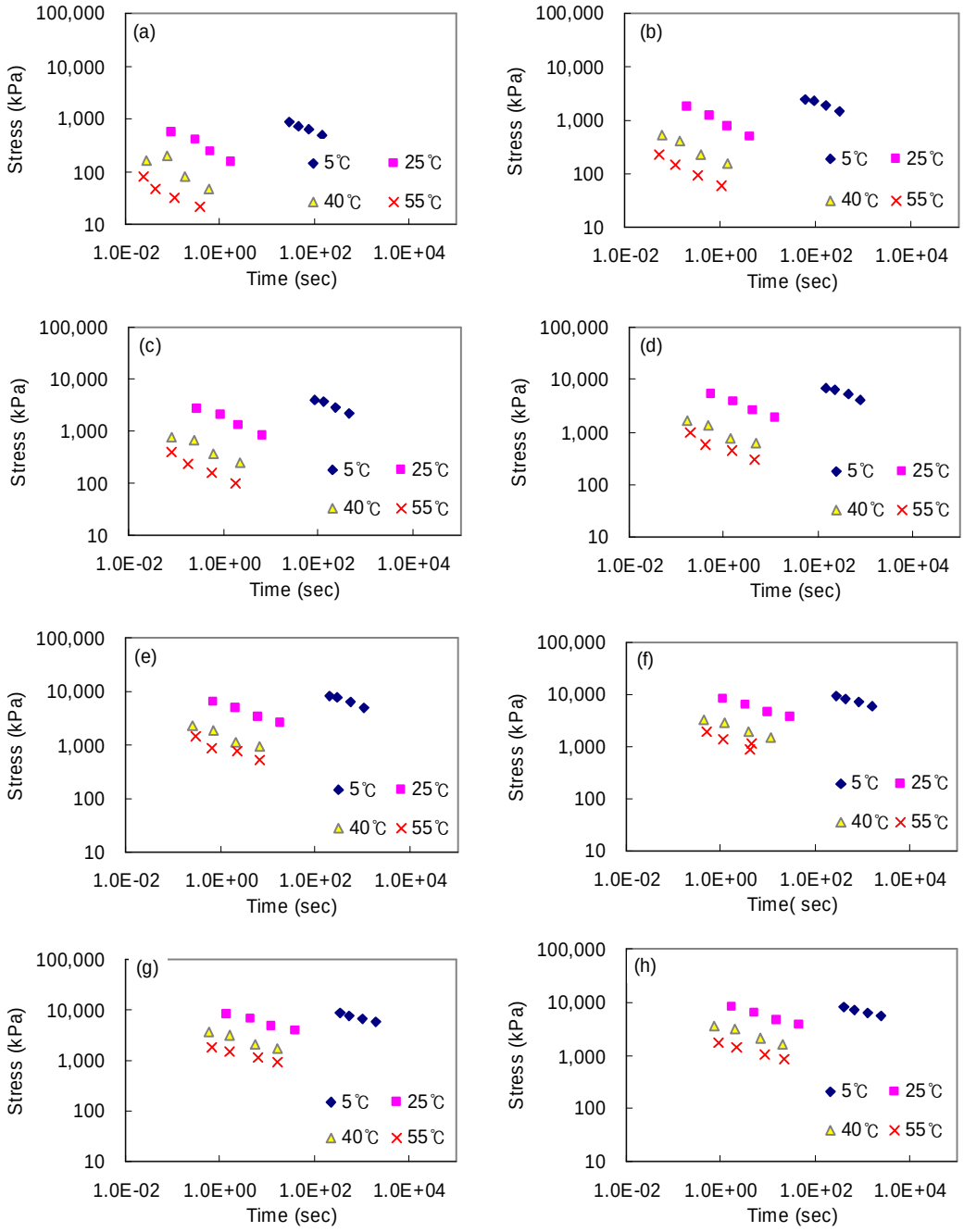

Figure 5.5 Stress-time curves for the control mixture before the application of time-temperature shift Factors at: (a) 0.0001, (b) 0.0005, (c) 0.001, (d) 0.003, (e) 0.005, (f) 0.01, (g) 0.015, and (h) 0.02 strain levels under uniaxial conditions.

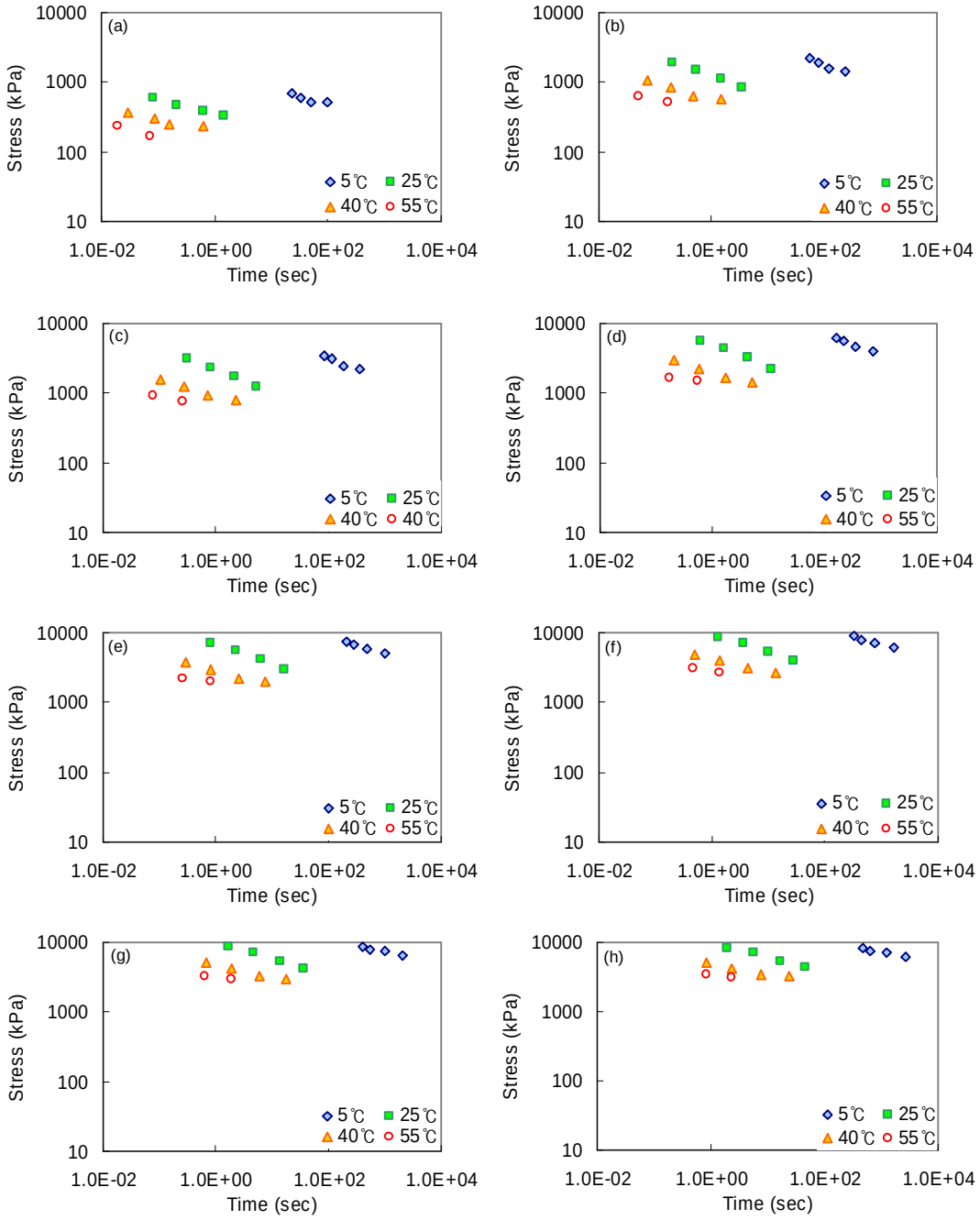

Figure 5.6 Stress-time curves for the control mixture before the application of time-temperature shift factors at: (a) 0.0001, (b) 0.0005, (c) 0.001, (d) 0.003, (e) 0.005, (f) 0.01, (g) 0.015, and (h) 0.02 strain levels under 500 kPa conditions.

If the t-TS principle is valid with growing damage, the resulting plots of stress and reduced time should appear continuous at all strain levels. This behavior is indeed observed for the compression tests under both the confined and unconfined conditions, as shown in Figure 5.7(a) and (b).

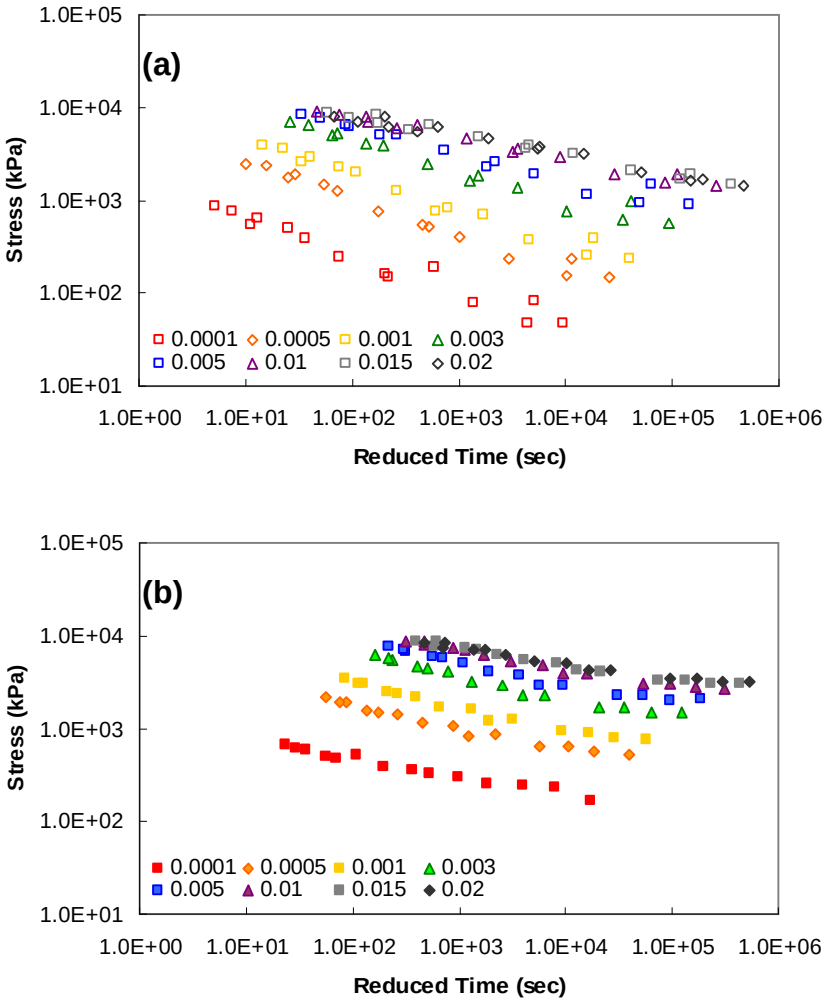

Figure 5.7 Stress mastercurves under: (a) uniaxial conditions and (b) triaxial conditions.

These results verify that the t-TS concept holds true for mixtures subjected to compressive loading as well as to tensile loading, even if there is severe damage and viscoplastic strain. However, to verify that the principle holds for the physical mechanisms behind the behavior of repetitive creep and recovery tests, more rigorous verification is needed. This verification compares VT test results at 40° and 55°C with the same reduced time histories. The results of these two tests are shown in Figure 5.8.

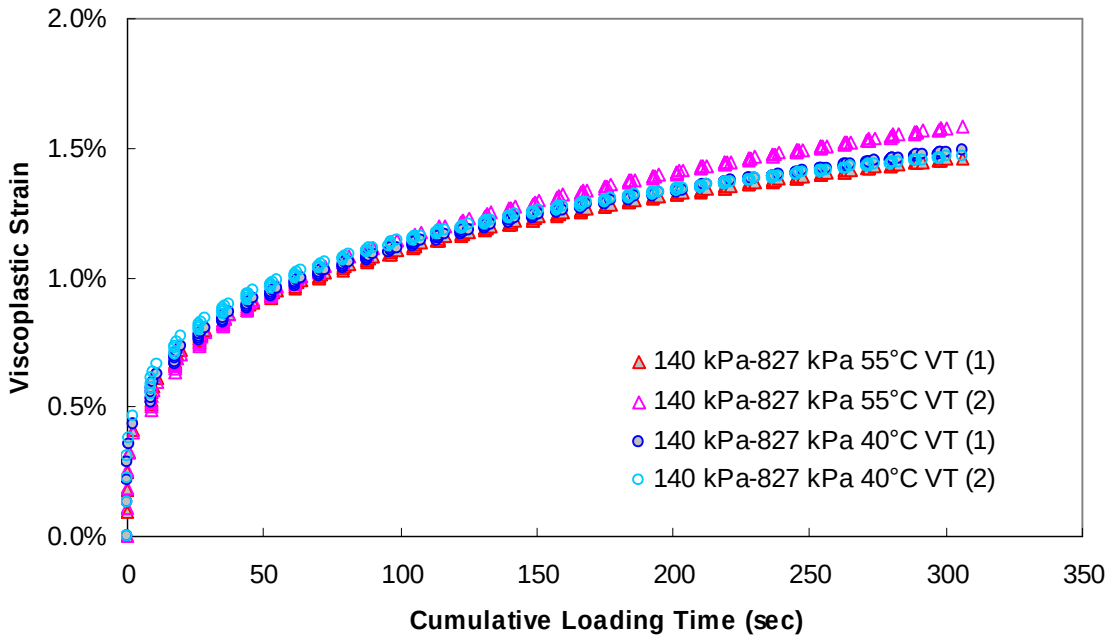

Figure 5.8 Viscoplastic strain vs. cumulative loading time (140 kPa confinement VT at 40° and 55°C).

As shown in Figure 5.8, viscoplastic strains measured at the end of rest periods are quite well matched to each other. This agreement confirms that the t-TS principle is applicable regardless of loading sequence and the amount of damage and viscoplastic strain in asphalt concrete.

5.2. STRAIN HARDENING IN THE VISCOELASTIC MEDIA

Although identifying the state of the viscoelastic media in HMA is critically important to model the viscoelastic behavior of the material with damage, there are no known test protocols to capture only viscoelastic behavior with damage at high temperatures because HMA exhibits complicated viscoelastic and viscoplastic behavior during the loading condition. Therefore, the viscoelastic continuum damage (VECD) modeling technique – which is known to be able to predict the viscoelastic stress-strain behavior of asphalt concrete under various loading histories with varying rates of loading, stress/strain amplitudes, and temperatures in tension – is applied to identify the viscoelastic behavior of HMA in compression. The VECD modeling procedure and strain hardening observed as a result of this process are described in the following Section 5.2.1 using a possible physical mechanism.

5.2.1. VECD Model Characterization

Once the linear viscoelastic characterization is completed, a relaxation modulus can be determined using the viscoelastic interrelationships between the dynamic modulus and the unit response functions. Then, the constitutive relationship of the linear viscoelastic media in the uniaxial state of stress is in the form of the following convolution integral (Kim and Chehab 2004, Ha and Schapery 1998, and Park and Schapery 1998):

$$s = \int_0^x E(x - t)\frac{de}{dt}dt \ , \qquad (5.1)$$

where

s = uniaxial stress,

e = uniaxial strain,

$x = t/a_T$ = reduced time,

t = physical time,

a_T = time-temperature shift factor,

$E(t)$ = relaxation modulus, and

t = integration variable.

The pseudo strain is defined for a uniaxial state of stress as

$$e^R = \frac{1}{E_R}\int_0^x E(x-t)\frac{de}{dt}dt \ , \tag{5.2}$$

where

e^R = pseudo strain, and

E_R = reference modulus, which is an arbitrary constant.

Applying the definition of pseudo strain in Equation (5.2) to Equation (3.8) results in the following:

$$s = E_R e^R. \tag{5.3}$$

The linear viscoelastic relationship represented by the pseudo strain in Equation (5.3) is modified as follows when the microcracking damage grows:

$$s = C(S)e^R, \tag{5.4}$$

where

$C = \frac{s}{e^R \times I}$ = secant pseudo stiffness,

I = initial secant pseudo stiffness, and

S = damage parameter.

Converting Equation (5.4) to predict the viscoelastic strain yields

$$e_{ve} = E_R \int_0^x D(x-t) \frac{d\left(\frac{s}{C(S)}\right)}{dt} dt \ , \qquad (5.5)$$

where,

$D(t)$ = creep compliance.

Equation (5.5) requires the determination of an internal state variable, *S*, to quantify damage. This internal state variable quantifies any microstructural changes that result in observed stiffness reduction. In tension modeling, this parameter is attributed to horizontal microcracking, whereas in this research for compression modeling it represents the weakening of the material's ability to withstand the applied load due to vertical microcracking. A detailed description of the *S* calculation method is described in relevant other references (Kim and Chehab 2004).

Equation (5.5) is the VECD model. The crux of the VECD model is that a unique damage characteristic relationship exists between C and S, regardless of loading type (monotonic versus cyclic), loading rate, and stress/strain amplitude (Daniel and Kim 2002). In addition, the application of the t-TS principle with growing damage to the C versus S relationship

at varying temperatures yields the same damage characteristic curve in the reduced time scale. The only condition that must be met in order to produce the damage characteristic relationship is that the test temperature and loading rate combination must be such that only the elastic and viscoelastic behaviors prevail with negligible, if any, viscoplasticity. When the test temperature is too high or the loading rate is too slow, it is found that the C versus S curve deviates from the characteristic curve. To ensure that the test temperature is low enough and the loading rate is fast enough not to induce any significant viscoplastic strain, the tests are performed at a low temperature (typically 5°C) with varying loading rates. If the C versus S curves at different rates overlap to form a unique relationship, the combination of the temperature and loading rate is sufficient to develop the damage characteristic relationship.

Data from the monotonic constant crosshead rate tests at 5°C are used for the viscoelastic damage characterization. Pseudo strains are calculated using Equation (5.2) and plotted against the stress in Figure 5.9. It can be seen from Figure 5.1(a) that the stress versus pseudo strain curves follow the line of equality (LOE) during the early part of loading when the damage is minor. This phenomenon occurs because the E_R value of one that is used in this

research makes the pseudo strain equal to the linear viscoelastic stress. As the stress and strain increase, the stress versus pseudo strain curves begin to deviate from the LOE, indicating the damage growth.

The stresses and pseudo strains are used to calculate the C and S values. It can be seen in Figure 5.9(b) that the C versus S curves overlap nicely for different loading rates, indicating that the viscoplastic strain under these testing conditions is minimal. Also in Figure 5.9(b), the damage characteristic curve from tension is plotted. It is found that the damage characteristic curve from compression is positioned higher than that from tension. In tension, the primary damage at 5°C is the microcracking in the perpendicular direction to the loading direction, whereas the primary damage in compression is the vertical cracking along the loading direction. Because the vertical cracking in compression is due to the horizontal tensile stress induced by the vertical compression loading, for the same amount of microcracking (i.e., the same value of S), the resistance of the material to cracking (i.e., C) is greater in compression than in tension. The C values at the peak stress obtained from the different rate tests are found to be between 0.3 and 0.35.

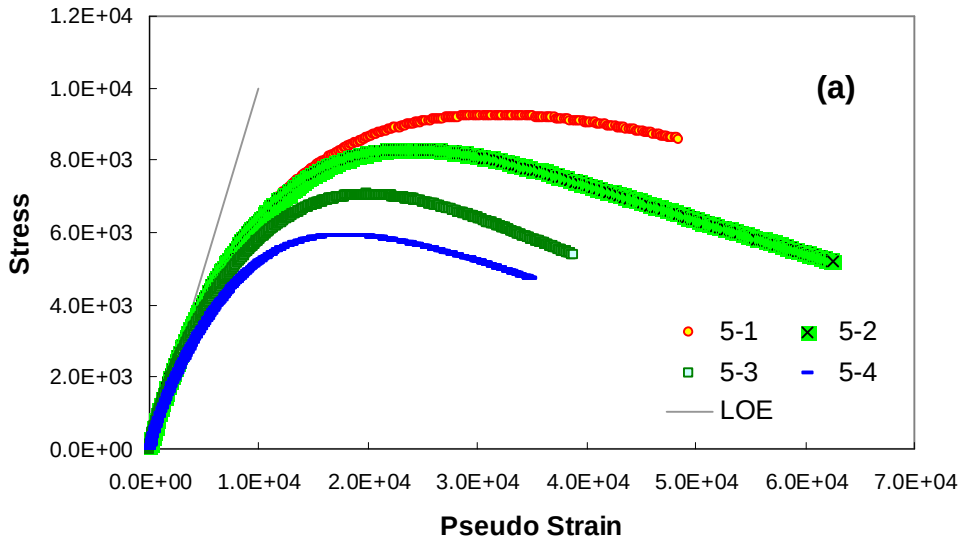

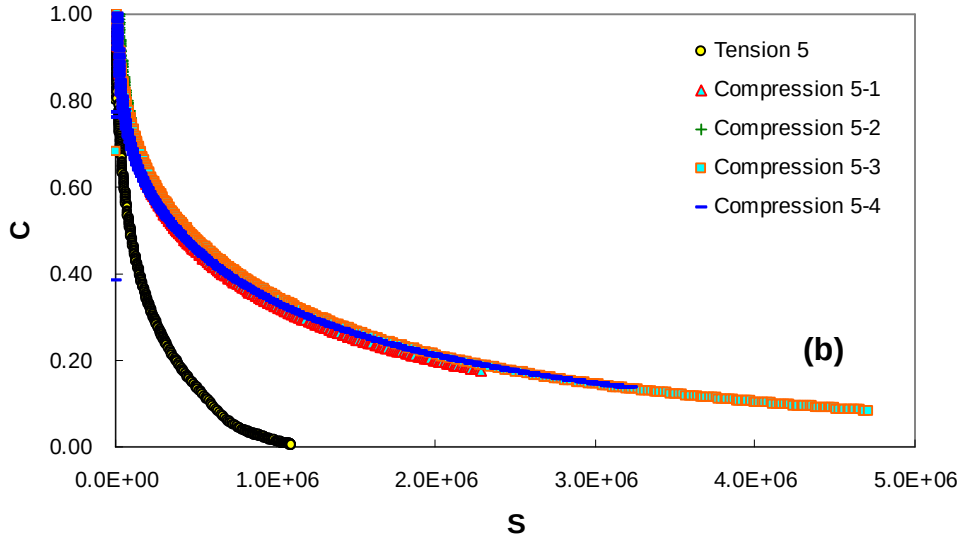

Figure 5.9 (a) stress vs. pseudo strain and (b) damage characteristic curves at 5°C

5.2.2. Strain Hardening Due to Aggregate Interlocking

A typical stress versus pseudo strain curve for 55°C is shown in Figure 5.10(a). It can be seen from the figure that the stress versus pseudo strain curve changes from a simple softening shape to a more complex shape. That is, at 5°C, the stress versus pseudo strain relationship curve starts along the LOE (i.e., the viscoelasticty dominates the behavior with minimal microcracking damage) and then changes to a softened curve, indicating the stiffness reduction due to microcracking in the vertical direction. At the peak stress or slightly over the peak stress, the localization starts; this marks the beginning of the macrocrack propagation.

In order to display this hardening and softening behavior of HMA in compression more effectively, the ***apparent*** pseudo secant stiffness (C_A) is calculated and presented in Figure 5.10(b). The pseudo secant stiffness in this figure is called ***apparent*** because the true pseudo secant stiffness is calculated using the viscoelastic strain only.

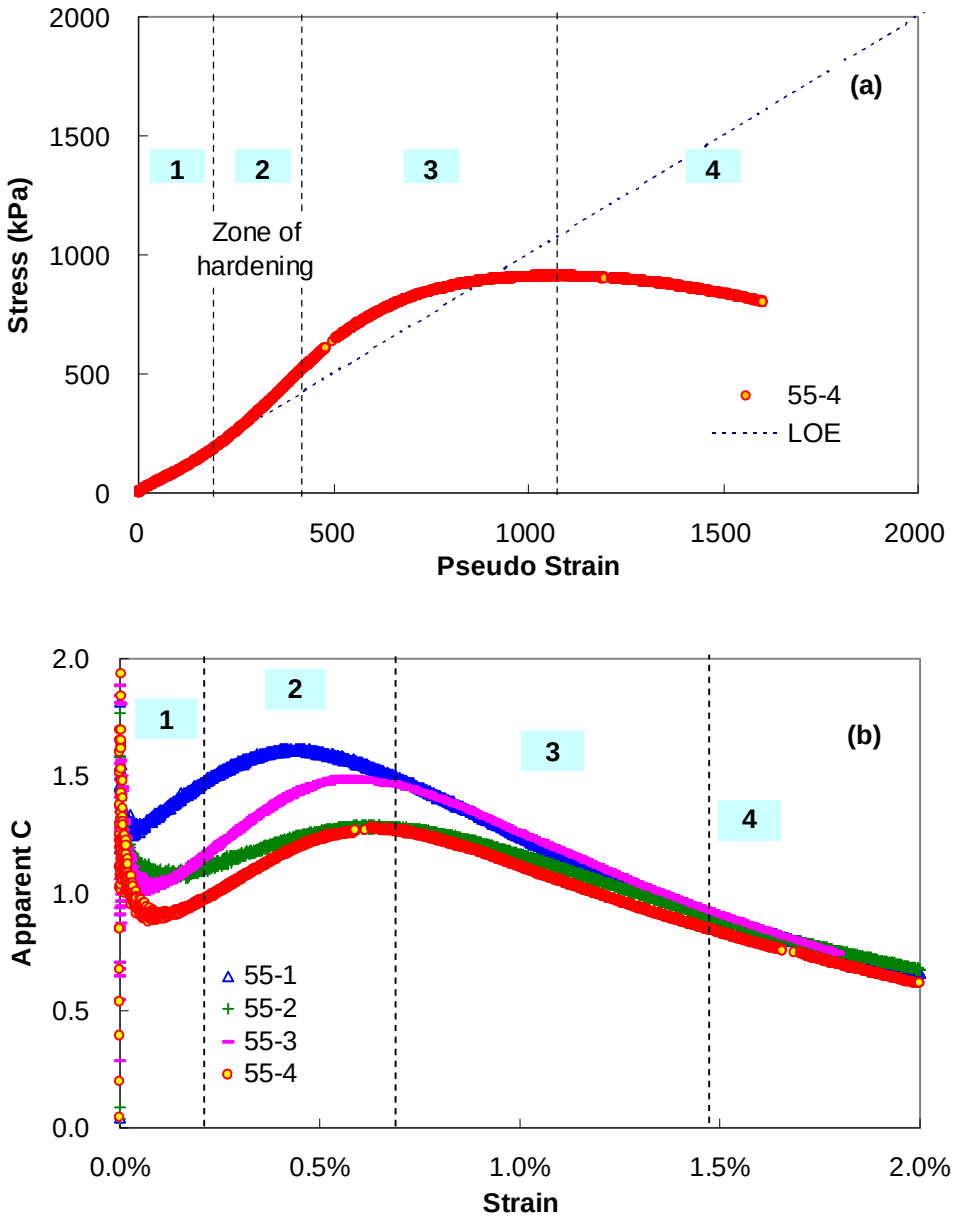

Figure 5.10 Effects of temperature and loading rate on (a) the stress vs. pseudo strain relationship and (b) the apparent *C* vs. strain relationship at 55°C

In this figure, the apparent pseudo secant stiffness is calculated using the total strain, which

includes both viscoelastic and viscoplastic strains and the aggregate interlocking effect on these strains. In Figure 5.10 for 5°C, the C value decreases all the way to failure as the strain increases.

As the temperature becomes higher and the strain rate becomes slower (Figure 5.10), the S-shape of the C_A versus strain curve becomes more evident. It is noted that the peak in the C_A versus strain curve occurs between 0.4 to 0.6% strain. The peak stress in the stress-strain curve is found to be between 1 and 1.6% strain regardless of the temperature and strain rate.

The primary mechanisms that govern the constitutive behavior of HMA in tension are viscoelasticity, the plastic flow of the binder, and cracking. In compression, it is well known that the interlocking of aggregate particles is an important factor that affects the behavior of HMA. The effect of aggregate interlocking increases as the binder viscosity decreases, which happens when the temperature increases and the rate of loading decreases. The primary characteristic of aggregate interlocking is that it stiffens and becomes more significant as the deformation of the HMA increases until the aggregate particles begin to slip. The observations made from Figure 5.10are well supported by the expected behavior of HMA due to aggregate interlocking. It must be noted that this behavior cannot be detected in the stress

versus strain plots because of the combined effects of viscoelasticity and aggregate interlocking. The benefit of using pseudo strain (i.e., eliminating the viscoelasticity from the plot) is clearly demonstrated in these Figure 5.9 and Figure 5.10.

A comparison of Figure 5.9 and Figure 5.10 reveals that the behavior of HMA in compression at high temperatures can be divided into four zones, as shown in Figure 5.10. In the first zone, the viscoelasticity and the flow of the binder dominate the HMA behavior and, as a result, the stress versus pseudo strain curve shows the softening behavior. In this zone 1, aggregate particles become closer and the air voids collapse, but noticeable aggregate interlocking has not yet formed. The beginning of Zone 2 indicates the onset of aggregate-to-aggregate interlocking. As the aggregate particles lock together, the stiffness of the mixture increases (i.e., the hardening behavior), as also shown in Zone 2. In Zone 3, aggregate interlocking degrades slowly as the load increases. At the peak stress, the aggregate particles slip away from each other; this causes shear failure, shown by the descending stress versus pseudo strain curve in Zone 4.

Investigation into the various relationships determined from the constant crosshead rate monotonic data suggests that the stiffening effect of aggregate interlocking must be taken

into account to model the compression behavior of HMA accurately. For the viscoelastic media of HMA, the viscoelastic damage characteristics are found to differ in the compression and tension loading modes, with the compression mode showing the more favorable results (i.e., less reduction in the pseudo stiffness, *C*, for the same amount of increase in the damage parameter, *S*). These results are also consistent with the hypothesis that the damage parameter, *S*, is related to crack density or crack volume, and that the primary direction of this cracking is perpendicular to the tensile loading direction or parallel to the compressive loading direction.

5.3. RATE-DEPENDENT HARDENING-SOFTENING IN VISCOPLASTIC MEDIA

In many of the constitutive concepts of plasticity, the state of the material is considered basically as a function of plastic strain and, therefore, most of the experimental efforts for material modeling are intended to correlate the material state and the plastic strain. However, although this concept and related experimental work have been proven to be reasonably valid for various elastoplastic and elastoviscoplastic materials, the validity of the concepts in terms of viscoelastoplastic material has not been rigorously evaluated through experimental

investigation. In this section, observations on the behavior of HMA under repetitive creep and recovery loadings, which are designed to identify the characteristic viscoplastic behavior of HMA, are discussed using possible physical mechanisms of HMA in compression.

5.3.1. Creep and Recovery Tests with Long Rest Periods

Although quantifying the variation of the viscoplastic strain or viscoplastic strain rate under a given loading condition is necessary to identify the actual behavior of the material directly, no test protocol is available that can capture only the viscoplastic strain or strain rate, because HMA shows rate-dependent viscoelastic strain, too. However, trends for viscoplastic strain and its respective rates that have been developed in repetitive creep and recovery testing can be evaluated by analyzing the VT test results.

Figure 5.11 represents viscoplastic strain development of VT tests at 500 kPa confinement with 1600 kPa deviatoric stress with respect to cumulative loading time. The loading history for this testing condition is described in Section 4.4.3.

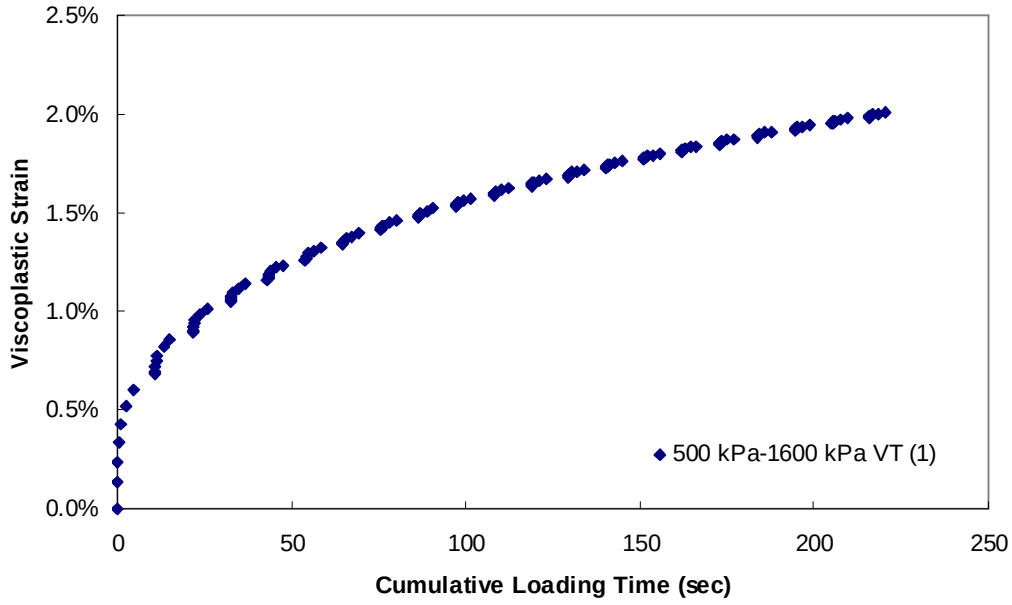

Figure 5.11 Viscoplastic strain vs. cumulative loading time (500 kPa confinement, 1600 kPa deviatoric stress)

It can be seen that the viscoplastic strain versus cumulative loading time behavior in each loading group with increasing pulse durations takes a power form similar to the hardening behavior shown for the entire VT data. This pattern repeats as the loading group of various pulse durations repeats; however, the effect of increasing pulse duration on the viscoplastic strain reduces as the loading group repeats more (i.e., as the viscoplastic strain increases).

In order to quantify the patterns described above, the *apparent* incremental viscoplastic strain rates is defined by dividing the incremental viscoplastic strain at the end of a square loading

cycle by pulse time (i.e., the duration of a square loading cycle). This variable is call ed the apparent viscoplastic strain rate because the real viscoplastic strain during loading is unknown and it represents the average viscoplastic strain rate for the entire loading duration. The apparent incremental viscoplastic strain rates are calculated for all the loading cycles in Figure 5.11 and plotted against the viscoplastic strain in Figure 5.12, it can be seen in Figure 5.12 that, at 1% viscoplastic strain, the *apparent* viscoplastic strain rates from 0.05-second loadings (approximately $2.0E^{-3}$) are much greater than those from 6.4-second loadings (approximately $8.0E^{-5}$).

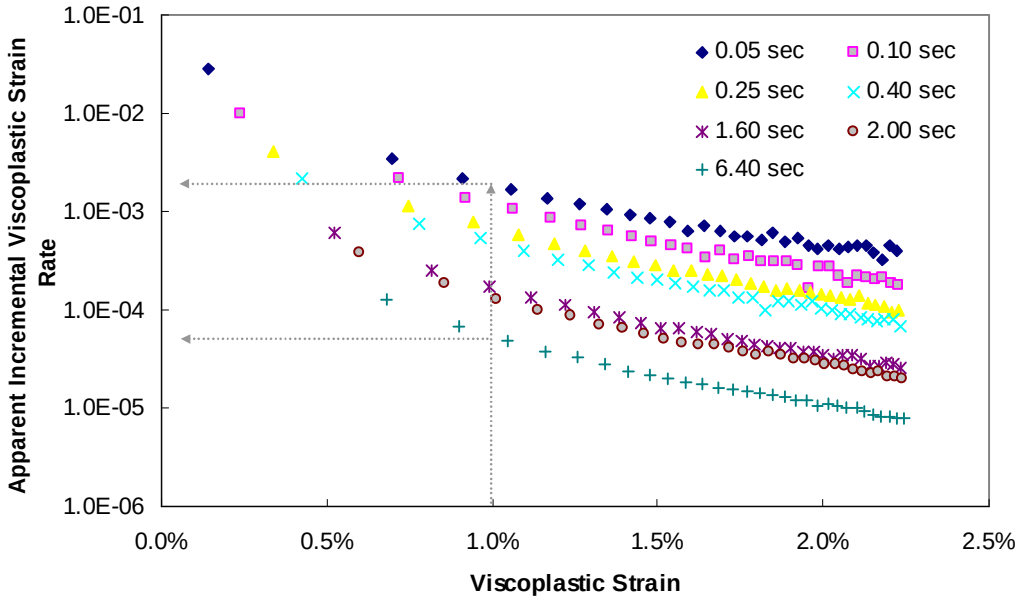

Figure 5.12 Incremental viscoplastic strain rate vs. viscoplastic strain (500 kPa confinement, 1600 kPa deviatoric stress)

Investigation of the patterns shown in Figure 5.11 and Figure 5.12 for different pulse times suggests that the most of the viscoplastic strain measured at the end of the square loading develops in the beginning of the loading period in the repetitive creep and recovery test. Therefore, the viscoplastic strain that develops during the remainder of the loading period is relatively small. It seems that during the long rest period (i.e., 200 seconds) the material relaxes and unlocks the interlocking among aggregate particles. Therefore, the large viscoplastic strain appears again in the next loading cycle. As the viscoplastic strain increases (i.e., as the material hardens due to more interlocking of aggregate), this early viscoplastic strain increase diminishes Figure 5.13 schematically depicts the effect of the overall hardening and the softening during rest period on the viscoplastic strain development under an imaginary VT test consisting of three different pulse durations.

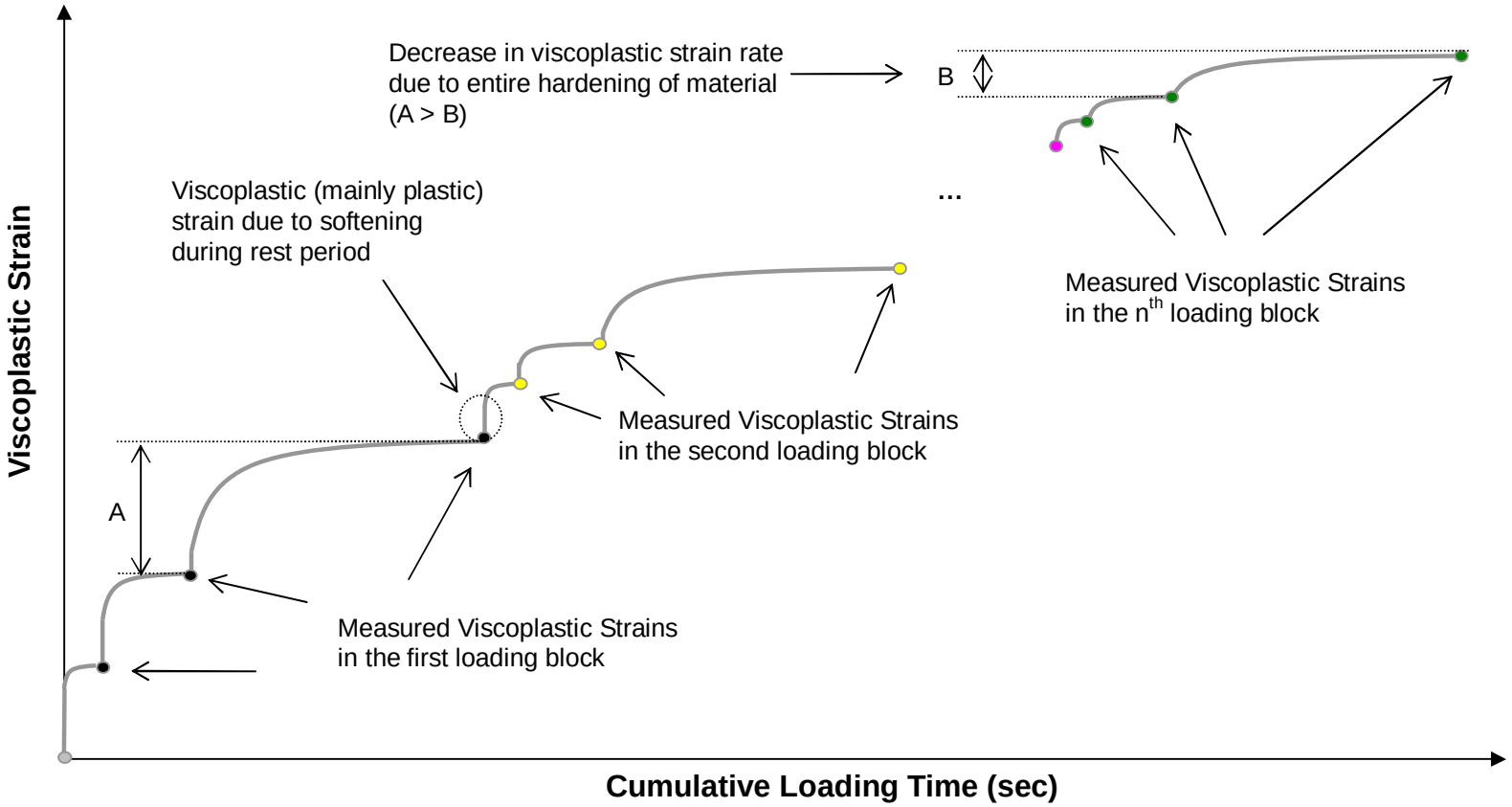

Figure 5.13 Schematic representation for viscoplastic strain development under variable loading time (VT) test

Figure 5.14 presents the viscoplastic strain history for each loading condition of the VT and CLT tests with a confining pressure of 500 kPa. The CLT tests were designed to capture the effect of the rate-dependent hardening and softening on viscoplastic strain development, and the VT tests with different deviatoric stress levels were designed to identify the significance of the load level effect relative to the pulse time. As shown in Figure 5.14 more viscoplastic strain was observed in the CLT tests that consist of shorter pulse times at a given cumulative loading time. Even considering the ramp time of 0.005 second for all tests, which is not taken into account in the cumulative loading time, the difference in the viscoplastic strains is quite significant. For example, at 150 seconds of cumulative loading time, the viscoplastic strain in 1800 kPa CLT testing with a 0.4-second pulse time was over 3%, whereas it was around 1.5% in 1800 kPa CLT testing with a 1.6-second pulse time. The fact that different viscoplastic strains are observed from the CLT tests with different pulse times at a given cumulative loading time can be explained mainly by the softening mechanism during the unloading.

It is noted that, for a given cumulative loading time, the number of cycles and thus the number of rest periods differ among the CLT tests with different pulse times. For example, the cumulative loading time of 100 seconds yields 1,000 cycles of 0.1-second pulse time, whereas the same cumulative loading time results in 200 cycles of 0.5-second pulse time. Because a sufficient rest period is introduced after each loading cycle, the 0.1-second pulse time CLT test has five times more opportunities to soften during the rest periods than the 0.5-second pulse time CLT test in this example; therefore, greater viscoplastic strain is evident

even though the cumulative loading time is the same as shown in Figure 5.14. However, by comparing viscoplastic strains under VT loading with RVT loading, as shown in Figure 5.15, it is found that the effect of the loading sequence on viscoplastic strain development decreases as the material stiffens, and that the effect is relatively small compared to the effect of that rest period has on viscoplastic strain development.

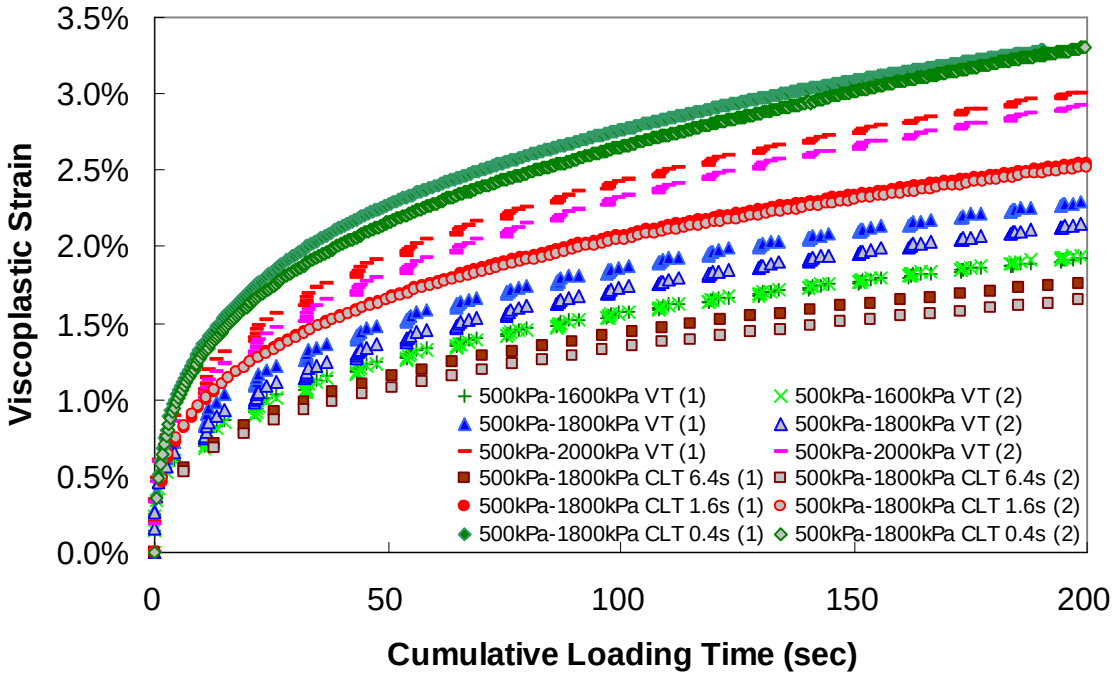

Figure 5.14 Viscoplastic strain vs. cumulative loading time (500 kPa confinement)

It should be noted that the first point of the n+1th viscoplastic strain group in VT testing must compared with the last point of the nth viscoplastic strain group under RVT conditions in order for viscoplastic strain to develop at the same cumulative loading time and rest period, because the test conditions were the same for both tests, with the exception of the sequence

of loading. However, in both cases, the discontinuous viscoplastic strain history that indicates rate-dependent hardening-softening is also observed.

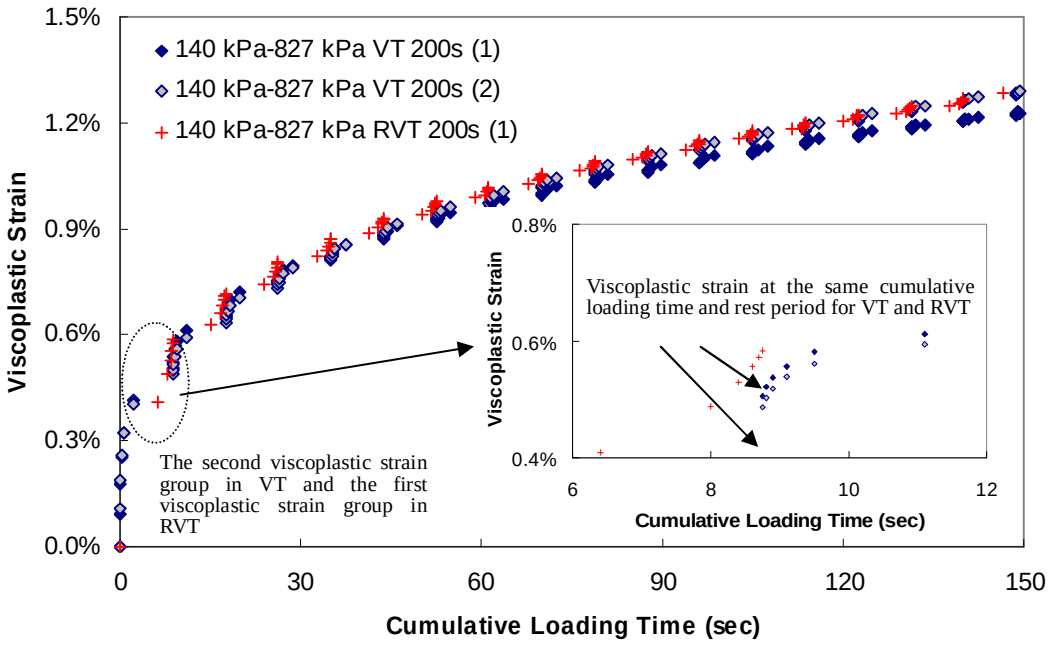

Figure 5.15 Viscoplastic strain vs. cumulative loading time (140 kPa confinement-827 kPa deviatoric stress VT, RVT).

5.3.2. Creep and Recovery Tests with Short Rest Periods

The VT test with the a short rest period was performed in order to investigate the effect of the rest period on the change in material state. Two additional VT tests with 0.1-second and 0.05-second rest periods were performed at a confining pressure of 140 kPa; these test results were compared with the results from VT testing with 200 seconds of rest. The test conditions were identical, i.e., the number of loadings and rest periods were the same for each test, except for

the length of the rest period, as shown in Figure 5.16. Figure 5.16 presents the viscoplastic strains measured at the end of the rest periods. The first number in the test ID is the confining pressure, the second number indicates deviatoric stress, and the third number indicates the rest period following each loading pulse. For the VT tests with 0.05 second and 0.1 second of rest, pure viscoplastic strains were measured only at the end of the test where a rest period of 200 seconds was allowed, because it was not possible to measure pure viscoplastic strain immediately after 0.05 second or 0.1 second of rest. A test with a deviatoric stress of 552 kPa was performed to evaluate the relative significance of the rest period effect on viscoplastic strain development.

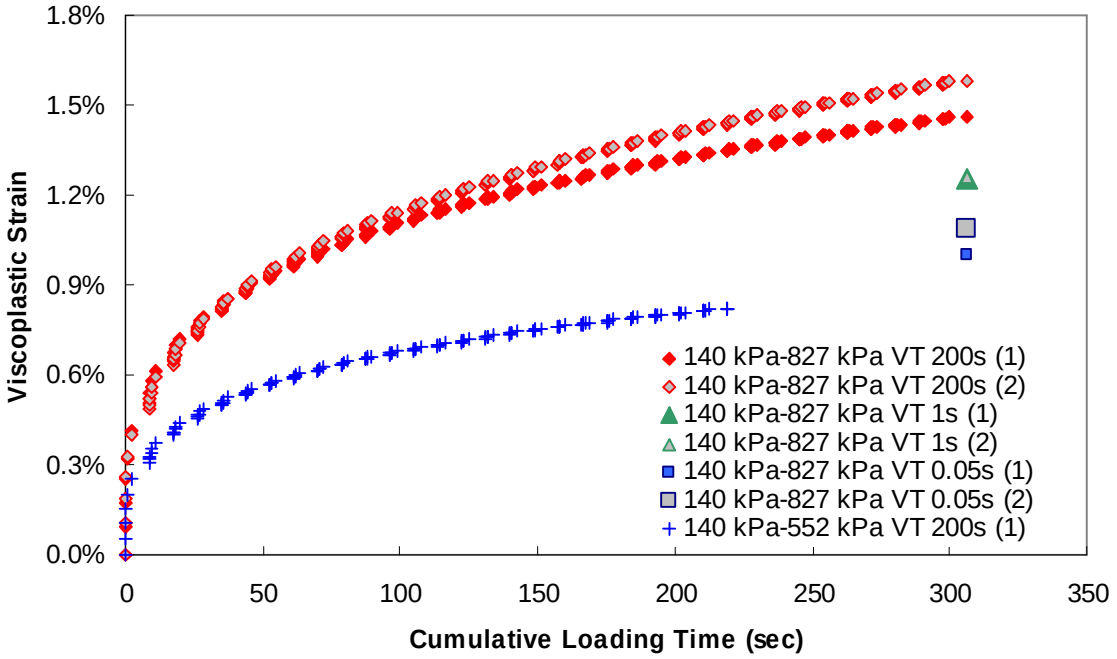

Figure 5.16 Viscoplastic strain vs. cumulative loading time (140 kPa confinement VT)

As seen in Figure 5.16, even though the loading histories are identical except for the length of the rest period, a smaller viscoplastic strain develops as the rest period becomes shorter. The effect of the rest period on viscoplastic development thus can not be ignored considering the amount of viscoplastic strain when using 552 kPa deviatoric stress and 200 seconds of rest. This experimental observation clearly demonstrates the significant effect of rate-dependent softening during unloading. Furthermore, it is not beyond reason to suppose that this softening behavior could be rate-dependent when the viscoplastic strain of the VT test with 0.05 second of rest is compared to that of the VT tests with 0.1 second and 200 seconds of rest.

Based on the observations made above, it seems a reasonable interpretation that the governing mechanism for this rate-dependent state of the material is related to the aggregate interlocking during loading and to the softening during unloading. More specifically, the mixture hardens during loading as a result of the interaction of aggregate particles and softens during the following unloading due to the viscoelastic recovery of the binder that pushes the aggregate particles to their original positions. Therefore, when the mixture is reloaded after a sufficient rest period, the state of the material at the beginning of reloading is different from the state of the material at the end of the preceding loading. Once the material is reloaded, the rapid hardening as a resulted of interlocking of the aggregate particles and the rate-dependent hardening as a result of the slippage of the aggregate-binder govern the overall hardening rate and viscoplastic strain development. A schematic representation for this behavior is shown in Figure 5.17 in which the viscoplastic strain due to continuous

loading is compared to viscoplastic strain due to discontinuous loading with rest periods at the same cumulative loading time. As shown in the Figure 5.17, the material state variable that represents resistance to flow is not only a function of viscoplastic strain but is also rate-dependent which appears to be related to the stress or/and stress rate (e.g., at B the state of the material under continuous loading is different from the state under discontinuous loading even though the viscoplastic strain is the same). Therefore, existing viscoplastic models for HMA that are founded on conventional plasticity theory, which mainly represent the behavior of metals or polymers under monotonic loading or ratcheting, are not adequate to represent the characteristic behavior of HMA, because such viscoplastic models are not capable of capturing either the rapid local hardening during repeated loading or the softening during unloading.

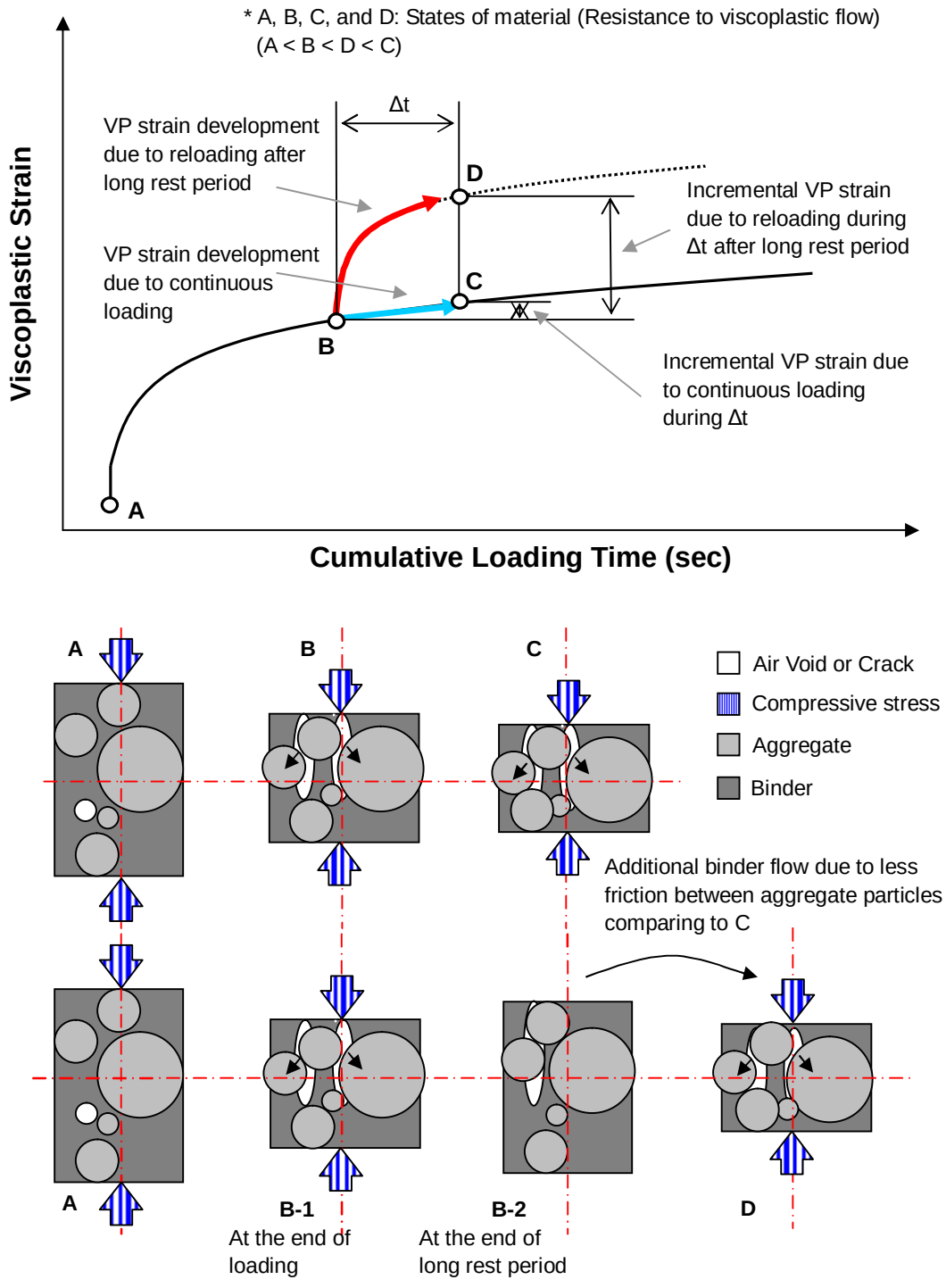

Figure 5.17 Schematic representation of hardening during loading and softening during unloading

6. VISCOPLASTIC MODELING OF ASPHALT CONCRETE IN COMPRESSION

6.1. FLOW RULE AND YIELD FUNCTION FOR DEVELOPED VISCOPLASTIC MODEL

As an expansion of Equation (2.5), a general flow rule for materials that exhibit kinematic and isotropic hardening is represented in Equation (6.1). m amplifies or reduces the stress rate dependency of the model, and D determines the viscosity in the viscoplastic flow. When D is a constant, it is assumed that the effect of the change in viscosity on the response of the material is taken into account by the yield stress function.

$$\dot{\varepsilon}_{ij}^{vp} = \left\langle \frac{f(s-a)-r}{D} \right\rangle^{m} \frac{\partial f}{\partial s_{ij}}, \tag{6.1}$$

where

a = kinematic hardening function,

g = isotropic hardening function,

D = viscosity parameter,

s = stress,

f = yield function, and

m = rate-dependency parameter.

A 1-D viscoplastic constitutive model that incorporates Perzyna's flow rule with a yield criterion is suggested, as shown in Equation (6.2) for the viscoplastic modeling of HMA in this research.

$$\dot{\varepsilon}^{vp} = \left\langle \frac{s - G}{D} \right\rangle^{m} \frac{s - G}{|s - G|}, \tag{6.2}$$

where

D, m = material constants,

s = stress, and

G = yield stress.

As discussed in Section 5.3, rate-dependent hardening and softening, which imply the existence of a multiple state of the material at a certain viscoplastic strains, must be introduced into the viscoplastic constitutive model in order to describe the difference between the viscoplastic strain development under continuous loading and under discontinuous loading at a certain cumulative loading time. Therefore, the mathematical expression that represents the rate-dependent material behavior is used as the yield stress function in this research. Equation (6.3) and Equation (6.4) are two forms of the yield stress rate that are conceptually the same as the equations used to represent rate-dependent linear viscoelastic material behavior. In the theory of linear viscoelasticity, $\dot{\sigma}$ in Equation (6.3) and $\dot{\varepsilon}$ in Equation (6.4) represent stress and viscoelastic strain, respectively.

$$\dot{G} = g\left(\dot{\varepsilon}_{vp}, e_{vp}, G\right), \text{ or} \tag{6.3}$$

$$\dot{G} = g\left(\dot{\varepsilon}_{vp}, s, G\right). \tag{6.4}$$

In Equation (6.3) and Equation (6.4), $\dot{G}$ represents the isotropic hardening-softening rate and is considered to be the rate of the reaction force that resists the plastic flow. Equation (6.3) is appropriate for materials that exhibit viscoplastic hardening and softening as a function of the viscoplastic strain rate under the creep loading condition, whereas Equation (6.4) is appropriate for materials exhibiting continuous viscoplastic hardening regardless of the viscoplastic strain rate under the creep loading condition. Equation (6.3) and Equation (6.4) can be solved using the state variable approach in order to reduce computational time, as shown in Equation (6.5) and Equation (6.6), respectively.

$$G^{n+1} = z_0^{n+1} + \sum_{i=1}^{m} z_i^{n+1}, \tag{6.5}$$

where

$$z_0^{n+1} = \left[e_{vp}^{t^{n+1}} - e_{vp}^{t^n} \right] E_0,$$

$$z_i^{n+1} = \left[e^{-\frac{\Delta t}{r_i}} z_i^n + e^{-\frac{\Delta t}{2r_i}} \left[e_{vp}^{t^{n+1}} - e_{vp}^{t^n} \right] E_i \right],$$

$e_{vp}^{t^{n+1}}$ = viscoplastic strain at time step $n+1, t^{n+1}$,

$e_{vp}^{t^n}$ = viscoplastic strain at time step n, t^n,

r_i = relaxation time,

$\Delta t = t^{n+1} - t^n$, and

E_0, E_i = Prony coefficients.

$$G^{n+1} = z_0^{n+1} - \sum_{i=1}^{m} z_i^{n+1}, \tag{6.6}$$

where

$$z_0^{n+1} = \left[D_0 + \sum_{i=1}^{m} D_i \right] \left[s^{t^{n+1}} - s^{t^0} \right],$$

$$z_i^{n+1} = \left[e^{-\frac{\Delta t}{r_i}} z_i^n + e^{-\frac{\Delta t}{2r_i}} \left[s^{t^{n+1}} - s^{t^n} \right] D_i \right],$$

$e_{vp}^{t^{n+1}}$ = viscoplastic strain at time step $n+1, t^{n+1}$,

$e_{vp}^{t^n}$ = viscoplastic strain at time step n, t^n, and

r_i = retardation time,

$\Delta t = t^{n+1} - t^n$, and

D_0, D_i = Prony coefficients.

Equation (6.7) represents the derivation procedure introduced in this research for Equation (6.6).

$$
\begin{aligned}
G^{n+1} &= \int_0^{t^{n+1}} D\left(t^{n+1} - t\right)\frac{ds}{dt}dt \\
&= \int_0^{t^{n+1}} \left[D_0 + \sum_{i=1}^{m} D_i \left(1 - e^{-\frac{t^{n+1}-t}{r_i}} \right) \right] f'(t)\, dt \\
&= \left[D_0 + \sum_{i=1}^{m} D_i \right] \int_0^{t^{n+1}} f'(t) - \sum_{i=1}^{m} D_i \int_0^{t^{n+1}} \left(e^{-\frac{t^{n+1}-t}{r_i}} f'(t)\, dt \right) \\
&= \left[D_0 + \sum_{i=1}^{m} D_i \right] \left[s^{t^{n+1}} - s^{t^0} \right] - \sum_{i=1}^{m} D_i \int_0^{t^{n+1}} \left(e^{-\frac{t^{n+1}-t}{r_i}} f'(t)\, dt \right)
\end{aligned}
\tag{6.7}
$$

where

$$
f'(t) = f\left(\frac{t^{n+1} + t^n}{2} \right) = \left(\frac{f\left(t^{n+1}\right) - f\left(t^n\right)}{\Delta t} \right),
$$

$s^{t^{n+1}}$ = stress at time step $n+1$,

s^{t^0} = stress at time step 0,

$e_{vp}^{t^{n+1}}$ = viscoplastic strain at time step $n+1, t^{n+1}$,

$e_{vp}^{t^n}$ = viscoplastic strain at time step n, t^n,

r_i = retardation time,

$\Delta t = t^{n+1} - t^n$, and

D_0, D_i = prony coefficients.

Because it is a reasonable assumption that the yield stress is never larger than the applied stress unless the material has previously experienced the same level of stress, the upper bound of $D(t)$, which is a unit response function representing the development of yield

stress under unit creep loading, is set to one. Therefore, under the unit creep loading, the yield stress approaches the applied stress as the loading time increases, as shown schematically in Figure 6.1.

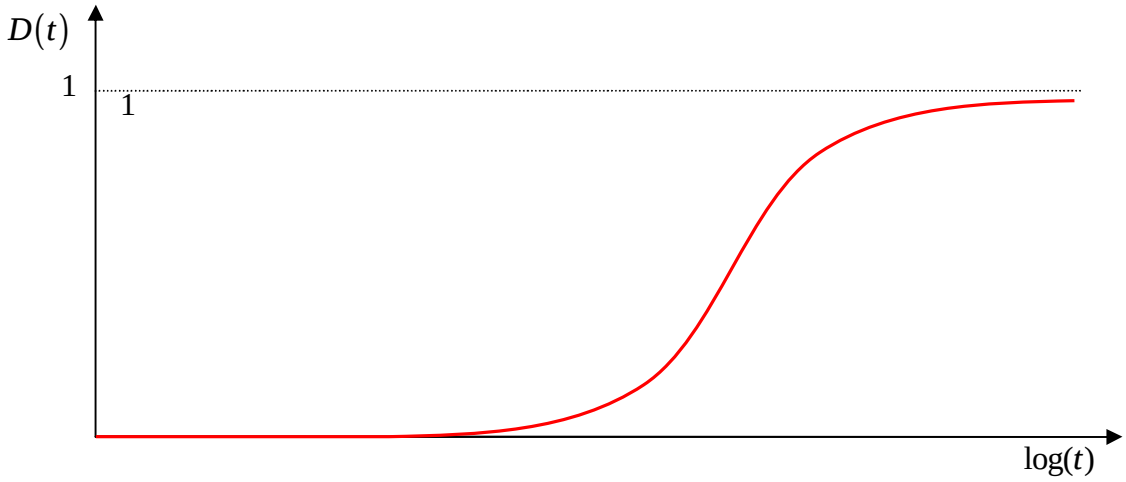

Figure 6.1 Variation of yield stress under unit creep loading.

As discussed in Section 5.3, the rate dependence of the yield stress during loading and unloading varies as the viscoplastic strain increases. Also, the rate dependence of the material during loading must be differentiated from the rate dependency during unloading because the hardening rate increases as the viscoplastic strain increases, whereas the softening rate decreases as viscoplastic strain increases. However, using two separate and distinct unit response functions to represent the rate-dependent behavior under loading and unloading requires significantly more computational time for both calibration and prediction. Therefore, a shifting technique is adapted in this research with the reasonable assumption that the variations in rate dependence of the yield stress can be captured with one comprehensive

mathematical representation without a significant increase in computational time, as follows. First of all, r_i in Equation (6.7), which determines the rate dependency of the material, is considered to be a function of an internal state variable, $H_{Loading}$, as shown in Equation (6.8).

$$r_{Loading} = r_{i,0} / 10^{H_{Loading}} \tag{6.8}$$

where

$r_{i,0}$ = initial retardation time, and

$H_{Loading}$ = internal state variable for loading condition.

The internal state variable, $H_{Loading}$, is introduced as a governing state variable that basically is determined by the history of the viscoplastic strain rate that develops during the loading condition (i.e., $s > G$). Based on the relationship represented in Equation (6.9) and Equation (6.10), $r_{Loading}$ decreases as viscoplastic strain increases, and it determines the amount of horizontal shifting of the unit response function for the loading condition.

$$H_{Loaing} = b_1 \left(1 - e^{b_2 h^{b_3}}\right) \tag{6.9}$$

where

b_1, b_2, and b_3 = material fitting parameters.

$$\Delta h = \dot{\varepsilon}_{vp} \cdot a_1 e^{\left(-a_2 \cdot \dot{\varepsilon}_{vp}\right)} \cdot \Delta t \tag{6.10}$$

where

$\dot{\varepsilon}_{vp}$ = viscoplastic strain rate,

a_1, a_2 = material fitting parameters, and

Δt = incremental time.

With the assumption that the rate dependence of both the hardening and softening evolve with the internal state variable which varies only under the loading condition, Equation (6.11) is introduced as a state variable for the unloading condition.

$$H_{Unloading} = \left(H_0 - \left(H_{Loading} \right)^{g_1} \right), \tag{6.11}$$

where

H_0, g_1 = material fitting parameters.

Equation (6.12) represents the relationship between $H_{Unloading}$ and $r_{Unloading}$. Similarly, $r_{Unloading}$ determines the amount of horizontal shifting of the unit response function for the unloading condition (i.e., $s < G$), and it increases as the viscoplastic strain increases.

$$r_{Unloading} = r_{i,0} / 10^{H_{Unloading}} \tag{6.12}$$

Figure 6.2(a) shows typical variations of the unit response function for both loading and unloading, and Figure 6.2(b) shows the variations of the yield stress according to the variations in rate dependence for both the loading and unloading conditions.

The Prony series is a convenient mathematical expression to represent especially the unit response function used in this study, but it has lots of coefficients (e.g., D_0 and D_i) to be determined during the calibration process, as shown in Equation (6.7). In order to reduce the

number of coefficients in the developed model, the following approach is used in this study.

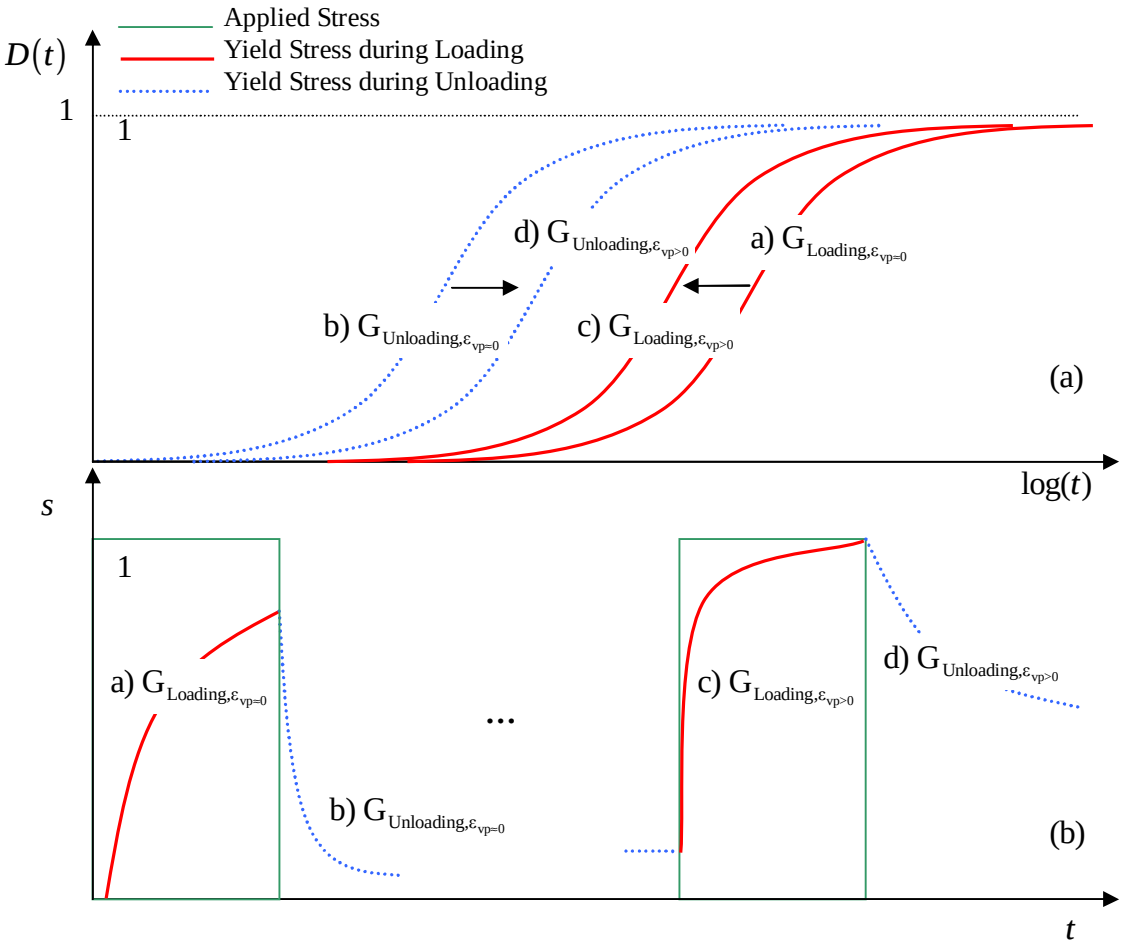

Figure 6.2 The variations of: (a) unit response function and (b) yield Stresses as a function of viscoplastic strain under repetitive creep and recovery

When the unit response function in Figure 6.1 is represented by a sigmoidal function as shown in Equation (6.13), a and $a+b$ in Equation (6.13) determine the lower and upper asymptotes of the unit response function, respectively. Because the upper asymptote is assumed as one, the relationship between a and b is $a+b=0$. Therefore, Equation (6.13)

reduces to Equation (6.14).

$$\log\left(D(t)\right) = a + \frac{b}{1+e^{\left(c-d\log(t)\right)}} \tag{6.13}$$

$$\log\left(D(t)\right) = a\left(1 - \frac{1}{1+e^{\left(c-d\log(t)\right)}}\right) \tag{6.14}$$

where,

$D(t)$ = unit response function for yield stress,

t = time, and

a, b, c, and d = fitting coefficients.

Once the unit response function is represented by the sigmoidal function, the coefficients in the Prony series are fitted to the sigmoidal function and used for the yield stress calculation.

6.2. CHARACTERISTICS OF THE DEVELOPED MODEL FOR ARBITRARY STRESS HISTORIES

In Sections 6.2.1 and 6.2.2, in order to confirm the characteristics of the viscoplastic model, a simplified model form is suggested by incorporating Equation (6.2) with Equation (6.15) and the following predictions are made for the arbitrary stress histories in the simplified model. In this analysis, it is assumed for the sake of simplicity that the rate dependences of the yield stress for both loading and unloading are identical and that they are independent of the viscoplastic strain. Equation (6.15) is considered to be a yield stress function in this

analysis because it is the simplest differential equation that represents the rate-dependent yield stress and residual yield stress.

$$\dot{G} = \frac{E_1 E_2}{h_2} \dot{e}^{vp} + E_1 \dot{e}^{vp} - \left(\frac{E_1 + E_2}{h_2} \right) G, \tag{6.15}$$

where,

E_1, E_2, h_1, h_2 = material constants.

Figure 6.3 presents a schematic concept of the variation in yield stress subjected to a creep and recovery loading condition.

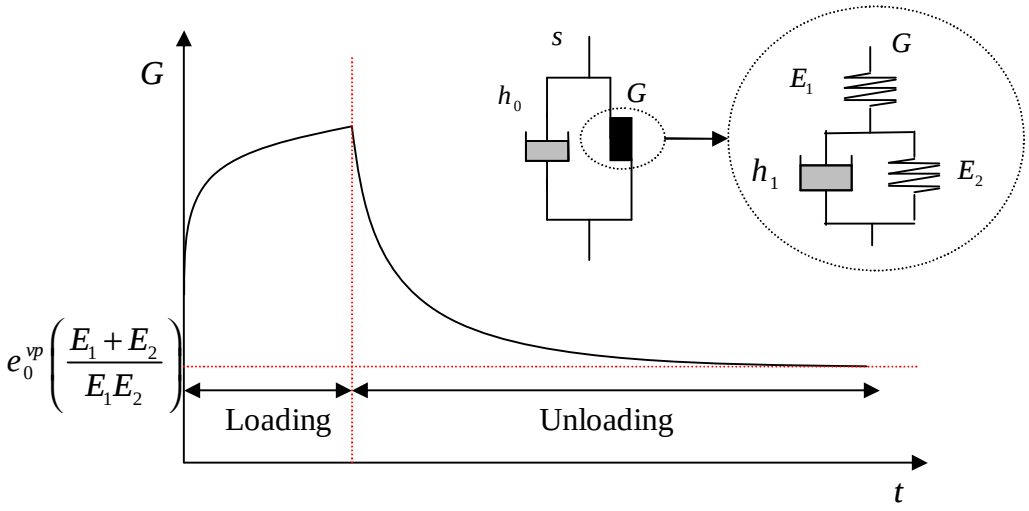

Figure 6.3 Variation of yield stress (standard linear solid model).

The remaining yield stress, which is the yield stress at the asymptote, is governed by the viscoplastic strain at the end of the loading condition, e_0^{vp}, and material constants, E_1 and

E_2. The decreasing yield stress during unloading allows a multiple viscoplastic strain rates at a certain viscoplastic strain. Table 6.1 presents the material constants that have been determined to show characteristics of the model in this analysis.

In Section 6.2.3, the case study results are presented to evaluate more specifically the effect of separated hardening and softening functions on the variations in the yield stress more.

Table 6.1 Material coefficients used for sensitivity analysis

D	m	η_1	η_2	E_1	E_2
2	3000	10	50000	500	200

6.2.1. Effect of Rest Period

Figure 6.4 shows two different stress histories that are used to evaluate the sensitivity of the viscoplastic model to rest periods. For both stress histories, the stress level and the cumulative loading time were fixed to 2000 kPa and 160 seconds, respectively. However, for the first stress history, 8.0 seconds of rest between the loading pulses were allowed, whereas only 1 second of rest was allowed for the second loading history. Figure 6.5 presents the variation of yield stress for each stress history and, as expected, the model shows different yield stress developments depending upon the rest period. Figure 6.6 presents the viscoplastic strain developed by each stress history, and it shows more viscoplastic strain for a longer rest period. This finding corresponds to the experimental observations made in Section 5.3.

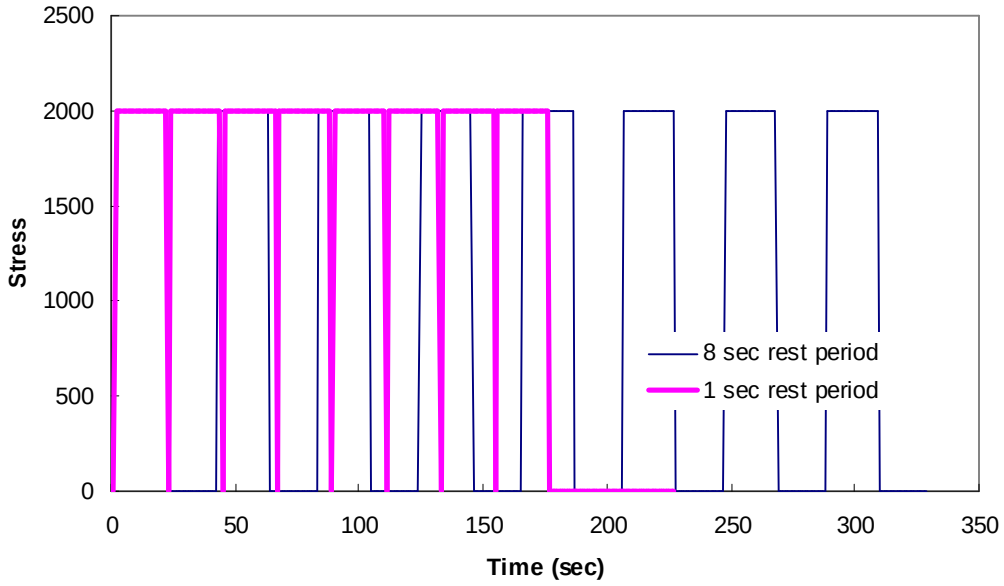

Figure 6.4 Stress histories for rest period analysis.

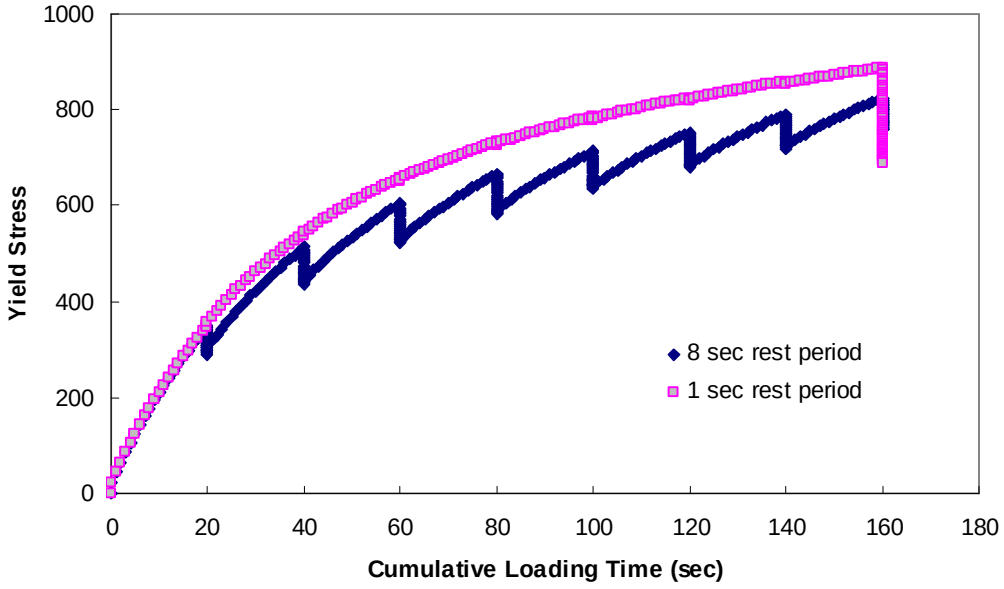

Figure 6.5 Yield stress vs. cumulative loading time (rest period analysis).

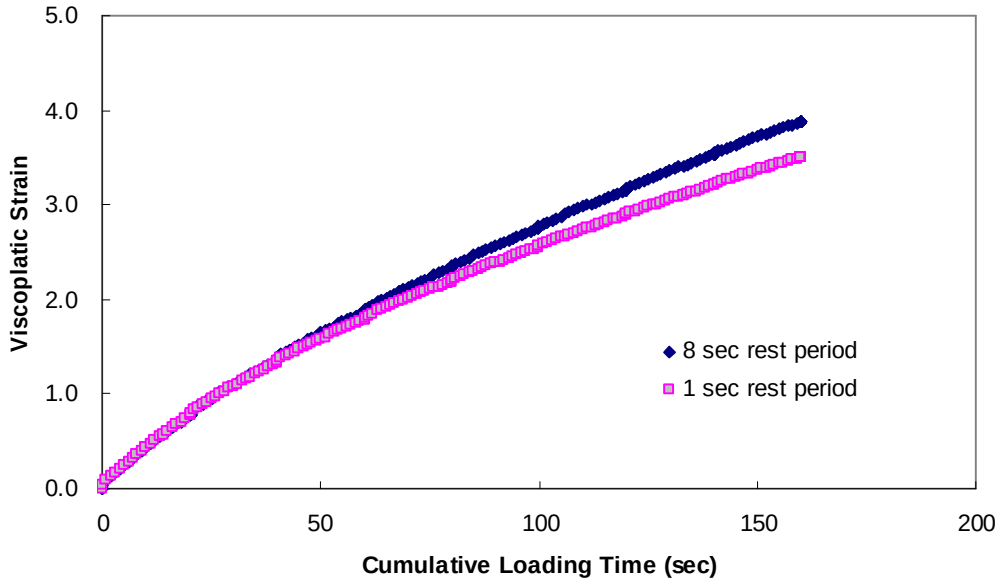

Figure 6.6 Viscoplastic strain vs. cumulative loading time (rest period analysis).

6.2.2. Effect of Loading Time

Figure 6.7 presents a set of stress histories that are used to evaluate the effects of loading time. For these stress histories, the load level, rest period and cumulative loading time were fixed to 2000 kPa, 4 seconds and 66 seconds, respectively. However, the first loading history consists of 6 pulses 11 seconds long, and the second loading history consisted of 22 pulses 3 seconds long. The analysis results for the given stress histories are shown in Figure 6.8.

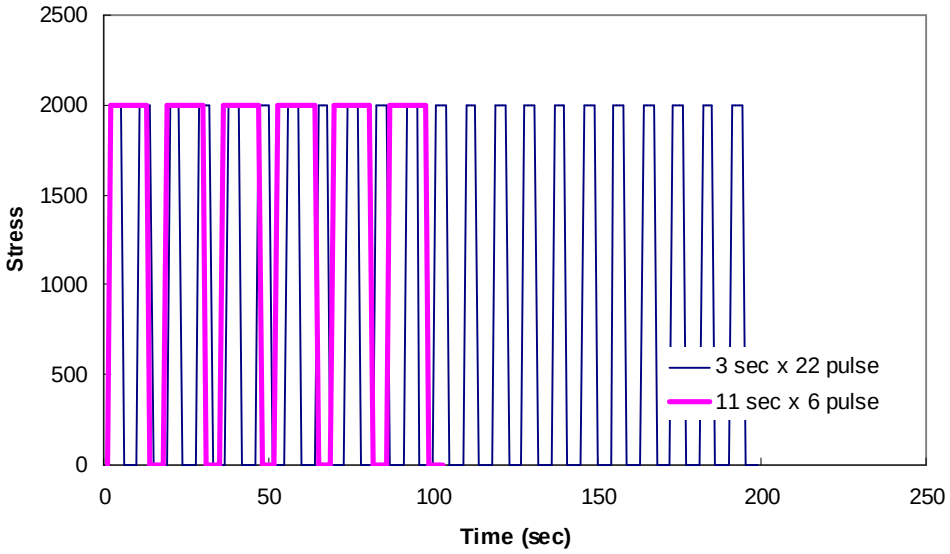

Figure 6.7 Stress histories for loading time analysis.

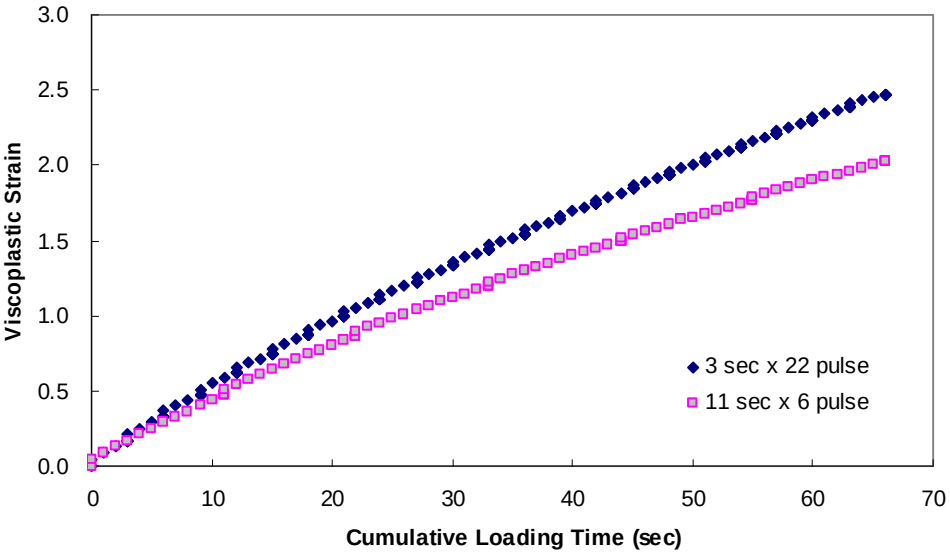

Figure 6.8 Viscoplastic strain vs. cumulative loading time (loading time analysis).

The loading history with shorter individual loading times shows more viscoplastic strain,

which is identical to the CLT test results. As shown, the viscoplastic model that incorporates the softening rule appears to account for the pulse time effect. As shown in Figure 6.6 and Figure 6.8, the viscoplastic model with the rate-dependent hardening-softening capability can account for the effects of loading time.

6.2.3. Effect of Separate Hardening and Softening Functions

In order to evaluate the effect of the separate hardening and softening functions on the variation in yield stress, three cases were considered in this analysis as shown in Figure 6.9. A creep and recovery test with 6.4 seconds of pulse time and a 0.9 second rest period was repeated five times and is thereby considered as a loading history.

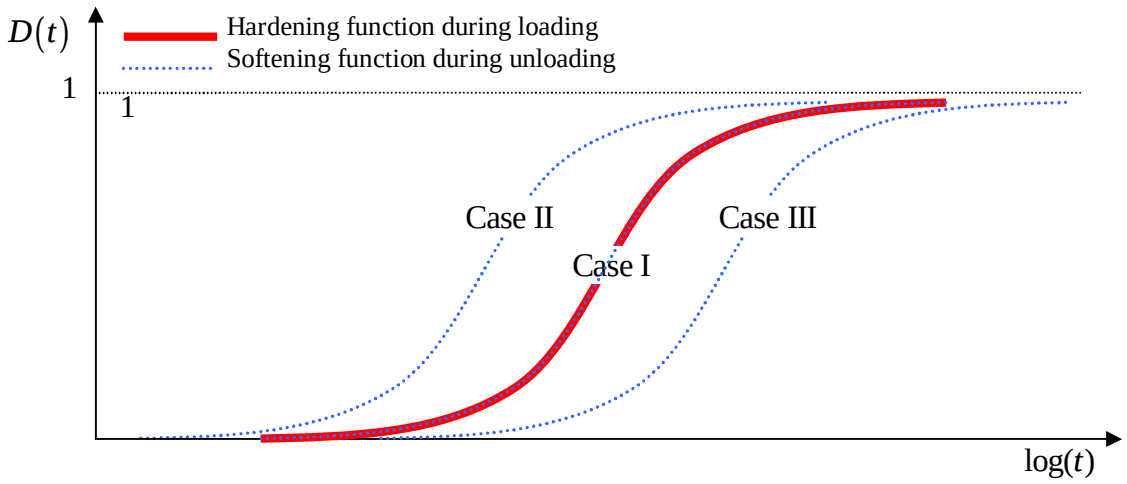

Figure 6.9 The schematic representation for hardening and softening functions

In the Case I, the same unit response function is used as both a hardening and softening

function to represent the variation in yield stress for the given stress history. In the Case II, the softening function is shifted to the left side of the hardening function, whereas it is shifted to the right side of the hardening function in the Case III. Also, it is assumed that all hardening and softening functions do not evolve for the entire loading history to simplify the variation in the yield stress.

Figure 6.10 presents the variation in yield stress, which is dependent on the position of the softening function with respect to the hardening function. As clearly shown in Figure 6.10, the lowest decreasing rate of yield stress during unloading is observed in Case III, whereas the fastest decreasing rate of yield stress is observed in Case II, as is expected from the theory of linear viscoelasticity. Considering the trend of viscoplastic strain development observed in Figure 5.11 and Figure 5.12, it seems that the Case II is a reasonable representation of the viscoplastic strain development in the primary region, whereas Case II is a reasonable representation of the viscoplastic strain development in the secondary region. It should be noted that when the unit response function that represents softening is positioned far away from the unit response function that represents hardening one the right side (i.e., that no softening occurs during unloading or an extreme condition of Case III), the developed viscoplastic model is simplified to a viscoplastic model with only rate-dependent hardening, which is a general viscoplastic model form used for metals and polymers. A more realistic case, i.e., the variation in yield stress with varying hardening and softening behavior as functions of viscoplastic strain, is shown in Figure 6.2.

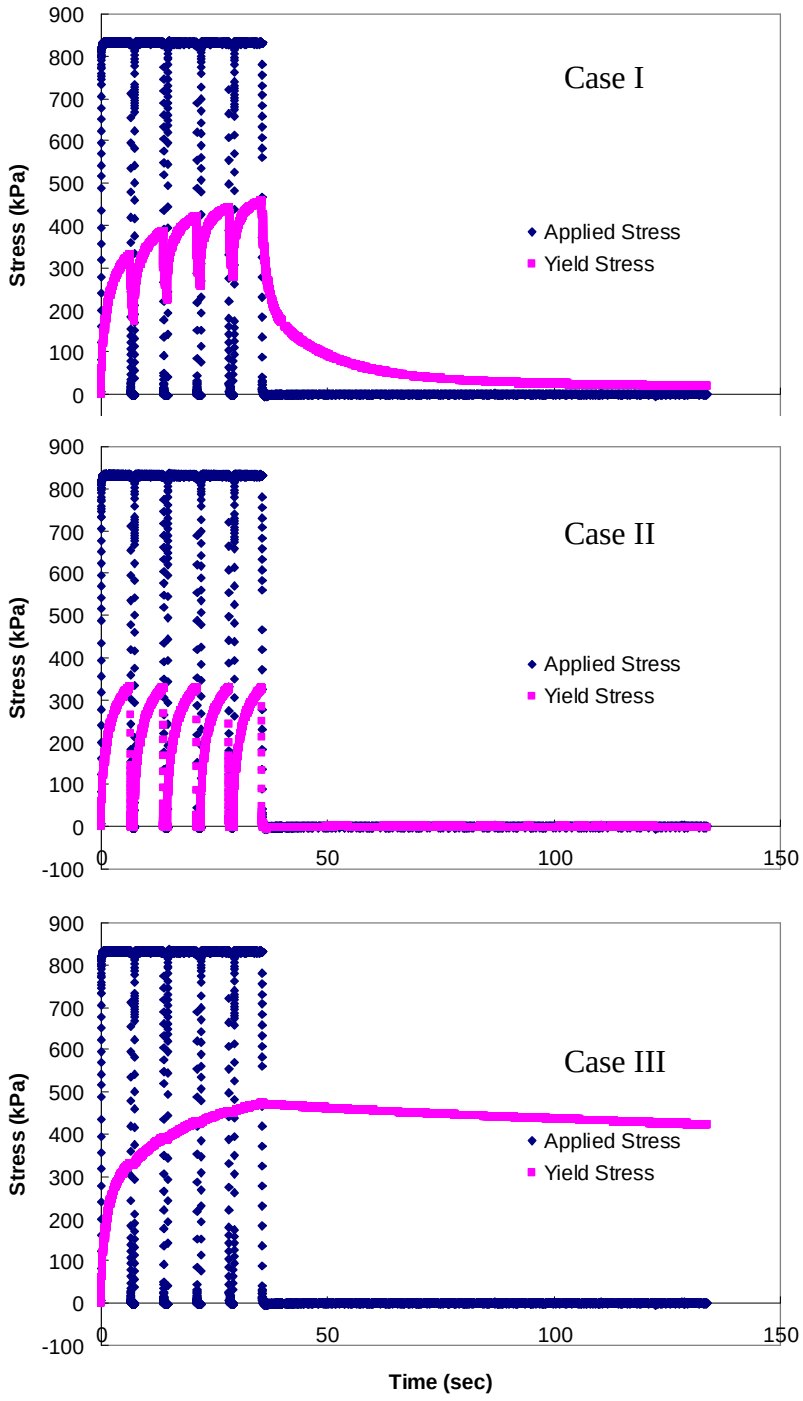

Figure 6.10 The variation of yield stress with separated hardening and softening functions

6.3. CALIBRATION OF THE DEVELOPED MODEL

Prior to the calibration process, data points acquired during the unloading periods are filtered to reduce the computational time. Strains measured at the end of the rest periods are defined as the objective function and the nonlinear optimization function (lsqnonlin) in Matlab^{TM} is utilized to minimize errors between the measured and predicted viscoplastic strains. For the calibration, the VT test is used to characterize the rate-dependent hardening of the material, and the VTVR test is used to characterize the rate-dependent softening of the material. Therefore, model coefficients, D, m, a_1, a_2, b_1, b_2, b_3, a, c, and d are calibrated for the VT test first and then g and H_0 are calibrated for the VTVR test. Table 6.2 shows the coefficients determined from the calibration process for 140 kPa and 500 kPa confining pressures.

Table 6.2 Compression viscoplastic material model coefficients

Confining Pressure (kPa)	D	m	a	c	d	α_1
140	599975	2.77	-6.999	1.800	0.687	1.500
500	869488	2.788	-7.0000	1.802	0.687	1.200
Confining Pressure (kPa)	α_2	β_1	β_2	β_3	γ	H_0
140	999999999	10.000	10.006	0.660	0.800	7.300
500	5099578	8.228	10.026	0.677	1.000	0.000

Because the effect of the varying rest periods is not considered in testing at 500 kPa confining pressure, the coefficients g and H_0 are set to 1 and 0, respectively, so that the

rate dependency of the yield stress during the unloading condition is exactly the same as during the loading condition. Also, the model is calibrated separately for each confining pressure condition without considering the effect of hydrostatic stress, because the objective of this research is to develop a 1D viscoplastic constitutive model in terms of rate-dependent hardening-softening behavior.

Figure 6.11 and Figure 6.12 present the calibration results of the VT and VTVR tests at 140 kPa confining pressure in normal scale and in semi-log scale, respectively, and Figure 6.13 presents the calibration results for the VT tests at 500 kPa confining pressure. In general, the predicted viscoplastic strains match very well to the measured viscoplastic strains for both confining pressure conditions in normal scale. It seems that the predictions are acceptable for the given stress histories considering the complicated behavior of HMA although the predicted slopes do not perfectly match the measured slopes in semi-log scale.

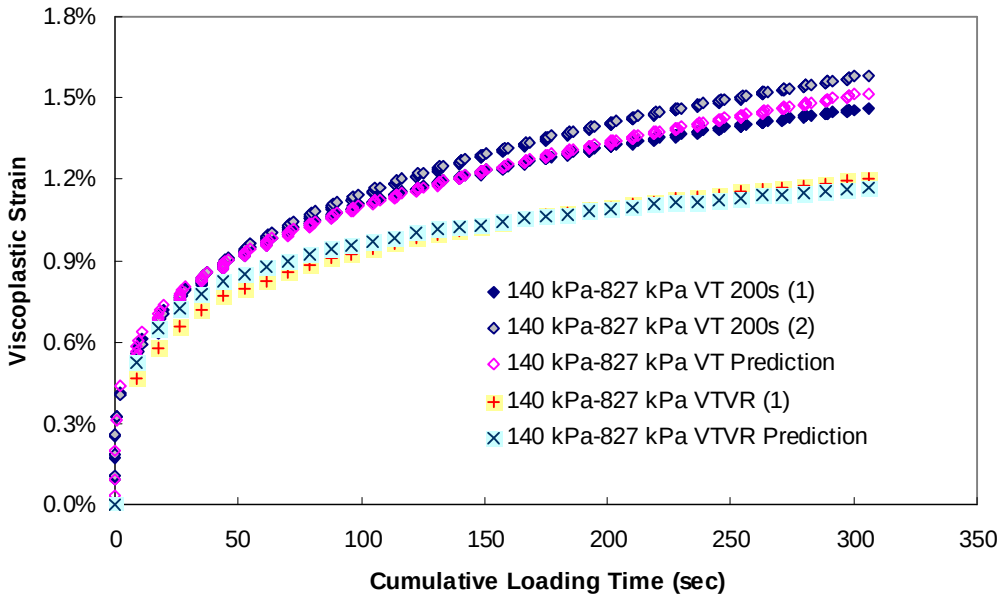

Figure 6.11 Calibration results with VT and VTVR testing at 140 kPa confinement in normal scale.

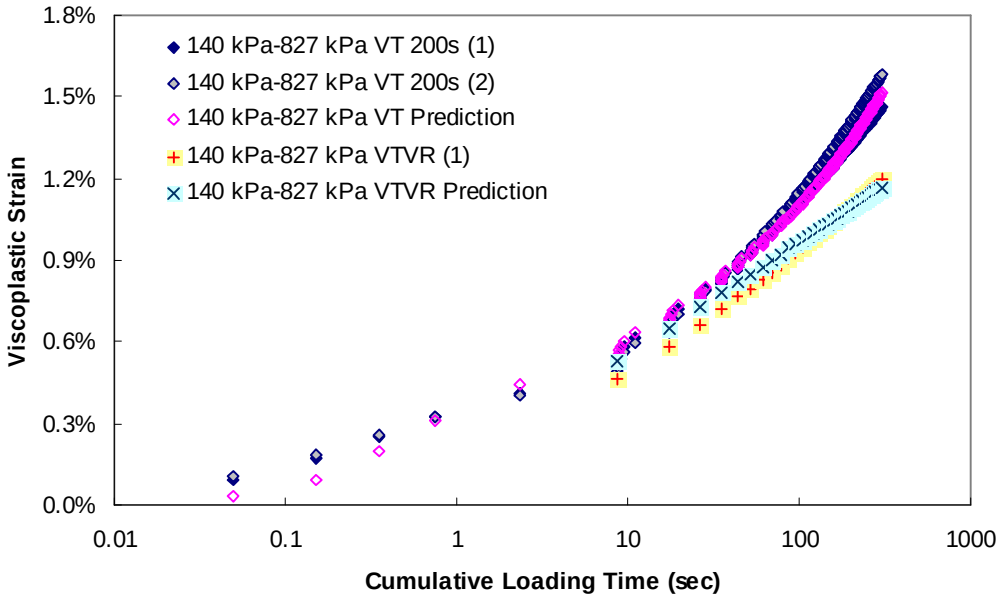

Figure 6.12 Calibration results with VT and VTVR testing at 140 kPa confinement in semi-log scale.

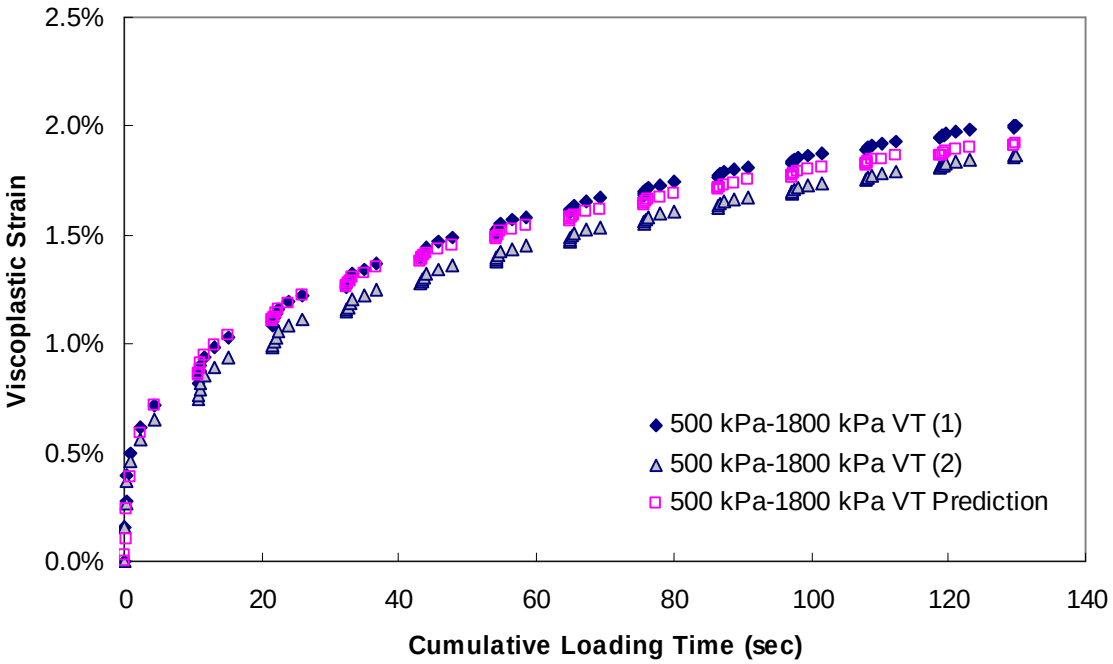

Figure 6.13 Calibration results with VT at 140 kPa confinement in normal scale.

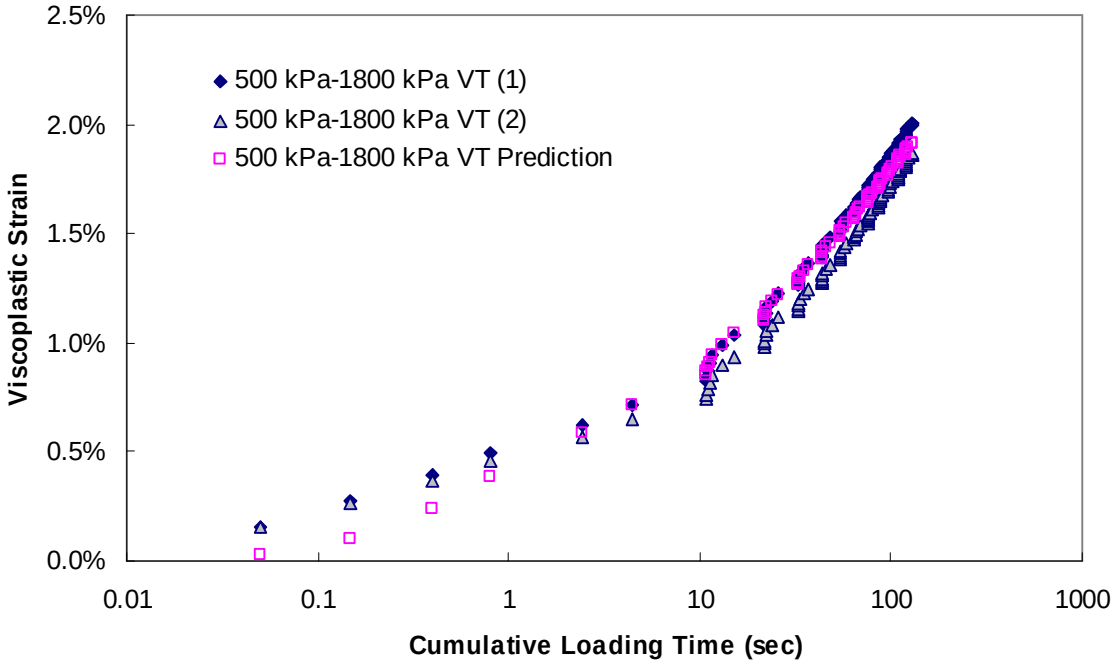

Figure 6.14 Calibration results with VT at 140 kPa confinement in semi-log scale.

6.4. VERIFICATION OF THE DEVELOPED MODEL

Based on the model calibrated using the VT and VTVR tests, the viscoplastic strains of the other loading conditions, such as the VT with two short rest periods, the RVT, VL, VLT, CLT, flow number, and the combination of the VT and flow number tests can be predicted. Each testing condition is designed to evaluate the accuracy of the developed model for the viscoplastic behavior of the material under characterized loading conditions, as described in Section 4.4. For example, flow number tests are designed to evaluate the performance of the model calibrated with square pulses for haversine pulses whereas CLT tests are designed more specifically for rate-dependent hardening-softening behavior.

6.4.1. Verification for the Confining Pressure of 140 kPa

Viscoplastic strain predictions for tests at 140 kPa confining pressure are presented in Figure 6.15 to Figure 6.20. Figure 6.15 clearly shows that the developed model is capable of considering the effects of rest periods in the viscoplastic strain prediction, which can not be accounted for by existing viscoplastic constitutive models for HMA. In Figure 6.15, as described in Section 4.4, for VT tests at 0.05 second and 1 second were performed with rest periods of 0.05 second and 1 second, respectively, until the end of testing, and VT tests at 200 seconds were performed with 200 seconds of rest. Figure 6.16 and Figure 6.17 represent the predictions for VT tests with a lower deviatoric stress of 552kPa and for RVT tests with the deviatoric stress of 827kPa, respectively. As shown in Figure 6.16 and Figure 6.17, the

predictions agree with the measurements quite well for both cases.

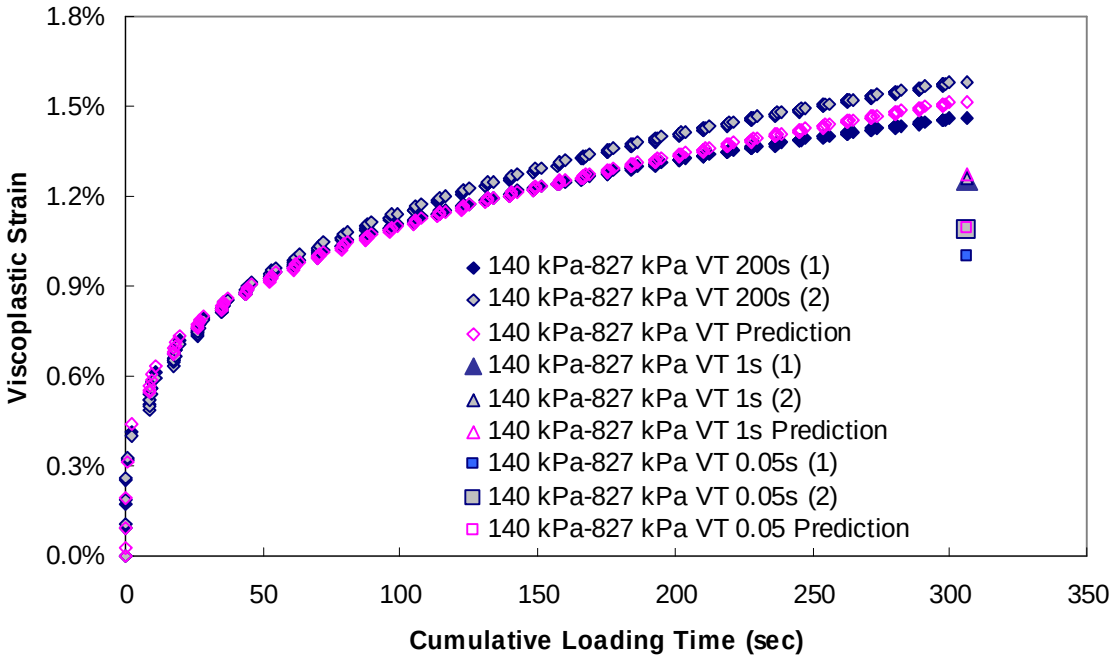

Figure 6.15 Viscoplastic strain vs. cumulative loading time (140 kPa confinement -827kPa deviatoric stress –VT tests with 3 different rest periods).

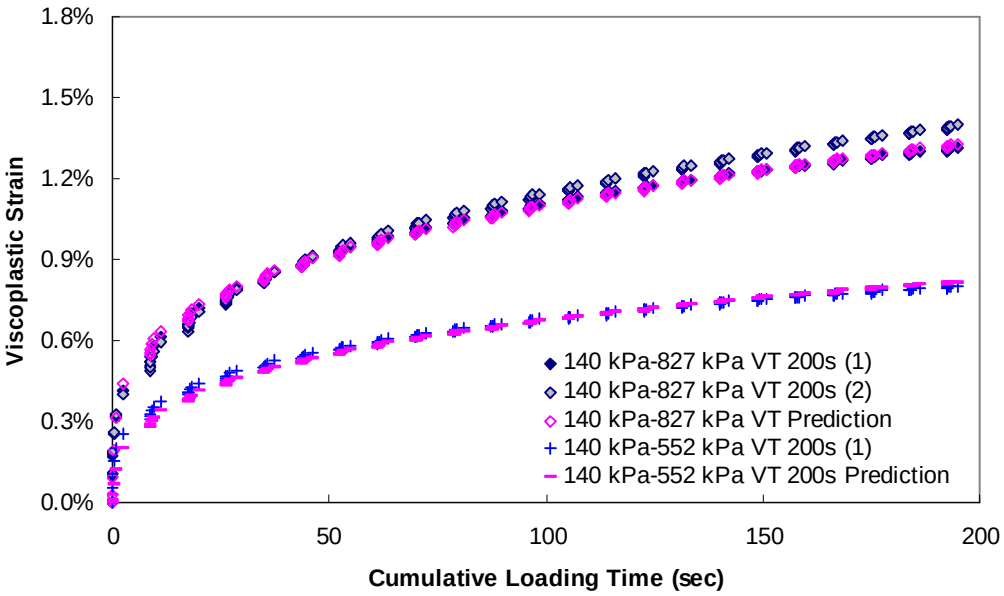

Figure 6.16 Viscoplastic strain vs. cumulative loading time (140 kPa confinement –VT test with 552 kPa and 827 kPa of deviatoric stress).

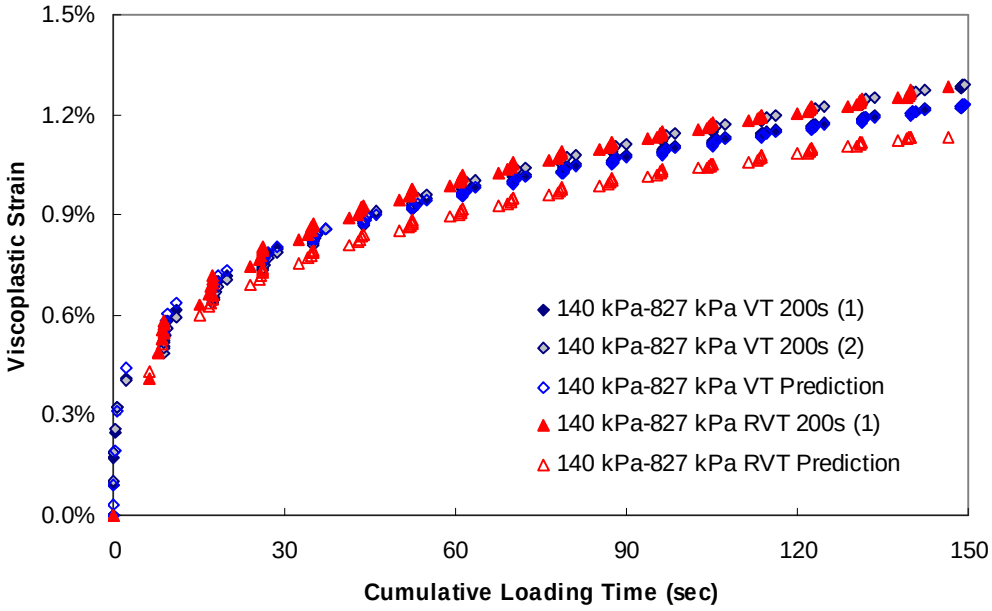

Figure 6.17 Viscoplastic strain vs. cumulative loading time (140 kPa confinement -827kPa deviatoric stress-RVT test).

Figure 6.18 and Figure 6.19 show the predictions for the VL and VLT tests and the loading histories for both conditions are represented in Figure 4.4 and Figure 4.6, respectively. Although some discrepancy is observed between the prediction and the measurement in the VL testing, the results nonetheless seem acceptable considering that most discrepancy is caused by the last pulse of the 5^{th} loading group whose deviatoric stress is 2120kPa. As shown in Figure 5.4, the strain levels at the peak stresses measured in monotonic testing at 55°C with 0 kPa and at 500 kPa confinement pressures are about 1.1% in total strain. The additional total strain developed by the last pulse of 5^{th} loading group is 0.7% in the VL test and, thus, the state of the material seems to be close to the boundary between the secondary and tertiary regions, considering the peak strain level in the monotonic test. Also, the predictions for a wide range of stress levels can be improved by adding the hydrostatic stress concept to the existing model when the model is expanded to a triaxial model. Meanwhile, the prediction for VLT testing shows quite good agreement with measurements for the entire loading history, even though the maximum load level (2030 kPa) was about the same as for VL testing. In this case, the additional total strain caused by the maximum loading is about 0.45% and is relatively lower than that in VL testing. Considering the accuracy of prediction up to these high stress levels (over 2000 kPa), it seems that viscoplastic strain is not a strong function of hydrostatic stress and, therefore, the yield stress of this material may be able to be represented with a simple yield criterion, such as von-Mises, without loosing accuracy of the predictions.

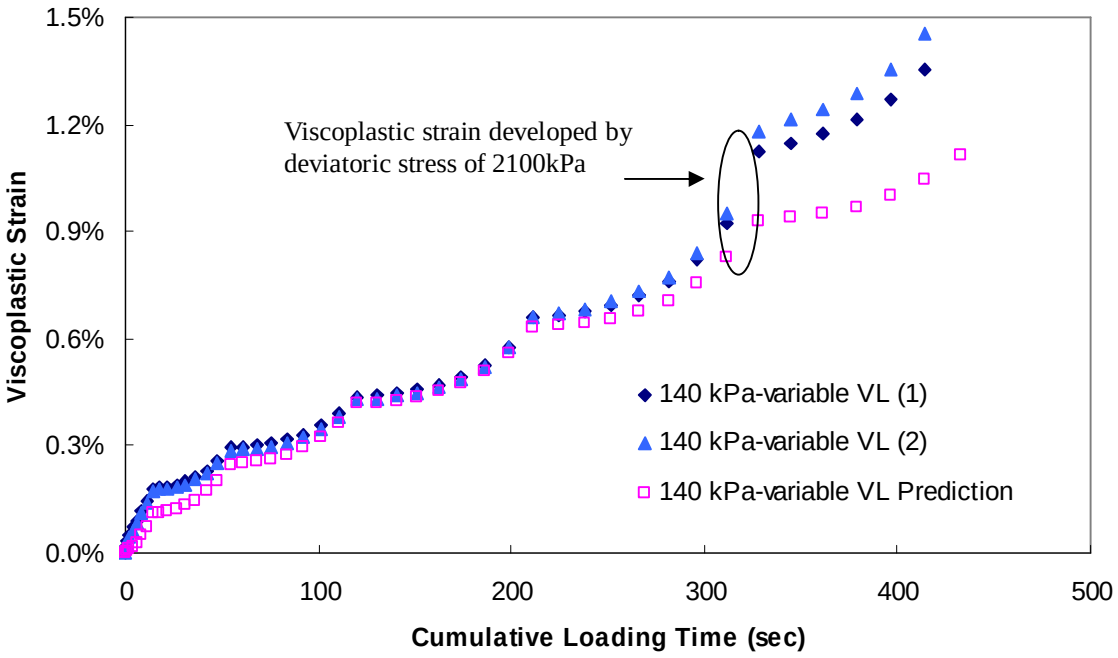

Figure 6.18 Viscoplastic strain vs. cumulative loading time (140 kPa confinement-VL).

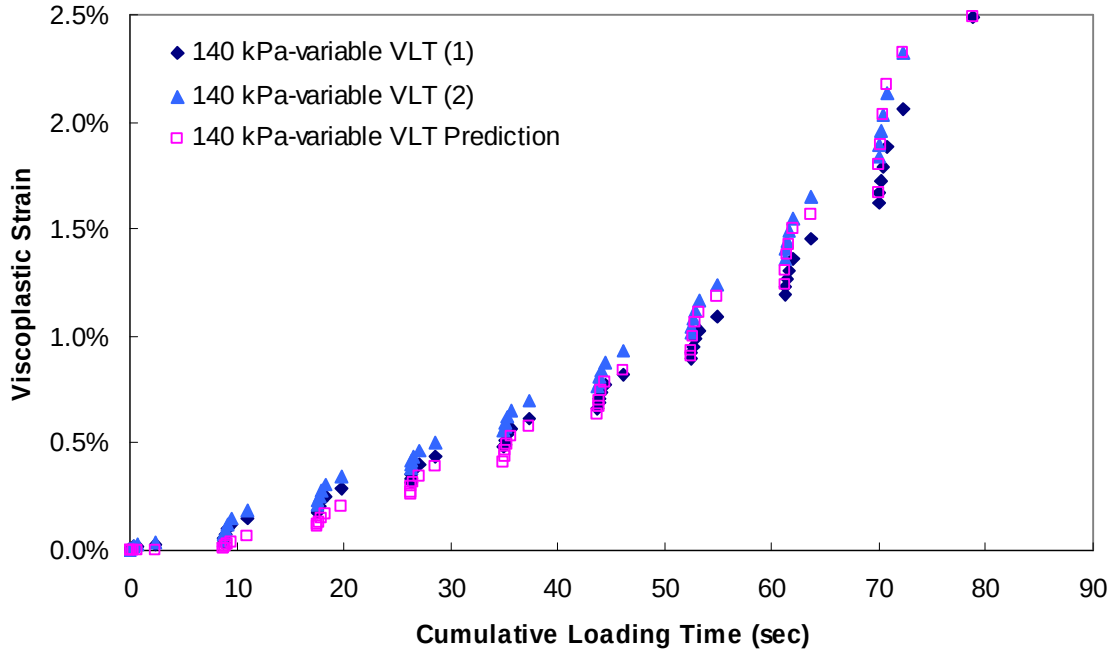

Figure 6.19 Viscoplastic strain vs. cumulative loading time (140 kPa confinement-VLT).

Figure 6.20 and Figure 6.21 represent measured and predicted viscoplastic strains for the CLT tests, and Figure 6.22 and Figure 6.23 present measured and predicted viscoplastic strains for the flow number tests in normal scale and in semi-log scale, respectively. The loading histories used for these testing conditions are described in Table 4.5 and Table 4.8. Also, the averaged viscoplastic strains measured for each loading pulse are presented in Figure 6.24 and Figure 6.25 to show the development of the viscoplastic strains more clearly. Overall, the predicted viscoplastic strains agree with the measured viscoplastic strains for each given loading history in normal scale except for three loading conditions; the CLT test at 0.1 second, the flow number test as 0.1 second, and the flow number test at 0.4 second. However, as presented in Figure 6.26, the slopes of the predicted viscoplastic strains from the CLT test in semi-log scale do not completely match the slopes of the measured viscoplastic strain, because the model over-predicts viscoplastic strain at lower viscoplastic strain levels as the pulse time decreases. Also, the trend (i.e., that a shorter pulse generates more viscoplastic strain) that is observed in other relevant tests, such as the VT test with rest periods of 1 second or 0.05 second, and the VTVR test and CLT test with rest periods of 200 seconds at 500kPa, is not clearly reproduced in both the CLT and flow number tests, although the predicted viscoplastic strain levels follow the trend. It appears that there is an additional complicated hardening-softening mechanism affects the behavior of the material under, especially repetitive short loadings and short rest periods. As shown in Figure 6.24 and Figure 6.25, the slopes of the tests in semi-log space decrease as the viscoplastic strain increases compared to other longer pulse tests, regardless of pulse shape, although tests with

shorter pulses generate more viscoplastic strain in both the CLT and flow number tests at the beginning of the testing. It seems that the 0.1 second loading time in the CLT test is not long enough to develop viscoplastic strain when the aggregate friction developed during loading is significant and is released during such a short unloading period. To address this behavior using current viscoplastic theory, it seems reasonable to introduce a sudden jump in the yield stress at the beginning of the loading, as shown in Figure 6.27. However, it is difficult to quantify the length of the pulse that is affected by the friction, because the chance is good that the amount of hump in the yield stress is a function of the load level and preceding rest period. Also, it would be difficult to represent the nonlinear yield stress with a proper mathematical expression.

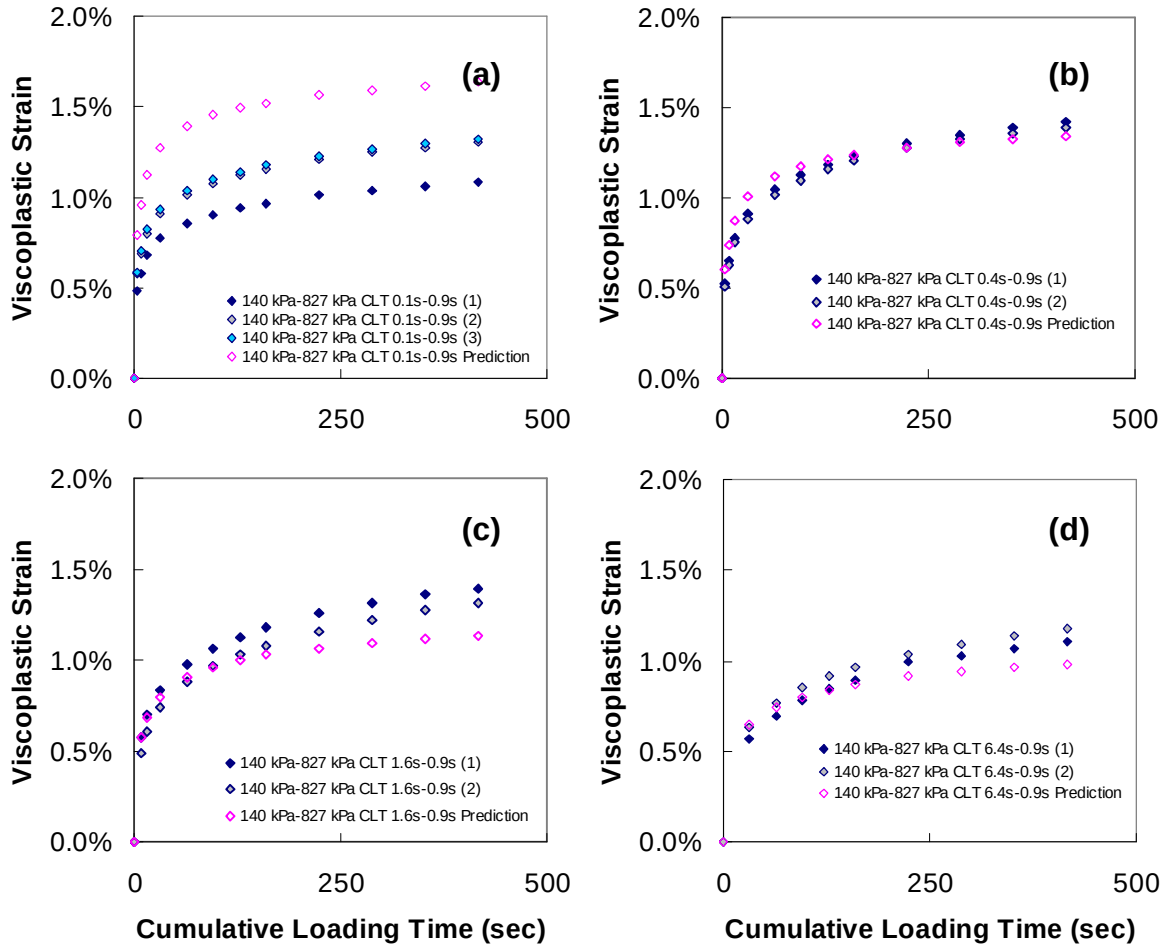

Figure 6.20 Viscoplastic strain vs. cumulative loading time in arithmetic scale (140 kPa confinement: CLT tests at (a) 0.1-0.9 second, (b) 0.4-0.9 second, (c) 1.6-0.9 second, and (d) 6.4-0.9 second).

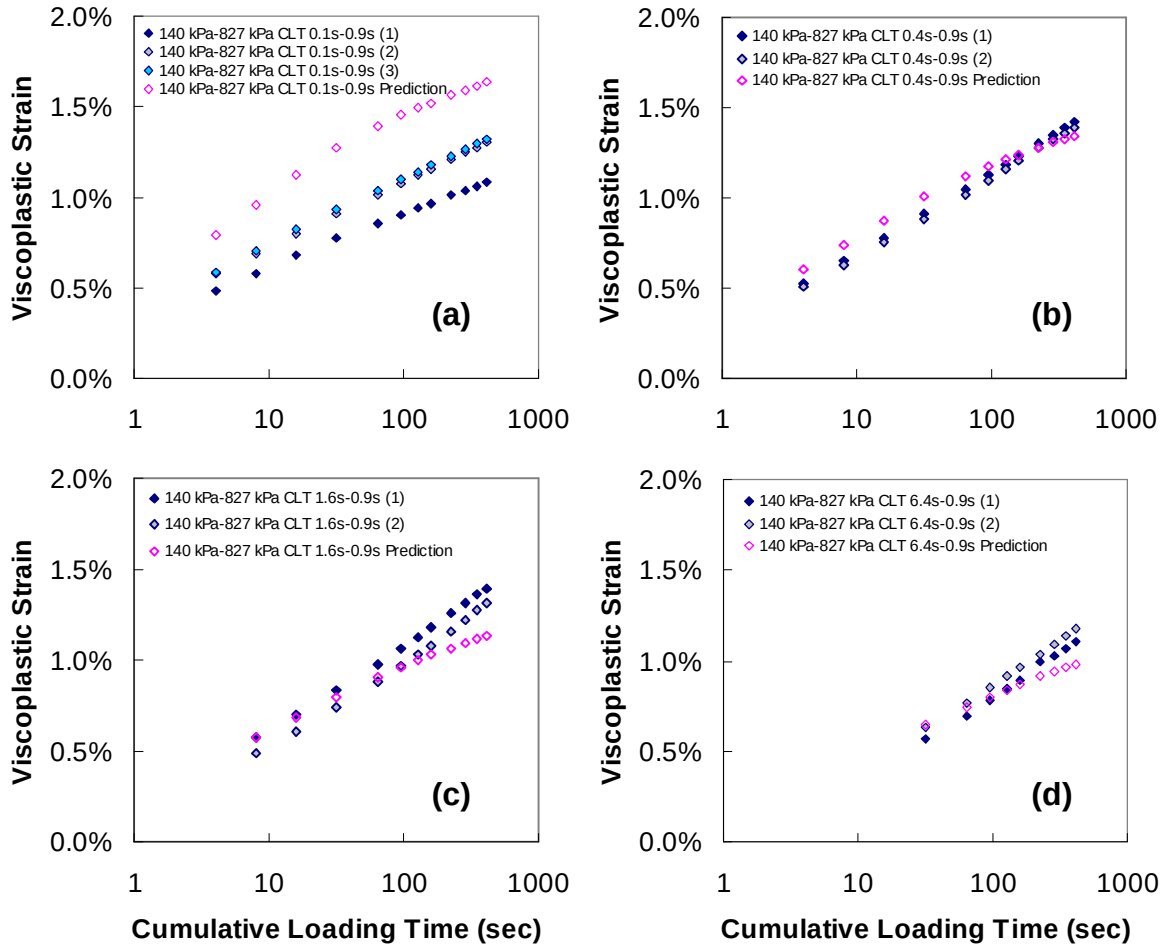

Figure 6.21 Viscoplastic strain vs. cumulative loading time in semi-log scale (140 kPa confinement: CLT tests at (a) 0.1-0.9 second, (b) 0.4-0.9 second, (c) 1.6-0.9 second, and (d) 6.4-0.9 second).

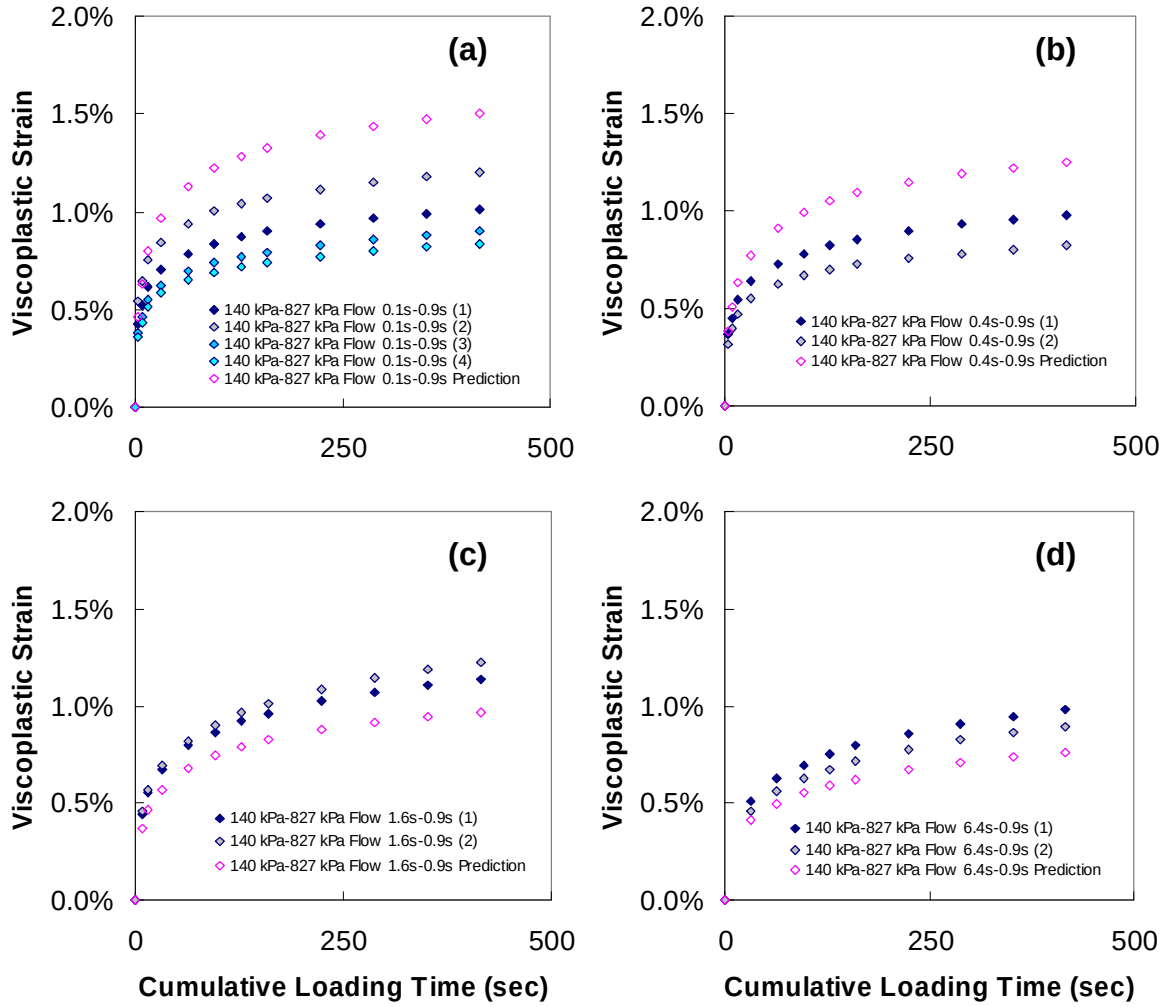

Figure 6.22 Viscoplastic strain vs. cumulative loading time in arithmetic scale (140 kPa confinement: flow number tests at (a) 0.1-0.9 second, (b) 0.4-0.9 second, (c) 1.6-0.9 second, and (d) 6.4-0.9 second).

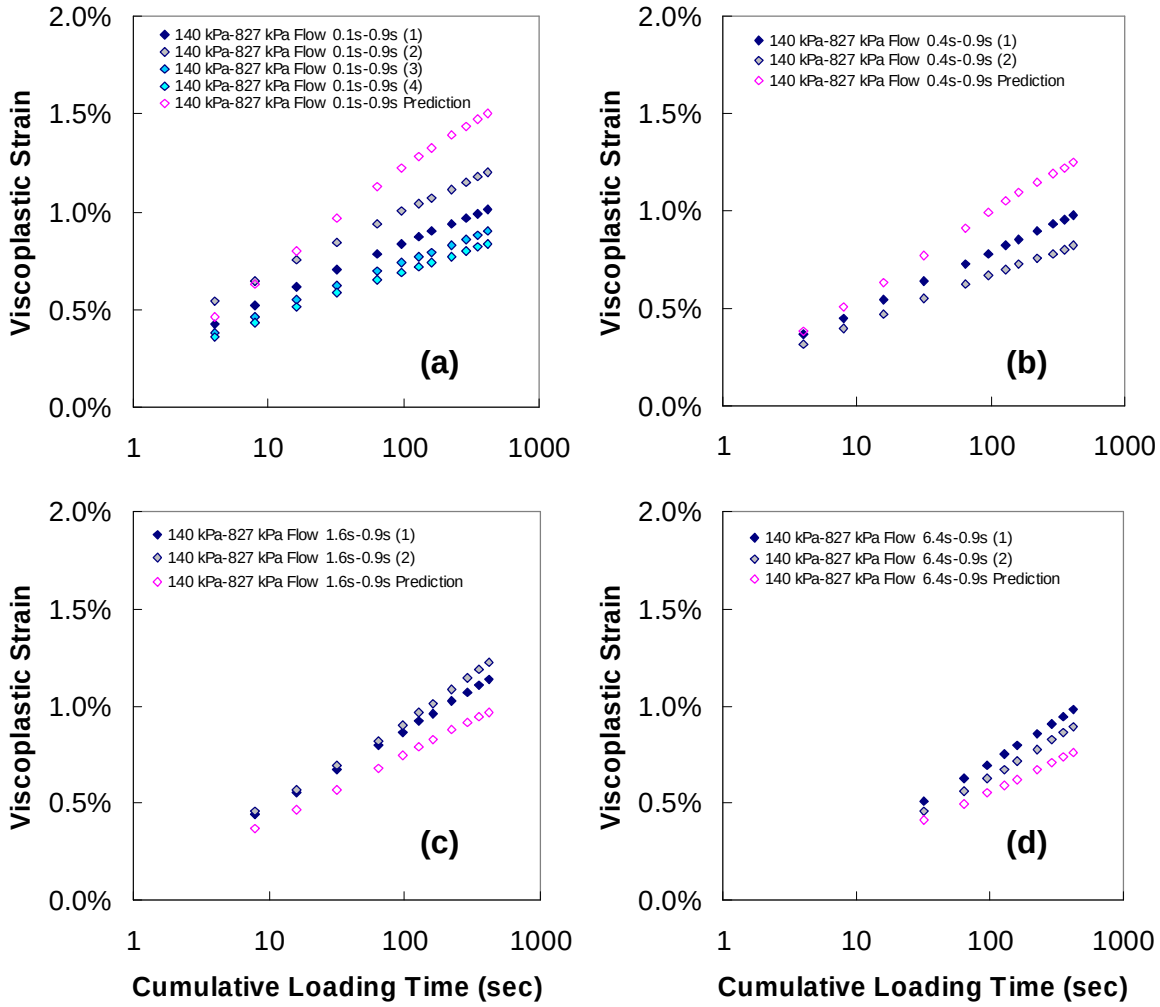

Figure 6.23 Viscoplastic strain vs. cumulative loading time in semi-log scale (140 kPa confinement: flow number tests at (a) 0.1-0.9 second, (b) 0.4-0.9 second, (c) 1.6-0.9 second, and (d) 6.4-0.9 second).

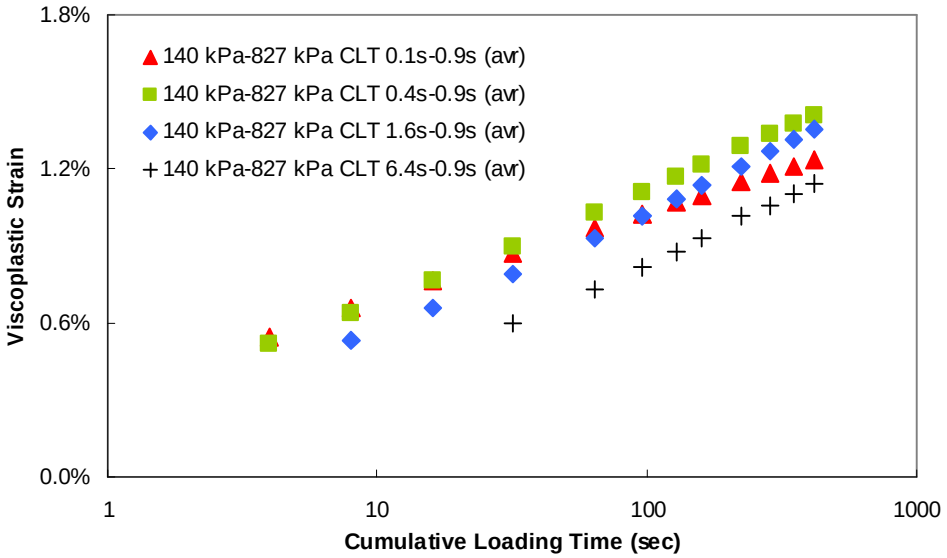

Figure 6.24 Viscoplastic strain vs. cumulative loading time in semi-log scale (140 kPa confinement: CLT tests at 0.1-0.9 second, 0.4-0.9 second, 1.6-0.9 second, and 6.4-0.9 second, averaged).

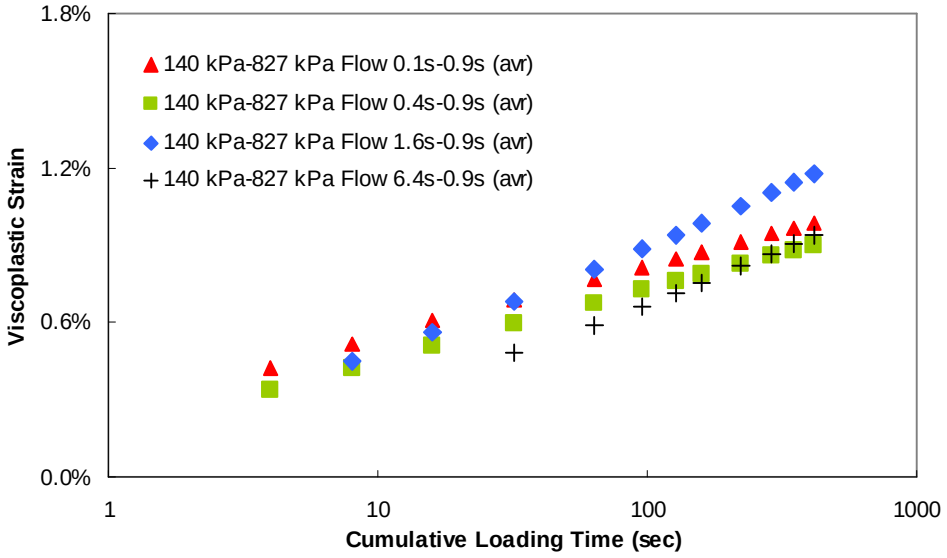

Figure 6.25 Viscoplastic strain vs. cumulative loading time in semi-log scale (140 kPa confinement: flow number tests at 0.1-0.9 second, 0.4-0.9 second, 1.6-0.9 second, and 6.4-0.9 second, averaged).

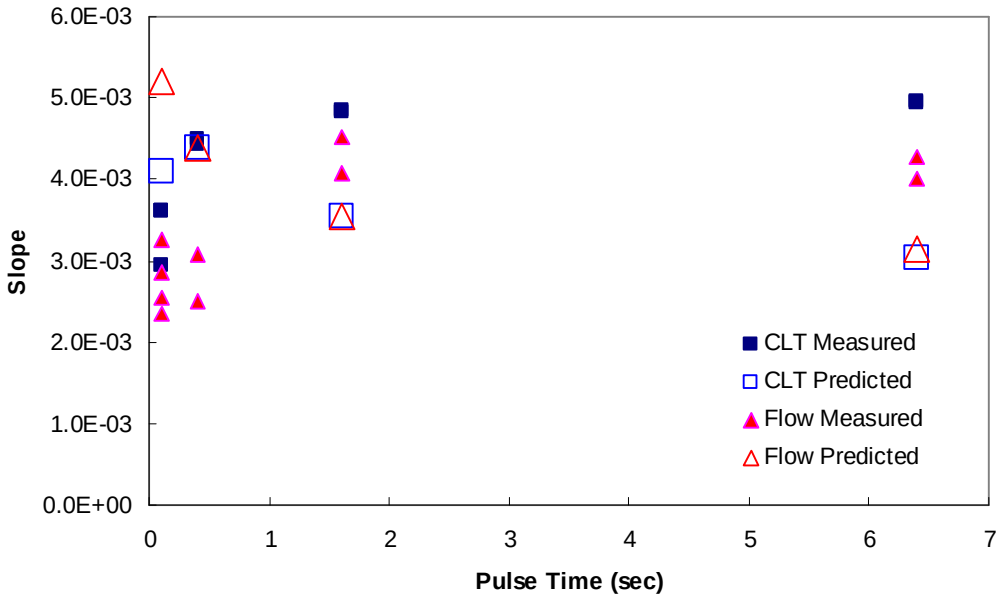

Figure 6.26 Slope vs. pulse time for CLT and flow number tests with various pulse times

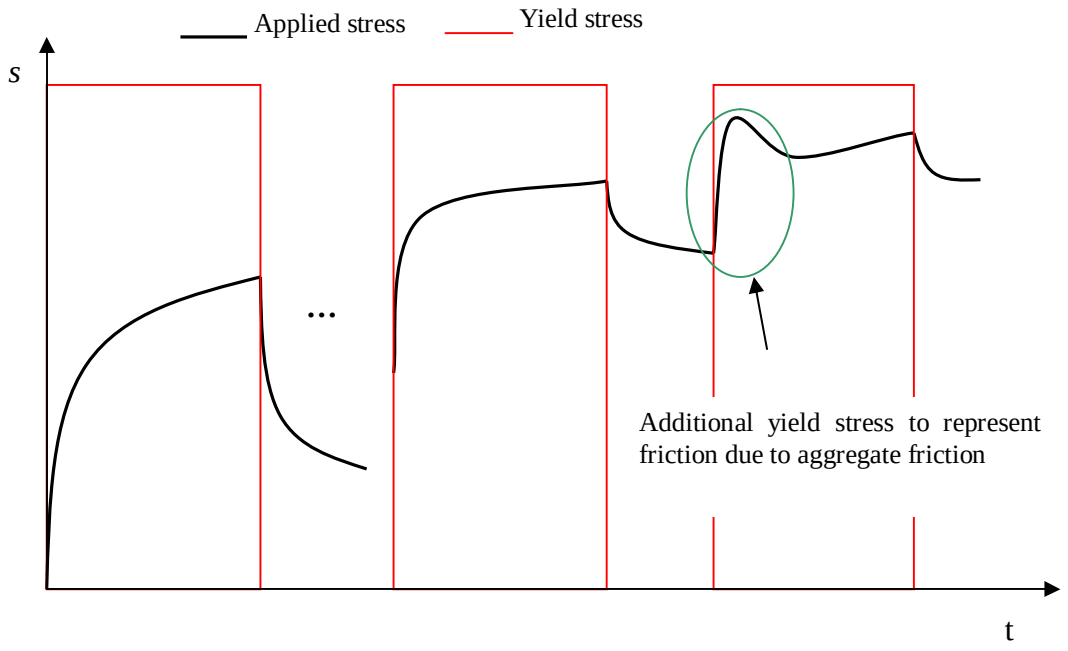

Figure 6.27 Schematic representation for ideal yield stress.

Figure 6.28 presents predictions for a complex loading history, which is a combination of the VT test results and the flow number test results. Overall, the prediction of the viscoplastic strain matches well with the measured viscoplastic strain considering the complexity of the stress history used in this test, as described in Section 4.4.5.

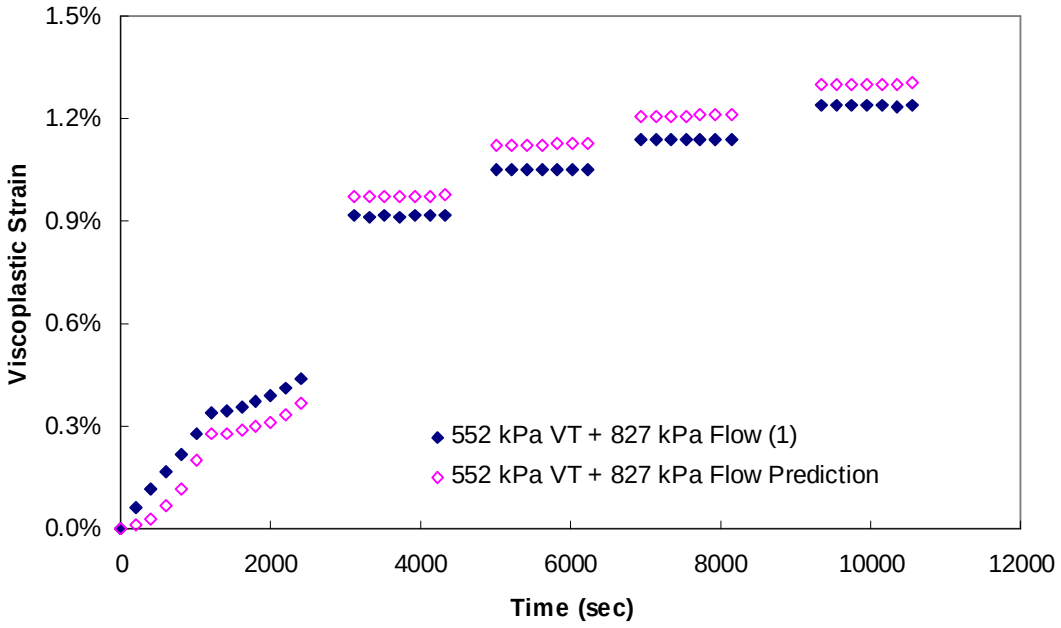

Figure 6.28 Viscoplastic strain vs. cumulative loading time (140 kPa confinement –VT + flow number test).

6.4.2. Verification for the Confining Pressure of 500 kPa

Figure 6.29 to Figure 6.35 present the viscoplastic strain predictions made for the 500 kPa confining pressure tests. As shown, the developed model shows good predictions for the VT tests under two different deviatoric stress conditions, whereas it shows relatively large errors for the VL and VLT tests. Considering that the model over-predicts viscoplastic strain at a

low deviatoric stress and under-predicts viscoplastic strain at high deviatoric stress in the VL and VLT tests, the prediction can be improved when hydrostatic stress is introduced in the model as described for the VL test at 140 kPa confinement pressure.

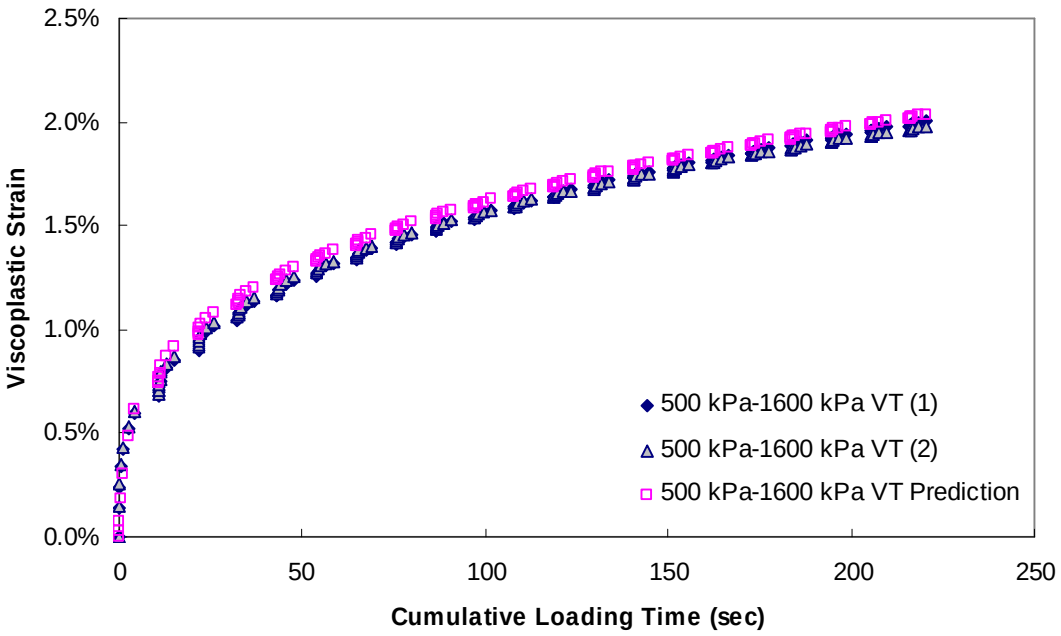

Figure 6.29 Viscoplastic strain vs. cumulative loading time (500 kPa confinement-1600 kPa deviatoric stress VT test).

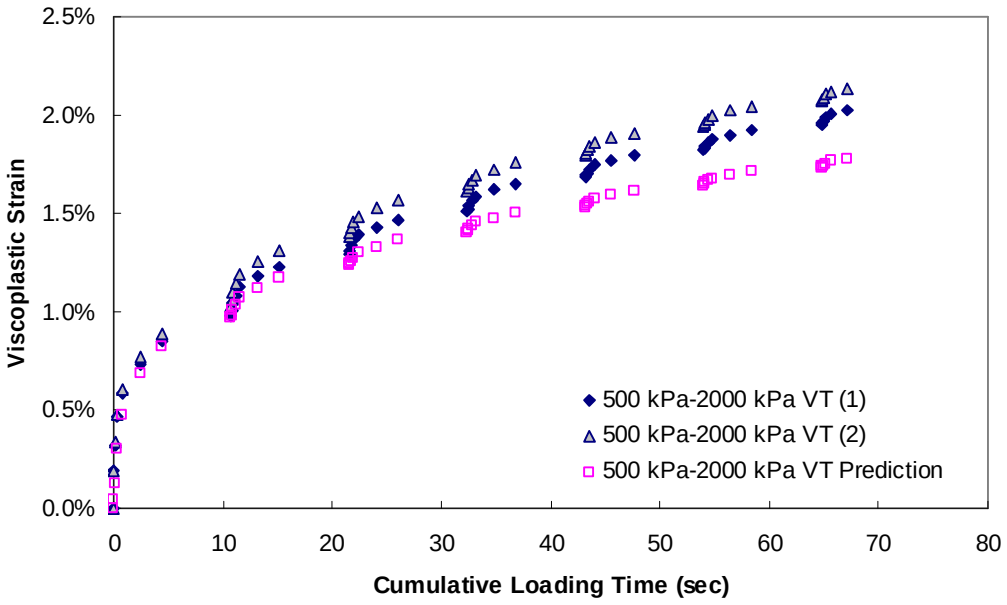

Figure 6.30 Viscoplastic strain vs. cumulative loading time (500 kPa confinement-2000 kPa deviatoric stress, VT test).).

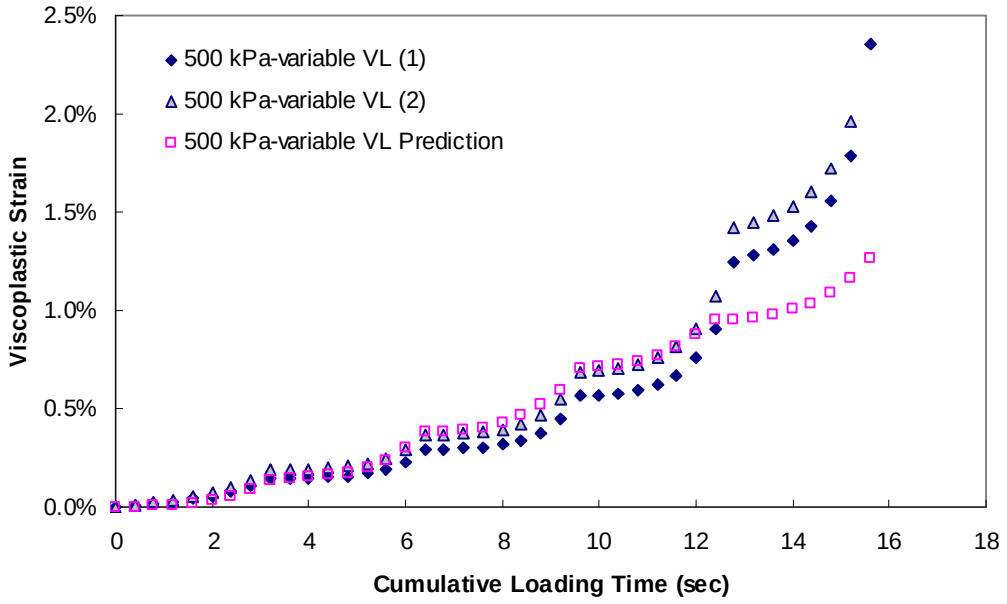

Figure 6.31 Viscoplastic strain vs. cumulative loading time (500 kPa confinement-VL test).

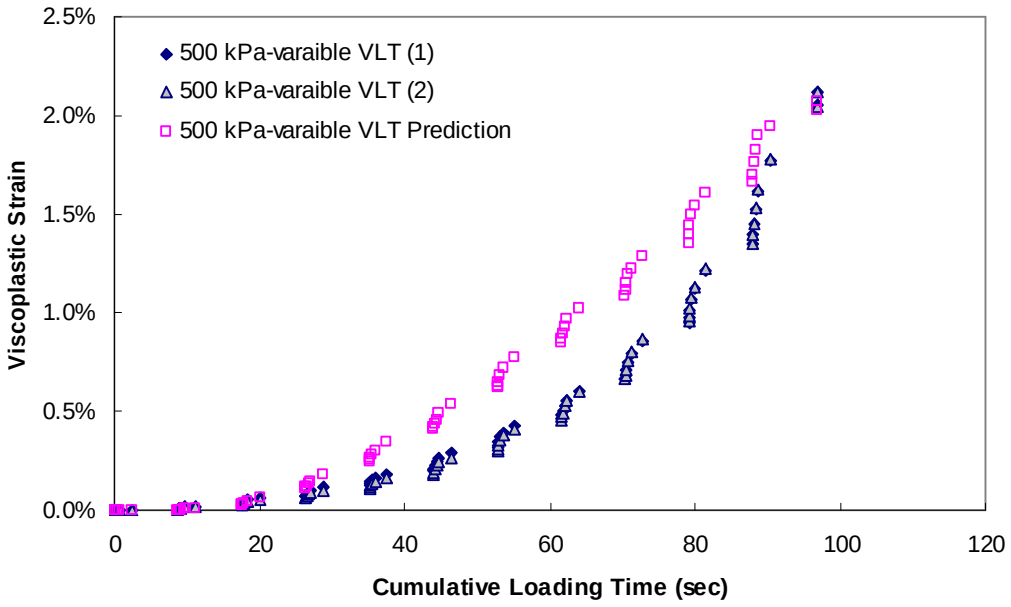

Figure 6.32 Viscoplastic strain vs. cumulative loading time (500 kPa confinement-VLT test).

Figure 6.33, Figure 6.34, and Figure 6.35 present predictions for the CLT test with three different pulse times (0.4 second, 1.6 seconds, and 6.4 seconds) and rest periods of 200 seconds. As described in Section 4.4.3, CLT tests with three different pulse times clearly show the effect of rest period and rate-dependent hardening of the yield stress on viscoplastic strain development. For this testing condition the predicted viscoplastic strain is quite well matched to the measured viscoplastic strain.

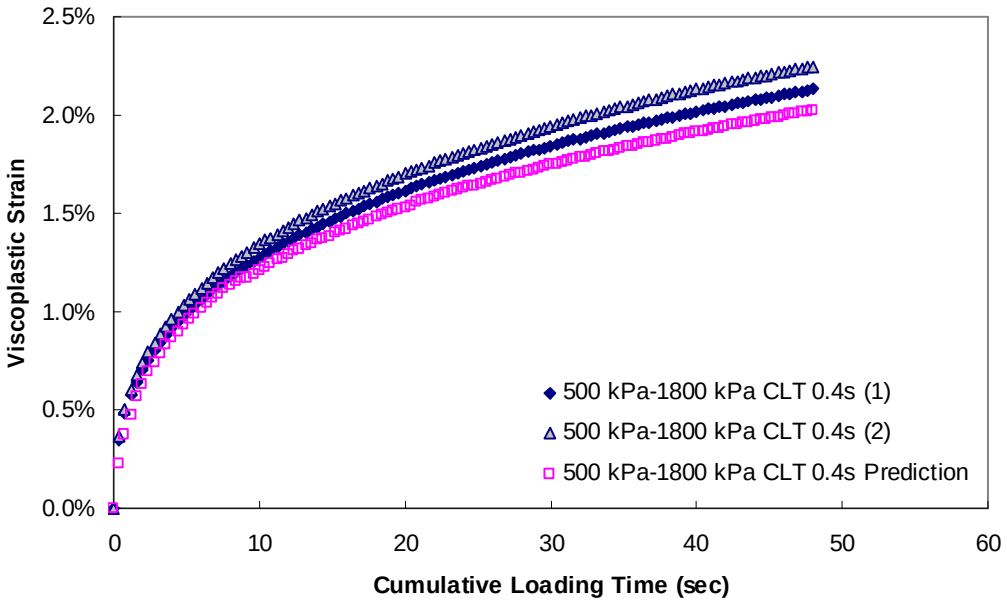

Figure 6.33 Viscoplastic strain vs. cumulative loading time (500 kPa confinement-1800 kPa deviatoric stress CLT test at 0.4 second).

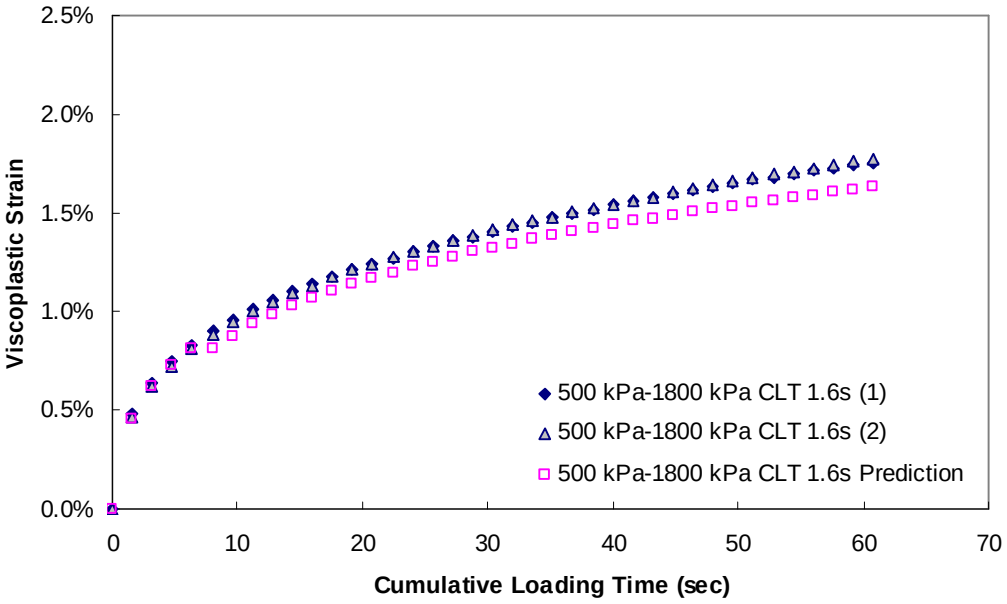

Figure 6.34 Viscoplastic strain vs. cumulative loading time (500 kPa confinement-1800 kPa deviatoric stress CLT test at 1.6 seconds).

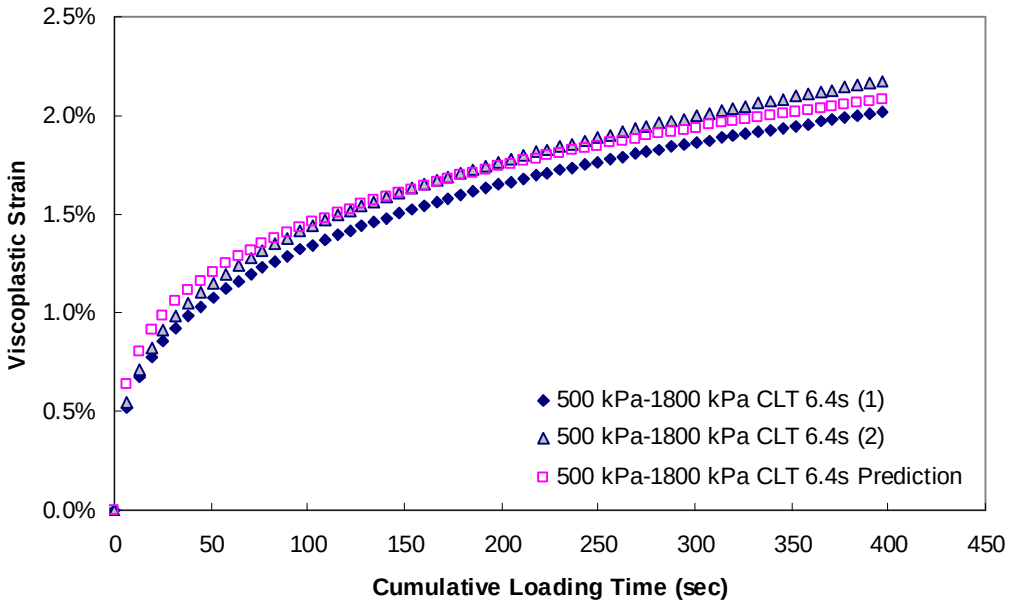

Figure 6.35 Viscoplastic strain vs. cumulative loading time (500 kPa confinement-1800 kPa deviatoric stress CLT test at 6.4 second).

Figure 6.36 presents measurements and predictions together for the testing and Figure 6.37 presents the fitting coefficient, B, determined by fitting the measured and predicted viscoplastic strains in Figure 6.36 to power functions ($e_{vp} = At^B$). As shown, the slopes of predicted viscoplastic strains match well with those of measured viscoplastic strains.

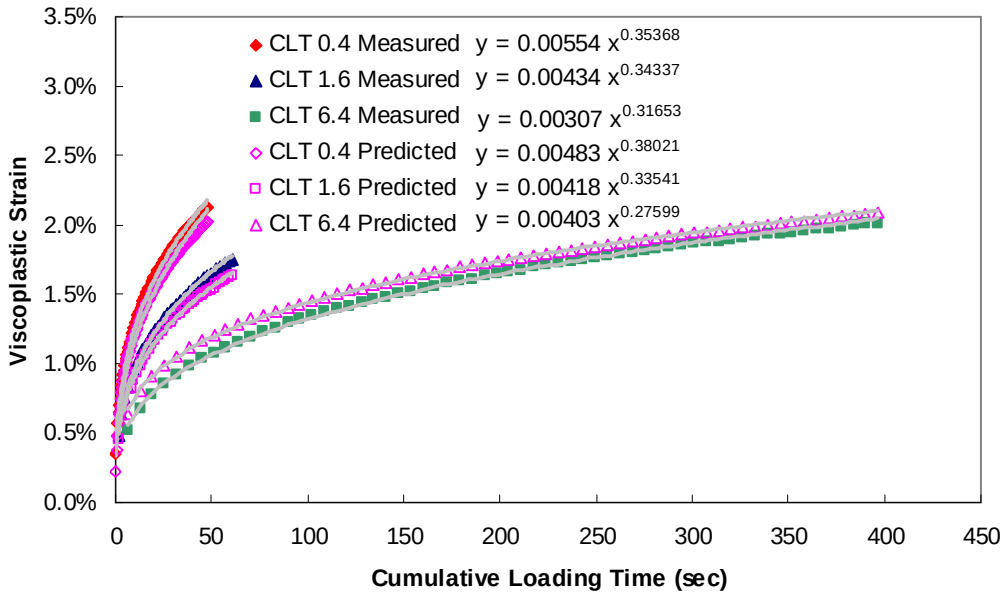

Figure 6.36 Viscoplastic strain vs. cumulative loading time (500 kPa confinement-1800 kPa deviatoric stress CLT tests).

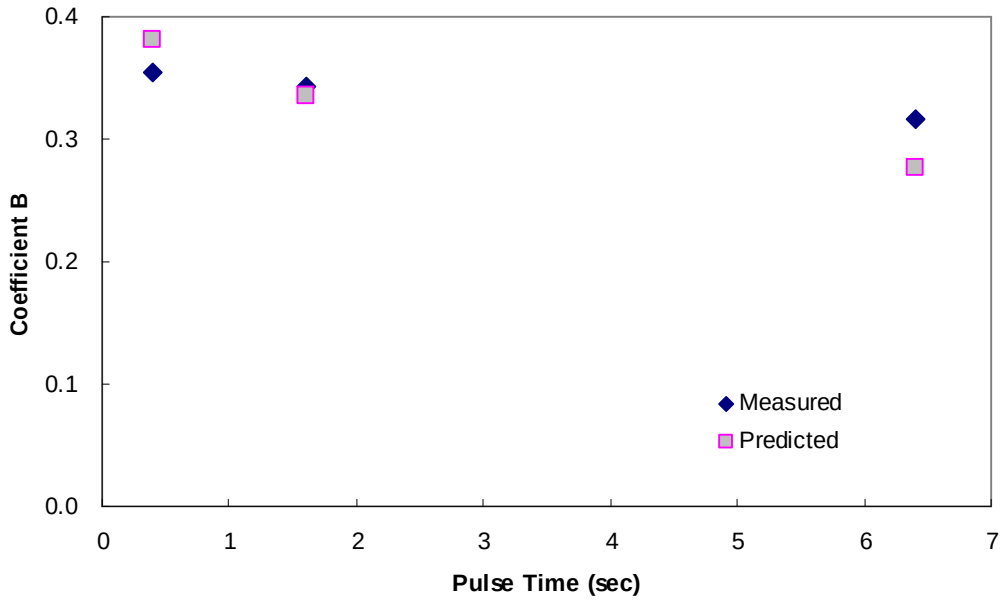

Figure 6.37 Coefficient B vs. pulse time for CLT tests at 500kPa confinement

7. CONCLUSIONS AND RECOMMENDATIONS

7.1. CONCLUSIONS

The main outcomes of this research, obtained through fundamental testing and analysis protocols, are: 1) the identification of the state dependent behavior of HMA in the small strain regime, 2) confirmation of the time and temperature relationship with growing damage/strain, and 3) the identification and modeling of the rate-dependent hardening and softening behavior in viscoplastic media, HMA.

From dynamic modulus testing at four different confining pressures, it is concluded that the dynamic modulus of HMA in compression is the same as that in tension-compression. However, it is shown that the dynamic modulus is especially dependent on confining pressure at conditions where the material is softest (high temperatures and low frequencies). Further, it is found that when affected by confining pressure, that the modulus increases as the confining pressure increases. Intensified aggregate interlocking is considered as a possible cause for this confining pressure dependent dynamic modulus. Also, it is concluded through a series of constant strain rate tests and repetitive creep and recovery tests that the time-temperature superposition principle holds true regardless of loading type and severity of damage or viscoplastic strain.

It is concluded that under compressive loading that a rate-dependent softening mechanism, which operates during unloading, and a rate-dependent hardening mechanism, which

operates during loading, must be considered as significant factors that affect the viscoplastic characteristics of asphalt concrete under compressive loading. In order to account for this characteristic behavior of HMA in the constitutive model, a rate dependent hardening-softening yield stress function with Perzyna's flow rule is suggested. This model adopt the time-temperature superposition (t-TS) principle with growing damage that has been verified for the wide range of the material state and thus reduces the calibration testing requirement significantly. A unit response function in linear viscoelasticity is successfully utilized to represent the rate-dependent hardening-softening yield stress. It is shown that the developed model is capable of accounting for the effects of rest period and pulse time on viscoplastic strain development and that the developed model performs well in predicting the viscoplastic strain development under various loading conditions. The model shows a reduced capacity in predicting the response to short loading pulse and rest period conditions; however, these predictions are still superior to those from existing viscoplastic models which ignore the softening mechanism. To better the predictions at these conditions it is suggested that the initial, elastic-like hardening should be studied.

7.2. RECOMMENDATIONS

In this research, the model parameters are determined for each specific confining pressure condition. Although the model is not insufficient to explain the general behavior hot mix asphalt pavements which experience almost uniform confining pressure for a certain time period, it seems reasonable to introduce a yield criterion that is capable of considering the

entire possible confining pressure especially in order to increase the accuracy of the predictions for low and high levels of stress loading.

The VT and VTVR tests are good experimental protocols to characterize both the hardening and softening behavior of HMA. However, a more complicated testing protocol may be required for the calibration of the model when the 1D model is expanded to triaxial model to account for the effect of hydrostatic stress on viscoplastic strain development.

Even though the current hardening-softening function considers rate-dependent hardening and softening of HMA reasonably, some over- and under-predictions are observed for certain stress histories with short rest periods. To improve the accuracy of the predictions, a study on hardening behavior which is related to aggregate friction at the beginning of loading is required as described in Section 6.4.2. Accordingly, investigation into a mathematical expression for the hardening behavior that would not cause a significant increase in computational time is also recommended.

As described in Section 5.2, the modeling technique used in the development of the VECD model in tension can not be directly applied to the behavior of HMA in compression because of viscoelastic strain hardening. From the point of view that hardening and softening of viscoplastic media show rate-dependent behavior, a study on the possible relationship between strain hardening in the viscoelastic media and hardening-softening in the viscoplastic media is recommended.

8. REFERENCES

Armstrong, P.J., Frederick, C.O. "A Mathematical Representation of the Multiaxial Bauschinger effect." CEGB Report No. RD/B/N 731. (1966).

Chaboche J.L. , "Time-Independent Constitutive Theories for Cyclic Plasticity". *International Journal of Plasticity* **2.** pp. 149–188 (1986).

Cernocky, E.P. and Krempl, E., "A Nonlinear Uniaxial Integral Constitutive Equation Incorporating Rate Effects, Creep and Relaxation." *International Journal of Nonlinear Mechanics*, 14, 183 (1979)

Chehab, G., Y. R. Kim, R. A. Schapery, M. Witczack, R. Bonaquist. "Time-Temperature Superposition Principle for Asphalt Concrete Mixtures with Growing Damage in Tension State." *Asphalt Paving Technology*, AAPT. Vol. 71: 559-593. (2002).

Chehab, G. "Characterization of Asphalt Concrete in Tension Using a Viscoelastoplastic Model." Ph.D. Dissertation, North Carolina State University, Raleigh, NC. (2002).

Chehab, G.R. and Y.R. Kim. "Viscoelastoplastic Continuum Damage Model Application to Thermal Cracking of Asphalt Concrete." *ASCE Journal of Materials in Civil Engineering*, (2003).

Desai, C. S., Somasundaram, S., and Frantziskonis, G. "A Hierarchical Approach for Constitutive Modeling of Geologic Materials." Int. J. Number. Analyt. Meth. Geomech., 10, 225-257. (1986)

Desai C.S. and Zhang D. "Viscoplastic Model for Geologic Materials with Generalized Flow Rule." *International Journal for Numerical and Analytical Methods in Geomechanics* **11**, pp. 603–620 (1987).

Desai, C.S. "Mechanics of Materials and Interfaces: The Disturbed State Concept." CRC Press, Boca Raton, Florida, CRC Press, Boca Raton, Florida, (2001).

Erkens, S. M., X. Liu, T. Scarpas, A. A. A. Molenaar, and J. Blaauwendraad. "Modeling of Asphalt Concrete – Numerical and Experimental Aspects, Recent Advances in Materials Characterization and Modeling of Pavement Systems" (E. Tutumluer, Y. M. Najjar, and E. Masad, eds.). Geotechnical Special Publication No. 123, ASCE. Reston, VA: 160-177. (2003).

Gibson, N.H., C.W. Schwartz, R.A. Schapery, and M.W. Witczak. "Viscoelastic, Viscoplastic, and Damage Modeling of Asphalt Concrete in Unconfined Compression." Transportation Research Record, No. 1860, pp. 3-15. (2003).

Gibson, N.H. "A Viscoelastoplastic Continuum Damage Model for the Compressive Behavior of Asphalt Concrete." Ph.D. Dissertation. University of Maryland. (2006).

Krempl, E., "Models of Viscoplasticity-Some Comments on Equilibrium (Back) Stress and Drag Stress." Acta Mech. 69, 25-42 (1987)

Krempl, E., Khan, F., "Rate (time)-Dependent Deformation Behavior: An Overview of Some Properties of Metals and Solid Polymers." *International Journal of Plasticity* 19, 1069-1095 (2003)

Krieg R.D. and Krieg D.B., "Accuracies of Numerical Solution Methods for the Elastic–Perfectly Plastic Model." *J. Press. Vess. Tech. ASME* **99**, pp. 510–515 (1977)

Kwnagsoo HO, "Unified Constitutive Equations of Viscoplastic Deformation: Development and Capabilities." *Japanese Society of Mechanical Engineers,* Vol.49, No. 1,2006 (2006)

Park, S. W. and R. A. Schapery. "Methods of Interconversion Between Linear Viscoelastic Material Functions. Part I – A Numerical Method based on Prony Series." *International Journal of Solids and Structures*. Vol. 36: 1653-1657. (1999).

Perzyna, P. "Thermodynamic Theory of Viscoplasticity." *Advances in Applied Mechanics*, 11:313-354 (1971).

Perzyna, P. "The Constitutive Equations for Rate Sensitive Plastic Materials." *Quart. Appl. Math.*, 20:321-332 (1963).

Prager, W. A New Method of Analyzing Stresses and Strains in Work Hardening Plastic Solids. *Journal of Applied Mechanics* **23**, pp. 493–496. (1956)

Saadeh, SAR. "Characterization of Asphlat Concrete Using Anisotropic Damage Viscoelastic-Viscoplastic Model." Ph.D. Dissertation. Texas A&M University (2005).

Scarpas, A., Al-Khoury, R., Van Gurp, C., Erkens, S. "Finite Element Simulation of Damage Development in Asphalt Concrete Pavements." In: Proceedings of the 8th International Conference on Asphalt Pavements, University of Washington, Seattle, WA, pp. 673–692. (1997)

Schapery, R.A. "A Simple Collocation Method for Fitting Viscoelastic Models to

Experimental Data.” GALCIT SM 61-23A. California Institute of Technology, Pasadena CA. (1961).

Schapery, R. A. “Correspondence Principles and a Generalized J-integral for Large Deformation and Fracture Analysis of Viscoelastic Media.” *Int. Journal of Fracture*. Vol. 25: 195-223. (1984).

Schapery, R. A. “Nonlinear Viscoelastic and Viscoplastic Constitutive Equations with Growing Damage.” *Int. Journal of Fracture*. Vol. 97: 33-66. (1999).

Uzan, J. "Asphalt Concrete Characterization for Pavement Performance Prediction.” *Asphalt Paving Technology*, AAPT. Volume 65: 573-607. (1996).

von Mises R. “Mechanik der plastischen Formanderung von Kristallen.” ZAMM 8:161–185 (1928)